LBL-1822

PHOSPHORESCENCE MICROWAVE DOUBLE RESONANCE STUDIES OF THE LOWEST EXCITED TRIPLET STATE OF p-DICHLOROBENZENE

Rodney Michael Panos
(Ph.D. Thesis)

June 1973

Prepared for the U. S. Atomic Energy Commission
under Contract W-7405-ENG-48

For Reference

Not to be taken from this room

LAWRENCE BERKELEY LABORATORY
UNIVERSITY OF CALIFORNIA
BERKELEY

LBL-1822

DISCLAIMER

This document was prepared as an account of work sponsored by the United States Government. While this document is believed to contain correct information, neither the United States Government nor any agency thereof, nor the Regents of the University of California, nor any of their employees, makes any warranty, express or implied, or assumes any legal responsibility for the accuracy, completeness, or usefulness of any information, apparatus, product, or process disclosed, or represents that its use would not infringe privately owned rights. Reference herein to any specific commercial product, process, or service by its trade name, trademark, manufacturer, or otherwise, does not necessarily constitute or imply its endorsement, recommendation, or favoring by the United States Government or any agency thereof, or the Regents of the University of California. The views and opinions of authors expressed herein do not necessarily state or reflect those of the United States Government or any agency thereof or the Regents of the University of California.

0 0 0 0 3 9 0 0 4 3 8

TABLE OF CONTENTS

ABSTRACT v

I. INTRODUCTION 1

A. Historical Background - Phosphorescence and the Triplet State 2

B. Benzene and p-Dichlorobenzene 8

II. THE TRIPLET STATE 12

A. The Antisymmetry Principle 12

B. The State Function 14

III. MAGNETIC INTERACTIONS AND PHOSPHORESCENCE 21

A. Zero-Field Splitting 21

B. Spin-Orbit Coupling 24

C. Spin-Orbit Perturbations 30

IV. ADIABATIC INVERSION 35

V. EXPERIMENTS 37

A. Descriptions 37

1. Triplet State Dynamics 37

2. Microwave Perturbations 41

B. Experimental Procedures 53

1. Basic Equipment 53

2. ODMR and PMDR Experiments 55

3. Adiabatic Inversion 57

VI. p-DICHLOROBENZENE -- PRELIMINARY STUDIES 61

A. Experiment and Results 61

1. Sample 61

2. Phosphorescence Microwave Double Resonance Spectroscopy (PMDR) 62

3. Adiabatic Inversion 66

B. Discussion 72

VII. p-DICHLOROBENZENE -- ENVIRONMENTAL EFFECTS 93

A. Experiment and Results 97

1. Systems Chosen for Study and Comparison 97

2. Sample Preparation 100

3. ODMR and PMDR Spectra 101

4. Delayed Inversion Experiments 102

B. Discussion 110

Appendix I. DCB In-Plane Spin-Spin Calculations 122

References 131

Acknowledgements 139

0 0 0 0 3 9 0 0 4 3 9

Phosphorescence Microwave Double Resonance Studies of the Lowest Excited Triplet State of p-Dichlorobenzene

Rodney Michael Panos

Inorganic Materials Research Division, Lawrence Berkeley Laboratory,
and Department of Chemistry; University of California
Berkeley, California 94720

ABSTRACT

Phosphorescence microwave double resonance (PMDR) spectra of p-dichlorobenzene (DCB) neat crystal have been obtained monitoring low temperature (~1.3°K) trap phosphorescence and used to make symmetry assignments of various vibronic bands present in the spectra. In addition, ratios of radiative rate constants of individual triplet spin-sublevels to several vibrational states, the intrinsic lifetimes of all three triplet spin sublevels, and selective polarized phosphorescence from individual spin sublevels in various vibronic transitions have been measured. An analysis of these data is presented along with explicit considerations of the p-chlorine perturbation on the aromatic ring. Finally, the relationships between the orbital symmetries and the sign and magnitude of the zero-field electron spin dipolar interactions in the triplet state are discussed and on these bases an assignment of the orbital symmetry of the lowest excited triplet state of p-dichlorobenzene is made.

Also, similar data, along with excitation dependent measurements of the relative populating rates into the individual triplet spin sublevels, have been obtained for the phosphorescent triplet state of various p-dichlorobenzene/host systems (p-dichlorobenzene/p-xylene, p-dichlorobenzene/p-dichlorobenzene-d_4, p-dichlorobenzene/p-dibromobenzene). A qualitative discussion of these data is presented in terms of an assessment of possible crystal field contributions to the properties of the p-dichlorobenzene phosphorescent triplet state.

0 0 0 0 3 9 0 3 4 4 0

I. INTRODUCTION

Toward the end of the last century, as spectroscopic techniques were being developed, investigators began exploring the nature of electronic transitions and of excited electronic states of atoms and molecules. Since then an enormous amount of information concerning these states and transitions has been published. At present, the theories which have survived the first half of the twentieth century can adequately describe many aspects of the excited electronic states and of electronic transitions of atomic, diatomic, and small polyatomic systems. The extension of these theories to larger molecular systems, however, even now yields inadequate results.

Of the larger molecular systems, perhaps the most extensively studied have been the aromatic hydrocarbons, principally benzene and its derivatives. The significant amount of attention which has been directed towards these molecules reflects the central position which they occupy among a large and important class of organic compounds. A comprehensive description of the nature and dynamics of the excited electronic states of these molecules is essential to any complete understanding of their chemistry. In the last few decades, investigators have made significant advances towards understanding the nature of the excited electronic states and of electronic transitions of these molecules, and yet many questions concerning them which were unanswered at the beginning of this century remain inconclusively answered today.

Historically, the task of obtaining the experimental data needed to delineate the properties of excited electronic states of aromatic hydrocarbons (as well as most other molecular and atomic systems) has fallen to the optical spectroscopist. Most of our present knowledge of the excited electronic states of benzene and its derivatives is the result of careful study of the gross and fine structure of optical absorption and emission spectra. Within the last thirty years, however, experimentalists have found increasing success in discerning the properties of excited multiplet electronic states through the use of magnetic as well as optical experimental "probes". In particular, great success has recently been achieved in the investigation of the properties of excited triplet states of aromatic molecules through the combination of optical spectroscopy with magnetic resonance techniques.

The following dissertation presents the results of an investigation into the nature and dynamics of the lowest excited triplet state of p-dichlorobenzene in low temperature crystalline solids, using the techniques of optical spectroscopy and optically detected electron spin resonance in zero field.

A. Historical Background -- Phosphorescence and the Triplet State

Late in the 19th century investigators made the observation that a number of organic compounds (quinine, aesculin and others) when placed in a solid solution exhibited a strong afterglow or phosphorescence following excitation by a mercury lamp. Some attribute this observation to Wiedemann in 1888,[1] while others believe that Dewar should receive primary credit as early as 1880.[2-4] This phosphorescence was found to

be of consistently longer wavelength than any accompanying fluorescence and to possess a lifetime which may vary from 10^{-4} to 10^{2} seconds. The 1930's produced explanations which accounted for these phosphorescent emissions in terms of three separate molecular states. During the early 1940's, Lewis, Lipkin and Magel,[5] and Terenin,[6,7] postulated that the phosphorescent transition was $T \rightarrow S$ in nature. Then, in 1944, Lewis and Kasha[8,9] completed an extensive study of phosphorescent emissions from organic molecules. The result of this study led them to label the emitting state as the lowest molecular triplet state. Lewis and Kasha observed that the phosphorescence intensity decays exponentially with time

$$I(t) = I(o)\, e^{-t/\tau} \quad .$$

The lifetime, τ, of the phosphorescence of aromatic hydrocarbons was found to be of the order of 10 seconds. Since τ is inversely proportional to the transition probability, this value for τ gave a transition probability about 10^{10} smaller than that of normally observed optical transitions (fluorescence). They therefore reasoned that since only spin-forbidden transitions can have such a low transition probability, the state from which the phosphorescence originated must be a molecular triplet state.

The triplet state has two electrons with parallel spins and should therefore exhibit paramagnetic behavior. Such a molecular state should also be metastable due to the spin-forbidden nature of the $T \rightarrow S_o$

transition. The search for evidence to support Lewis and Kasha's postulated phosphorescent triplet state therefore concentrated on the magnetic properties of phosphorescent compounds.

Lewis and Calvin[10] and later Lewis, Calvin and Kasha[11] examined an irradiated solution of fluorescein in boric acid glass and detected a reversible light-induced paramagnetic susceptibility. Later experiments of Evans[12] on fluorescein and triphenylene showed that the decay of phosphorescence intensity was exactly matched by the decay of paramagnetic susceptibility, thus directly linking the two phenomena. Finally, all ambiguity was removed by Hutchison and Mangum[13,14] in 1958 when they conducted magnetic resonance experiments which measured the electron spin of the phosphorescent state of naphthalene and found that it was indeed a triplet state. The results of Hutchison and Mangum's experiment revealed more than just the triplet nature of the molecular phosphorescent state. From their results, Hutchison and Mangum were able to evaluate the surprisingly high magnitude of the spin-spin dipolar interaction[15,16] within the triplet state and thereby found the cause of failure of the many previous attempts to observe the electron spin resonance (ESR) of organic triplet states. They placed a single crystal of durene containing 2 to 5 mole percent naphthalene in a high magnetic field at low temperature and carefully performed an orientation dependence study of the ESR signal. Their data subsequently demonstrated that the spin-spin dipolar interaction within the triplet state causes the three magnetic sublevels to be separated in zero field by an amount which is of the same order as that produced by the conventional ESR

magnetic fields (~6000 gauss). The electron spin-spin interaction therefore creates a local field inhomogeneity which is sufficient to have washed out any ESR signal which previous investigators had hoped to observe from randomly oriented and/or polycrystalline samples with conventional fields. It became evident with the discovery of the zero-field splittings of the triplet state magnetic sublevels that conventional ESR techniques would have only limited value to future study of organic triplet states. The need for properly prepared single crystal samples severely restricted the number of molecules which might be examined. The study of organic triplet states by conventional ESR was further limited by the inherent sensitivity of the technique. The observation of resonance by conventional ESR requires that a significant percentage of sample molecules be in the triplet state; therefore only molecules with relatively long phosphorescence lifetimes may be studied. Recently, however, a technique has been developed which overcomes many of the handicaps of conventional ESR methods.

In 1965, Geschwind, Devlin, Cohen and Chinn[17] applied the optical rf double resonance techniques of Brossel and Kastler[18] to a solid sample of Cr^{+3} in Al_2O_3 and succeeded in observing the metastable $\bar{E}^{(2E)}$ state of Cr^{+3}. In this classic experiment Geschwind, *et al.* used a high resolution optical spectrometer to monitor the change in intensity of one of the Zeeman components of the fluorescence $[\bar{E}^{(2E)} \rightarrow A_2]$ while saturating $\bar{E}$ with microwaves and sweeping the external magnetic field through resonance. The important feature of the experiment is the use of optical methods to detect the microwave resonance. Since

optical rather than microwave photons are being detected this technique offers a significant advantage in sensitivity over conventional magnetic resonance techniques.

The success of Geschwind, *et al.* in using optical detection methods to observe the electron spin resonance of a metastable state in a solid medium soon led others to the hope that similar methods might be employed to the detection of the ESR of organic molecules in their phosphorescent triplet state.

Sharnoff and Kwiram independently became the first to observe by optical techniques the ESR of an organic phosphorescent state. In 1967, Sharnoff reported the $\Delta M = 2$ transition of the lowest triplet state of naphthalene,[19] and Kwiram reported the $\Delta M = 1$ and $\Delta M = 2$ transitions of the phenanthrene phosphorescent triplet state.[20] Since their initial experiments, along with the improvement of optically detected magnetic resonance techniques (ODMR), the available data on organic phosphorescent triplet states has increased rapidly.

Important advances were made by Schmidt and van der Waals,[21] with the optical detection of ESR transitions of the lowest triplet states of many molecules in zero external magnetic field, and by Tinti, El-Sayed, Maki and Harris[22] with the incorporation of a high resolution optical spectrometer to isolate and examine the effect of the microwave transitions on individual vibronic bands in the phosphorescence spectrum. The latter authors also reported the first optically detected electron nuclear resonance (ENDOR) for nitrogen in 2,3-dichloroquinoxaline.[23]

Since these initial experiments, an impressive amount of data has been obtained concerning the lowest excited triplet state of many molecules. These data include not only the measured values for the zero-field splitting parameters of the excited triplet state,[28] but also measurements of other static quantities such as the electron-nuclear hyperfine interaction (^{14}N, ^{35}Cl, ^{37}Cl, ^{1}H, ^{79}Br, ^{81}Br)[37] and the nuclear quadrupole interaction (^{14}N, ^{35}Cl, ^{37}Cl, ^{79}Br, ^{81}Br),[38] all of which, until recently, had only been obtainable for electronic ground states.

ODMR techniques have also enabled experimentalists to accurately determine many dynamic quantities of individual magnetic sublevels of excited triplet states such as intersystem crossing rates,[45] radiative and total decay rates,[46] spin-lattice relaxation rates,[47] and, most recently, spin-spin relaxation rates.[48-50]

Equipped with these kinds of data, investigators are now easily able to determine the basic electronic structure of an excited triplet state and, in some cases, to arrive at more precise conclusions such as the spatial symmetry of the state.[43] These sort of data are also precisely what is needed to help delineate many of the intra- and intermolecular energy transfer processes in crystalline molecular solids and determine the pathways by which the excited state might acquire particular properties.

B. Benzene and p-Dichlorobenzene

The characterization of excited electronic states, and particularly, the classification of the orbital symmetries of excited electronic states of aromatic and substituted aromatic molecules is a problem which has received a considerable amount of attention from theoreticians and experimentalists alike. Benzene and its derivatives have certainly received the largest portion of this attention. The available literature concerning the electronic structure of benzene and its simple derivatives comprises the largest portion of the total literature dealing with the electronic structure of aromatic molecules.

The strong UV absorption band seen at about 2600 Å in benzene vapor and corresponding to the benzene S_1 system has been known and investigated since the early days of optical spectroscopy.[62] Historically, this absorption band was the first clear example of an electronic transition which was forbidden by dipolar symmetry selection rules and whose explanation required the application of vibronic selection rules.[63] The sharpness of the fine structure of this absorption stimulated additional investigations and provided a suitable system with which experimentalists might test theories of electronic transitions and vibronic coupling in large molecules.

The identification of the S_1 state associated with the 2600 Å absorption band in benzene proved, however, to be a relatively difficult problem. The conclusion that the orbital symmetry of the benzene S_1 state actually belongs to a $^1B_{2u}$ irreducible representation required

not only a detailed analysis of the vibrational structure of the absorption band, but also an analysis of its polarization and of the associated rotational structure[64] along with a refined theoretical calculation.[65-67] Benzene fluorescence studies finally confirmed this assignment.[66,68,69]

Although the characterization of the S_1 state of benzene was a relatively difficult problem, the problem of characterizing the first excited triplet state of benzene proved to be still more elusive. Sklar reported the weak absorption band observed in benzene at about 3400 Å as early as 1937[70] and the absorption spectrum of liquid benzene in the same region was reported by Lewis and Kasha in 1945.[71] Early efforts to characterize the T_1 state which gave rise to this absorption band relied on vibrational analysis of the phosphorescence emission from this state.[72-74] The authors of these efforts concluded that the transition was essentially dipole forbidden and that the weak phosphorescence activity originated from a vibronic coupling of the e_{2g} vibrations. This vibronic coupling of the e_{2g} modes has been cited as evidence for either a $^3B_{1u}$ or $^3B_{2u}$ assignment for the T_1 state,[72,75,76] since vibrations of this symmetry can induce mixing with dipole-allowed $^1E_{1u}$ character. The presence of a significant activity of a b_{2g} vibration has been presented as evidence to further limit the assignment to a $^3B_{1u}$,[72] since the b_{2g} vibration can induce mixing of dipole-allowed $^1A_{2u}$ character but only with a state having B_{1u} symmetry. Further vibrational analysis showed that the e_{2g} activity in the benzene phosphorescence was distinctly different than that found in the fluorescence spectrum,[71] suggesting that the phosphorescent transition was unlike the fluorescent

$^1B_{2u} \rightarrow {}^1A_{1g}$ transition and inferring that the T_1 state must then have B_{1u} symmetry. The conclusion that the benzene T_1 state has B_{1u} orbital symmetry could not, however, be formed on the basis of these arguments alone. The spin-forbidden nature of the transition makes such a characterization entirely ambiguous.

Later, the symmetry of the T_1 state of benzene was implied from studies of other molecules. Kearns showed that the behavior of the lowest triplet state in the catacondensed aromatic hydrocarbons extrapolates to a benzene assignment of $^3B_{1u}$.[77] On the other hand, polarization studies of the phosphorescence of crystalline hexachlorobenzene led to a proposed $^3B_{2u}$ assignment when taken into the benzene D_{6h} point group.[78]

In a classic study, Albrecht has set down the possible routes by which dipole-allowed character might find its way into the benzene $T_1 \rightarrow S_0$ transition.[79-81] His findings, along with considerations of the oscillator strengths and polarization of the phosphorescence, allowed him to propose the $^3B_{1u}$ assignment. Theorists have generally agreed that a $^3B_{1u}$ state would be lowest in energy and this assignment has since gained wide acceptance.[92]

The complete characterization of the lowest triplet state of the benzene-substituted benzene series, however, continues to retain certain ambiguities. From an early single crystal polarized $T_1 \leftarrow S_0$ absorption study, Castro and Hochstrasser[93a] have proposed a $^3B_{2u}$ assignment for the lowest triplet state of the p-dihalobenzenes, conflicting with the $^3B_{1u}$ assignment which would be deduced from the accepted benzene assignment, although recent Zeeman studies conducted by Hochstrasser and coworkers[93b] support the latter assignment.

As Albrecht has pointed out, the spin-forbidden nature of phosphorescence renders the interpretation of phosphorescence spectra ambiguous. The $T_1 \rightarrow S_0$ transition derives its transition probability from the admixing of singlet states into the triplet wavefunctions, primarily through spin-orbit coupling. It is not, then, generally possible to unambiguously assign the triplet orbital symmetry without a complete knowledge of the spin-orbit symmetries of all three triplet spin sublevels. In many cases, such as benzene itself, one must go beyond spin-orbit interactions and invoke vibronic and spin-vibronic considerations to characterize the triplet state and the phosphorescent transition.

The mechanisms whereby the singlet-triplet transitions become allowed in the optical spectrum are not well understood and this is precisely why studies of low-lying triplet states in aromatic molecules are of fundamental interest. The present work is concerned with the characterization of the lowest triplet state of the p-dihalobenzenes, employing the techniques of optically detected magnetic resonance in zero external field. Specifically, the objective of this work is the resolution of the spin-orbital-vibrational-electronic coupling mechanisms in the p-dihalobenzenes, including the unambiguous assignment of the orbital symmetry of the lowest excited triplet state, the determination of the nuclear framework in the excited triplet state, and the study of intermolecular interactions in the solid phase. The ability of ODMR techniques to selectively examine both the static and dynamic properties of individual triplet magnetic sublevels readily lends itself to this problem.

II. THE TRIPLET STATE

As a suitable point of entry into this investigation of the properties of the lowest excited triplet state of p-dichlorobenzene, a brief consideration of some fundamental aspects of the nature of the electronic triplet state lends itself most adequately.[94]

A. The Antisymmetry Principle

The electronic state of interest throughout this manuscript is that state which results from the excitation of a single electron out of a high-lying (in energy) occupied molecular orbital of a closed shell ground state electronic configuration into a low-lying unoccupied molecular orbital, thus forming an open shell excited electronic state with two singly occupied molecular orbitals. The potential "triplet" character of such a state owes its origin to restrictions imposed upon systems of electrons by the Pauli principle, which is a consequence of the antisymmetrization of electron wavefunctions. The following consideration of the consequences of the antisymmetry principle on many electron systems will clearly illustrate some basic aspects of the triplet state.

Consider two identical particles within a many-body system, each labeled with total position vectors, $\bar{\tau}_1 = (\nu_1,\sigma_1)$ and $\bar{\tau}_2 = (\nu_2,\sigma_2)$ (relative to an arbitrary origin), where ν_i represents a general spatial

coordinate and σ_i represents a spin coordinate (which is dependent upon the intrinsic spin of the particles). Then, if ψ is the wavefunction describing this two-particle system, the probability of finding particle (1) at point $\bar{\tau}_1$ and particle (2) at point $\bar{\tau}_2$ is given by

$$|\psi[\bar{\tau}_1(1),\bar{\tau}_2(2)]|^2 \, d\tau_1\tau_2 \quad . \qquad \text{(II-1)}$$

The two particles must be physically indistinguishable, since they are identical. Therefore, the probability of finding particle (2) at position $\bar{\tau}_1$ and particle (1) at position $\bar{\tau}_2$ is identical to that of finding particle (1) at $\bar{\tau}_1$ and particle (2) at $\bar{\tau}_2$, or,

$$|\psi[\bar{\tau}_1(1),\bar{\tau}_2(2)]|^2 \, d\tau_1\tau_2 \quad = \quad |\psi[\bar{\tau}_1(2),\bar{\tau}_2(1)]|^2 \, d\tau_1\tau_2 \quad . \qquad \text{(II-2)}$$

This expression embodies a fundamental symmetry law of quantum mechanics. That is, the outcome of any measurement of a physically measurable property, which depends on the coordinates of identical particles, must be independent of any attempt to label the particles of the system, i.e., the measureable property (or its operator) must be a symmetric function of the coordinates. In the absence of applied magnetic fields, the wavefunction ψ may always be chosen as real. Then,

$$\psi^2[\bar{\tau}_1(1),\bar{\tau}_2(2)] \quad = \quad \psi^2[\bar{\tau}_1(2),\bar{\tau}_2(1)] \quad , \qquad \text{(II-3)}$$

which has solutions:

$$\psi[\bar{\tau}_1(1),\bar{\tau}_2(2)] = \psi[\bar{\tau}_1(2),\bar{\tau}_2(1)] \qquad \text{(II-4)}$$

and

$$\psi[\bar{\tau}_1(1),\bar{\tau}_2(2)] = -\psi[\bar{\tau}_1(2),\bar{\tau}_2(1)] \quad . \qquad \text{(II-5)}$$

In the former case, ψ is designated to be symmetric with respect to the exchange of the coordinates of any two identical particles, while, in the latter case, ψ is designated to be antisymmetric with respect to such exchange. Particles which have integral spin angular momentum, or spin (in units of $\hbar$), are called bosons, obey Bose-Einstein statistics, and are described by symmetric wavefunctions, while particles which possess half-integral spin are called fermions, obey Fermi-Dirac statistics, and must be described by antisymmetric wavefunctions. Electrons are fermions with a spin of $1/2\ \hbar$ and, therefore, systems of electrons must be described with wavefunctions which are antisymmetric with respect to the interchange of coordinates (spatial and spin) of any pair of electrons. This requirement of electronic systems is known as the Pauli principle or the antisymmetry principle.

B. The State Function

The preceding section has shown that a wavefunction describing any state of a system of many electrons (state function) must be antisymmetric with respect to the exchange of any pair of electrons. The

following section will show that a "triplet" state arises as a consequence of the restrictions imposed by the antisymmetry principle on the state function describing the electronic state of interest to the present study (i.e., a single electron excitation out of a closed shell configuration).

The construction of proper state functions for a system of many electrons is, at best, a process of successive approximations. One of the simplest methods for constructing such functions, the LCAO (linear combination of atomic orbitals) molecular orbital method, has been used with very limited success. In this method, electrons are assigned to molecular orbitals, Φ_i, which are formed from a linear combination of atomic orbitals, ϕ_k; then

$$\Phi_i = C_A\phi_A + C_B\phi_B + C_C\phi_C + \cdots = \sum_k C_{i_k}\phi_k \quad . \qquad \text{(II-6)}$$

At most, two electrons are allowed to occupy the same MO, one with spin projection α, and the other with β. The total state function is then taken as a simple product of the Φ_i of all the electrons considered.

$$\Psi = \prod_i \Phi_i^{\alpha} \Phi_i^{\beta} \qquad \text{(II-7)}$$

The LCAO-MO approach to proper construction of electronic state functions suffers from several obvious faults. A detailed treatment of solutions to all of the faults of the LCAO-MO approach is both beyond the scope and outside the interest of this discussion. One failing

which is of interest here, however, is the failure of the LCAO-MO method to satisfy adequately the restrictions imposed by the antisymmetry principle. The solution to this problem begins with the explicit inclusion of spin functions into the basis functions from which the state function will be constructed. Molecular spin-orbitals (MSO) are, therefore, constructed such that

$$\psi_j^{\mu} = \psi_j(\nu^{\mu},\sigma^{\mu}) = \Phi_{i(j)}(\nu^{\mu})\ \eta_j(\sigma^{\mu}) \qquad \text{(II-8)}$$

where η_j^{μ} is a normalized function of the possible electron spin projections, i.e.,

$$\eta_j^{\mu} = C_{j\alpha}\ \alpha^{\mu} + C_{j\beta}\ \beta^{\mu} \quad ; \quad C_{j\alpha}^{*}\ C_{j\alpha} + C_{j\beta}^{*}\ C_{j\beta} = 1 \qquad \text{(II-9)}$$

with the superscript, μ, indexing the electrons, and the subscripts, j and i, indexing the MSO's and MO's, respectively. The total state function will automatically be antisymmetrized if it is taken as a Slater determinant of MSO's; thus,

$$\Psi = (N!)^{-\frac{1}{2}} \begin{vmatrix} \psi_1^1 & \psi_2^1 & \psi_3^1 & \cdots & \psi_N^1 \\ \psi_1^2 & \psi_2^2 & \cdots & \cdots & \psi_N^2 \\ \cdots & \cdots & \cdots & \cdots & \cdots \\ \psi_1^N & \psi_2^N & \cdots & \cdots & \psi_N^N \end{vmatrix} \qquad \text{(II-10)}$$

A state function formed in this manner is then inherently antisymmetric, since the determinant is antisymmetric under an exchange of any two of its rows, an operation equivalent to exchanging the coordinates of a pair of electrons. The more specific Pauli exclusion principle, which states that no atom or molecule may possess two electrons which have identical sets of quantum numbers, is also embodied in the determinant representation, since any determinant with two identical columns (two electrons with identical sets of quantum numbers) will vanish. State functions constructed in this manner have proven quite useful for describing molecular electronic systems.

At this point we should consider the state function explicitly describing the excited electronic configuration with which we are interested in this discussion. As has already been mentioned, we are primarily concerned with an excited molecular electronic configuration possessing only two singly occupied molecular orbitals, all other MO's being either filled or empty. Previous investigators have shown that many properties of such an electronic state may be adequately studied using approximate state functions which include only the two unpaired electrons.[95] All other electrons may then be treated as "core" electrons and a suitable adjustment of the core potential within the Hamiltonian operator for the two unpaired electrons may be performed in such a manner as to minimize errors produced by this "two electron" approximation. This procedure will be adequate for the purposes of this discussion.

Consider, then, two molecular orbitals, Φ_1, and Φ_2, and two possible spin functions, denoted α and β. We have four possible molecular spin orbitals,

$$\begin{aligned} \psi_1(\mu) &= \Phi_1(\mu)\,\alpha(\mu) \\ \psi_2(\mu) &= \Phi_1(\mu)\,\beta(\mu) \\ \psi_3(\mu) &= \Phi_2(\mu)\,\alpha(\mu) \\ \psi_4(\mu) &= \Phi_2(\mu)\,\beta(\mu) \end{aligned} \qquad \text{(II-11)}$$

where μ labels electrons. By taking these MSO's two at a time (since we are considering only two electrons), six possible state functions arise. Two of these functions place both electrons in a single MO and are therefore neglected. The remaining possible state functions have the following determinant forms:

$$\begin{aligned} \Psi_1 &= \frac{1}{\sqrt{2}} \begin{vmatrix} \Phi_1(1)\,\alpha(1) & \Phi_2(1)\,\alpha(1) \\ \Phi_1(2)\,\alpha(2) & \Phi_2(2)\,\alpha(2) \end{vmatrix} \\ \Psi_2 &= \frac{1}{\sqrt{2}} \begin{vmatrix} \Phi_1(1)\,\beta(1) & \Phi_2(1)\,\beta(1) \\ \Phi_1(2)\,\beta(2) & \Phi_2(2)\,\beta(2) \end{vmatrix} \\ \Psi_3 &= \frac{1}{\sqrt{2}} \begin{vmatrix} \Phi_1(1)\,\alpha(1) & \Phi_2(1)\,\beta(1) \\ \Phi_1(2)\,\alpha(2) & \Phi_2(2)\,\beta(2) \end{vmatrix} \end{aligned} \qquad \text{(II-12)}$$

$$\Psi_4 = \frac{1}{\sqrt{2}} \begin{vmatrix} \Phi_1(1)\ \beta(1) & \Phi_2(1)\ \alpha(1) \\ \Phi_1(2)\ \beta(2) & \Phi_2(2)\ \alpha(2) \end{vmatrix}$$

It will be shown later (Section III-A) that suitable state functions must also be eigenfunctions of the spin operators, $\bar{S}^2$ and $\bar{S}_z$. An examination of the above four functions reveals that, while Ψ_1 and Ψ_2 satisfy this requirement, Ψ_3 and Ψ_4 do not. However, the linear combinations

$$\Psi_{3'} = \frac{1}{\sqrt{2}} [\Psi_3 + \Psi_4] \qquad \text{(II-13)}$$

and

$$\Psi_{4'} = \frac{1}{\sqrt{2}} [\Psi_3 - \Psi_4] \qquad \text{(II-14)}$$

will yield two appropriate eigenfunctions of both $\bar{S}^2$ and $\bar{S}_z$.

If we now separate our four state functions into spatial and spin parts (this is possible for functions involving only two electrons), the "triplet" portion nature of this excited state will become apparent. In this separated form, one state function, $\Psi_{4'}$, appears unique, possessing a symmetric orbital function and an antisymmetric spin function, while the other three state functions, Ψ_1, Ψ_2 and $\Psi_{3'}$, have a common antisymmetric orbital function and three symmetric spin functions. These latter three state functions are degenerate under operation by a Hamiltonian operator which neglects spin interactions. Thus we are left with two non-degenerate states of different spin multiplicites, a singlet state,

$$^{1}\Psi = \Psi_{4'} = \frac{1}{\sqrt{2}}\,[\Phi_1(1)\Phi_2(2) + \Phi_1(2)\Phi_2(1)]\left\{\frac{1}{\sqrt{2}}\,[\alpha(1)\beta(2) - \alpha(2)\beta(1)]\right\}, \tag{II-15}$$

and a triplet state ,

$$^{3}\Psi = \begin{Bmatrix} \Psi_1 \\ \Psi_2 \\ \Psi_{3'} \end{Bmatrix} = \frac{1}{\sqrt{2}}\,[\Phi_1(1)\Phi_2(2) - \Phi_1(2)\Phi_2(1)]\begin{Bmatrix} \alpha(1)\alpha(2) \\ \beta(1)\beta(2) \\ \frac{1}{\sqrt{2}}\,[\alpha(1)\beta(2) + \alpha(2)\beta(1)] \end{Bmatrix}. \tag{II-16}$$

III. MAGNETIC INTERACTIONS AND PHOSPHORESCENCE

A. Zero-Field Splitting

While the three state functions which describe the triplet state are degenerate under zeroth-order Hamiltonian operation which includes only kinetic and electrostatic operators, they are non-degenerate under a Hamiltonian which includes magnetic interactions. In the absence of any externally applied magnetic field, the principal magnetic interaction present within the triplet state is a magnetic dipole-dipole interaction between the two unpaired electron spins. Such an interaction may be described by a Hamiltonian of the following form:[15,16,96]

$$\mathcal{H}_D = g^2 \beta^2 \frac{\bar{S}_1 \cdot \bar{S}_2}{r^3} - \frac{3(\bar{S}_1 \cdot \bar{r})(\bar{S}_2 \cdot \bar{r})}{r^5} , \qquad \text{(III-1)}$$

where g denotes the dimensionless Landé "g" factor, β denotes the electronic Bohr magneton and the vector $\bar{r}$ joins the two electrons, each with spin $\bar{S}_1$ and $\bar{S}_2$. Van Vleck has shown that this Hamiltonian may be rewritten as $\mathcal{H}_D = \bar{S} \cdot \bar{D} \cdot \bar{S}$; where $\bar{S} = \bar{S}_1 + \bar{S}_2$ and $\bar{D}$ is a symmetric tensor called the zero-field splitting tensor.[97] The components of $\bar{D}$ are given by averages over the electronic wave function:

$$D_{\mu\mu} = \tfrac{1}{2} g^2 \beta^2 \left\langle \frac{r_{12}^2 - 3\mu_{12}^2}{r_{12}^5} \right\rangle ; \quad D_{\mu\nu} = \tfrac{1}{2} g^2 \beta^2 \left\langle \frac{-3\mu_{12}\nu_{12}}{r_{12}^5} \right\rangle \qquad \text{(III-2)}$$

where $\mu;\nu = x,y,z$.

Since $\bar{D}$ is a symmetric tensor, a principal axis system may be chosen which diagonalizes $\bar{D}$, in which case $\mathcal{H}_D$ becomes

$$\mathcal{H}_D = -X\bar{S}_x^2 - Y\bar{S}_y^2 - Z\bar{S}_z^2 \qquad \text{(III-3)}$$

where

$$X = -D_{xx}; \quad Y = -D_{yy}; \quad Z = -D_{zz} \quad . \qquad \text{(III-4)}$$

Moreover, $\bar{D}$ is a traceless tensor and $\mathcal{H}_D$ may be rewritten in terms of only two independent parameters. Then,

$$\mathcal{H}_D = D(\bar{S}_z^2 - \tfrac{1}{3}\bar{S}\ ) + E(\bar{S}_x^2 - \bar{S}_y^2) \qquad \text{(III-5)}$$

where

$$D = \tfrac{1}{2}(X + Y) - Z;$$

and (III-6)

$$E = -\tfrac{1}{2}(X - Y)$$

with the axis convention $|X| \leq |Y| \leq |Z|$.

Or,

$$D = \tfrac{3}{4}\, g^2\, \beta^2 \left\langle \frac{r_{12}^2 - 3z_{12}^2}{r_{12}^5} \right\rangle \qquad \text{(III-7)}$$

and

$$E = \tfrac{1}{4}\, g^2\, \beta^2 \left\langle \frac{3y_{12}^2 - 3x_{12}^2}{r_{12}^5} \right\rangle \quad . \qquad \text{(III-8)}$$

The spin functions associated with the triplet state magnetic sub-levels as shown on p. 20 are eigenfunctions of $\bar{S}^2$ and $\bar{S}_z$ only, and if

$$
\begin{aligned}
|T_{+1}\rangle &= |\alpha_1\alpha_2\rangle \\
|T_0\rangle &= \frac{1}{\sqrt{2}}\,|\alpha_1\beta_2 + \beta_1\alpha_2\rangle \qquad \text{(III-9)} \\
|T_{-1}\rangle &= |\beta_1\beta_2\rangle \;,
\end{aligned}
$$

then the Hamiltonian matrix has the following form using these functions as basis states:

$$
\mathcal{H}_D = \begin{array}{c} \begin{array}{ccc} |T_{+1}\rangle & |T_0\rangle & |T_{-1}\rangle \end{array} \\ \begin{vmatrix} \frac{1}{3}D & 0 & E \\ 0 & -\frac{2}{3}D & 0 \\ E & 0 & \frac{1}{3}D \end{vmatrix} \end{array} \;. \qquad \text{(III-10)}
$$

If basis states are chosen which diagonalize the Hamiltonian matrix as:

$$
\mathcal{H}_D = \begin{array}{c} \begin{array}{ccc} |T_x\rangle & |T_y\rangle & |T_z\rangle \end{array} \\ \begin{vmatrix} +X & 0 & 0 \\ 0 & +Y & 0 \\ 0 & 0 & +Z \end{vmatrix} \end{array} \;, \qquad \text{(III-11)}
$$

then the basis states are

$$|T_x\rangle = \frac{1}{\sqrt{2}} |T_{-1} - T_{+1}\rangle = \frac{1}{\sqrt{2}} |\beta_1\beta_2 - \alpha_1\alpha_2\rangle$$

$$|T_y\rangle = \frac{i}{\sqrt{2}} |T_{-1} + T_{+1}\rangle = \frac{i}{\sqrt{2}} |\beta_1\beta_2 + \alpha_1\alpha_2\rangle \qquad \text{(III-12)}$$

$$|T_z\rangle = |T_0\rangle = \frac{1}{\sqrt{2}} |\alpha_1\beta_2 + \beta_1\alpha_2\rangle$$

These basis states are eigenfunctions of the Hamiltonian and $\bar{S}_x$, $\bar{S}_y$ and $\bar{S}_z$. Throughout the remainder of this discussion we will be concerned primarily with triplet spin sublevels which are described by these spin functions.

B. Spin-Orbit Coupling

The phosphorescence transition is spin-forbidden by nature and derives its transition probability primarily through the action of spin-orbit coupling. While an exact treatment of the spin-orbit coupling Hamiltonian is unnecessary for the purpose of this discussion, a brief description of the nature of forbidden transitions and the mechanism by which the spin-orbit coupling Hamiltonian can bring allowed character into such transitions would be in order.

Spectroscopists use the term "forbidden transition" to describe any transition with a probability that is much smaller than normal. The term "forbidden", then, only has meaning in a relative sense, i.e., relative to a fully allowed, "normal" transition.

An allowed transition has a transition probability greater than zero in zeroth-order approximation. That is, if

$$\mathcal{H}_0 = \sum_{j=1}^{N} \frac{\bar{p}_j^2}{2m} + V(\bar{r}_1, \bar{r}_2, \cdots, \bar{r}_N; R) \quad , \qquad \text{(III-13)}$$

(where R denotes nuclear coordinates and $\bar{r}_j$ labels the position coordinate of the jth electron), is the zeroth-order Hamiltonian describing a molecule with N electrons, then

$$|\langle\psi_n|G(\sum^{N} \bar{r}_j)\ |\psi_m\rangle|^2 \neq 0 \qquad \text{(III-14)}$$

for an allowed transition between eigenstates, ψ_n and ψ_m, of $\mathcal{H}_0$, where $G(\sum^{N} \bar{r}_j)$ represents the electric dipole operator. This definition may be formulated more explicitly as follows. The eigenfunctions ψ_n of $\mathcal{H}_0$ are functions of the spin variables $(S_1, S_2, \cdots, S_N)$ as well as of $\bar{r}_j$ and R. They may then be taken as eigenfunctions of the operators $\bar{S}^2$ and $\bar{S}_z$ as well as $\mathcal{H}_0$; where

$$\bar{S}^2 = (\sum_j^N \bar{S}_{jx})^2 + (\sum_j^N \bar{S}_{jy})^2 + (\sum_j^N \bar{S}_{jz})^2 \qquad \text{(III-15)}$$

$$\bar{S}_z = \sum_j^N \bar{S}_{jz} \quad . \qquad \text{(III-16)}$$

Then if

$$\bar{S}^2 \psi_n = s(s+1)\hbar \psi_n \qquad \text{(III-17)}$$

and

$$\bar{S}_z \psi_n = m_s \hbar \psi_n \quad , \qquad \text{(III-18)}$$

we may add spin quantum numbers and relabel ψ_n such that $\psi_n \equiv {}^{(2s+1)}\psi_{n;m_s}$. Since the necessary orthonormality condition requires that

$$\langle {}^k\psi_{n',i} | {}^\ell\psi_{m',j} \rangle = \delta_{k,\ell}\, \delta_{i,j}\, \delta_{n',m'} \qquad \text{(III-19)}$$

and since $G(\sum^N \bar{r}_j)$ does not operate on spin variables, then

$$\langle {}^k\phi_{n',i} | G(\sum^N \bar{r}_j) | {}^\ell\psi_{m',j} \rangle = \delta_{k,\ell}\, \delta_{i,j} \langle \psi_{n'} | G(\sum^N \bar{r}_j) | \psi_{m'} \rangle \quad . \qquad \text{(III-20)}$$

The definitions for "spin forbidden" and "spin allowed" transitions are now contained in the above equation, i.e., a transition is spin forbidden if $k \neq \ell$ or $i \neq j$ and spin allowed only if $k = \ell$ and $i = j$. Additionally, a transition is called dipolar or symmetry forbidden if

$$\langle {}^k\psi_{n',i} | G(\sum^N \bar{r}_j) | {}^k\psi_{m',i} \rangle = 0 \qquad \text{(III-21)}$$

and dipolar or symmetry allowed otherwise. The phosphorescence transition, i.e.,

$$I_{phos} = \sum_{m_s} A_{m_s} \left|\langle {}^1\psi_o \, G(\sum^N \bar{r}_j) | {}^3\psi_{1,m_s}\rangle\right|^2 , \qquad \text{(III-22)}$$

presents a clear example of a spin forbidden transition (which may or may not be dipolar forbidden). Responsibility for the finite probability of the phosphorescence transition rests chiefly with the spin-orbit coupling interaction, whose primary action may be represented by the Hamiltonian,[96-99]

$$\mathcal{H}_{so} = \frac{g\,\beta\,e}{2mc} \sum_i \left[\sum_k \frac{Z_k}{r_{ki}^3} \bar{\ell}_{ik} + \sum_{j\neq i} \frac{1}{r_{ij}^3} (2\bar{P}_j - \bar{P}_i)\times\bar{r}_{ij} \right] \cdot \bar{S}_i , \qquad \text{(III-23)}$$

where k labels nuclei and i, j label electrons,

Z_k = charge on nucleus k

$\bar{\ell}_{ik}$ = angular momentum of electron i around nucleus k, i.e.,

$$\bar{\ell}_{ik} = \bar{r}_{ki} \times \bar{P}_i$$

and $\bar{r}_{ij} = \bar{r}_i - \bar{r}_j$.

$\mathcal{H}_{so}$ represents the interaction of the electron spins with internal magnetic fields produced by the relative motion of electrons and nuclei, the first sum within the brackets representing the contribution due to the motion of electron i in the coulomb field of nucleus k and the second sum representing the contribution due to the relative motion of electrons i and j. Further considerations of the explicit form of $\mathcal{H}_{so}$

are unnecessary, since the relevant properties of $\mathcal{H}_{so}$ may be illustrated by group theoretical arguments alone.[100]

Consider first the general form of the matrix element

$$\langle {}^{k}\psi_{n,i} | \mathcal{H}_{tot} | {}^{\ell}\psi_{m,j} \rangle \quad , \qquad \text{(III-24)}$$

where $\mathcal{H}_{tot} = \mathcal{H}_o + \mathcal{H}_D + \mathcal{H}_{so}$. ${}^{k}\psi_{n,i}$ and ${}^{\ell}\psi_{m,j}$ are eignefunctions of $\mathcal{H}_o$ and may be taken as properly antisymmetrized linear combinations of products of molecular orbital functions and spin functions (cf. Chapt II). Then let

$$| {}^{k}\psi_{n,i} \rangle \rightarrow | {}^{k}\Gamma_n \Gamma_i \rangle \qquad \text{(III-25)}$$

where Γ_n and Γ_i denote the irreducible representations of the total orbital function and the total spin function respectively within the appropriate molecular point group, while k denotes the spin multiplicity, $k = (2s+1)$, if $s = \sum^{N} S_j$.

Since all point group symmetry operations may be taken as a combination of pure rotations and inversions, then all molecular operators and functions may be related to a representation of the continuous rotation group. The action of the molecular operators is thus examined by examining the transformation properties of the appropriate irreducible representation of the continuous rotation group. Applying this procedure to the present problem, several general properties may be deduced for the Hamiltonian, $\mathcal{H} = \mathcal{H}_o + \mathcal{H}_D + \mathcal{H}_{so}$. First, $\mathcal{H}$ must be a Hermitian

operator, and must then be invariant under any rotation of coordinates. Thus, $\mathcal{H}_o$, $\mathcal{H}_D$, and $\mathcal{H}_{so}$ must each be invariant under any rotation. $\mathcal{H}_o$ contains only kinetic and electrostatic functions and thereby cannot yield a finite matrix element between states of different spin multiplicities. Van Vleck has shown that $\mathcal{H}_D$ can be written as five products of an orbital and a spin factor such that the orbital factors form a basis for the irreducible representation $D^{(2)}$ of the continuous rotation group.[96] Since $\mathcal{H}_D$ must be invariant under any rotation, then the spin factors of $\mathcal{H}_D$ must also transform as $D^{(2)}$, i.e., the orbital and spin factors must transform contragradiently. Singlet state spin functions belong to totally symmetric representations and thereby must transform as $D^{(0)}$ while triplet state spin functions transform as rotation and belong to $D^{(1)}$ of the continuous rotation group. Therefore, $\mathcal{H}_D$ can mix triplet states with states whose spin functions transform as $D^{(2)} \otimes D^{(1)} = D^{(1)} + D^{(2)} + D^{(3)}$ and, obviously, $\mathcal{H}_D$ cannot give finite matrix elements between singlet states ($D^{(0)}$) and triplet states ($D^{(1)}$). The remaining term, $\mathcal{H}_{so}$, is linear in spin operators and thereby has spin factors which transform as angular momentum (rotations), or $D^{(1)}$ of the continuous rotation group. $\mathcal{H}_{so}$ is thus responsible for the phosphorescence transition since the cross product $D^{(1)} \otimes D^{(1)} = D^{(0)} + D^{(1)} + D^{(2)}$ contains the singlet state spin representation $D^{(0)}$.

Since the complete $\mathcal{H}_{so}$ must be invariant under any rotation of coordinates it transforms as the totally symmetric representation within a given molecular point group. Realizing that single state spin functions also belong to the totally symmetric representation, we may write,

$$\therefore \langle {}^1\psi_{n,i} | \mathcal{H}_{so} | {}^3\psi_{m,j} \rangle \rightarrow \langle {}^1\Gamma_n \Gamma_i | \Gamma \mathcal{H}_{so} | {}^3\Gamma_m \Gamma_j \rangle \rightarrow$$

$$\langle {}^1\Gamma_n || {}^3\Gamma_m \Gamma_j \rangle , \qquad \text{(III-26)}$$

where $j = x, y, z$.

The spin-orbit matrix element will therefore only be non-zero when the cross product ${}^1\Gamma_n \otimes {}^3\Gamma_m \otimes \Gamma_j$ contains the totally symmetric representation, or, in other words, when ${}^3\Gamma_m \otimes \Gamma_j \in {}^1\Gamma_n$. This relationship has a direct bearing on the experimental results which will be discussed in a later section (Chapters VI and VII). Its importance, along with further consequences of the spin-orbit interaction, may be seen in the following perturbation treatment of the spin-orbit coupling Hamiltonian.

C. Spin-Orbit Perturbations

The inclusion of the following section within this manuscript will serve two purposes. Expressions presented herein will demonstrate both the nature of spin-orbit effects on the properties of the T_1 state and also the nature of difficulties which experimentalists encounter in their attempts to realize a quantitative assessment of any specific spin-orbit interaction.

If we treat the spin-orbit coupling interaction as a perturbation on the Hamiltonian $\mathcal{H} = \mathcal{H}_o + \mathcal{H}_D$ then the first excited triplet state wavefunctions, T_{1u}, become:[101]

$$T_{1u'} = T^{\circ}_{1u} + \sum_{\ell}^{S} \frac{\langle S_\ell | \mathcal{H}_{so} | T^{\circ}_{1u} \rangle}{E_{T^{\circ}_{1u}} - E_{S_\ell}} \cdot S_\ell + \sum_{i=-1}^{1} \sum_{m}^{T} \frac{\langle T_{m_i} | \mathcal{H}_{so} | T^{\circ}_{1u} \rangle}{E_{T^{\circ}_{1u}} - E_{T_{m_i}}} \cdot T_{m_i}$$

$$+ \sum_{j=-2}^{2} \sum_{n}^{Q} \frac{\langle Q_{n_j} | \mathcal{H}_{so} | T^{\circ}_{1u} \rangle}{E_{T^{\circ}_{1u}} - E_{Q_{n_j}}} \cdot Q_{n_j} \qquad \text{(III-27)}$$

where T°_{1u} are eigenfunctions of $\mathcal{H}$ with u = x, y, z or -1, 0, +1 and S_ℓ, T_{m_i} and Q_{n_j} denote singlet, triplet and quintet state wavefunctions, respectively. Using these triplet wavefunctions, we now proceed to examine the effects of the spin-orbit interaction on measurable quantities which are relevant to the present study.

First, we examine the phosphorescence transition probability, $|\langle S_o | e\bar{r} | T'_{1u} \rangle|^2$. Substitution of the above wavefunction for T'_{1u} yields:

$$|\langle S_o | e\bar{r} | T'_{1u} \rangle|^2 = |\langle S_o | e\bar{r} | T^{\circ}_{1u} \rangle|^2 + \sum_{\ell}^{S} A^2_{\ell,u} |\langle S_o | e\bar{r} | S_\ell \rangle|^2$$

$$+ \sum_{i=-1}^{1} \sum_{m}^{T} B^2_{m,i,u} |\langle S_o | e\bar{r} | T_{m,i} \rangle|^2$$

$$+ \sum_{j=-2}^{2} \sum_{n}^{Q} C^2_{n,j,u} |\langle S_o | e\bar{r} | Q_{n,j} \rangle|^2 , \qquad \text{(III-28)}$$

where

$$A^2_{\ell,u} = \left| \frac{\langle S_\ell | \mathcal{H}_{so} | T^{\circ}_{1u} \rangle}{E_{T^{\circ}_{1u}} - E_S} \right|^2 , \qquad \text{(III-29)}$$

and similarly for $B^2_{m,i,u}$ and $C^2_{n,j,u}$, while $e\bar{r}$ represents the electric dipole moment operator. Then, assuming that the large energy difference between S_o and all excited states is sufficient to preclude the admixture of any triplet or quintet character into S_o, the expression becomes

$$|\langle S_o|e\bar{r}|T'_{1u}\rangle|^2 = \sum_{\ell}^{S} A^2_{\ell,u}|\langle S_o|e\bar{r}|S_\ell\rangle|^2 . \quad \text{(III-30)}$$

Several important points are embodied in this expression. As we mentioned in the preceding section, the symmetry of S_ℓ is uniquely determined by the spin-orbit symmetry of T^o_{1u}. That is, $A^2_{\ell,u}$ will be non-zero only when ${}^3\Gamma_1 \otimes \Gamma_u \in {}^1\Gamma_\ell$. Thus, since the transformation properties of $e\bar{r}$ are obvious and those of S_o are usually known, we may determine the symmetry of S_ℓ and thereby of T^o_{1u} by the strength of the phosphorescence transition, i.e., $|\langle S_o|e\bar{r}|S_\ell\rangle|^2 \neq 0$ when ${}^1\Gamma_o \otimes \Gamma_{\bar{r}} \in {}^1\Gamma_\ell$.

In addition, equations (III-28, and III-29) demonstrate the dependence of phosphorescence transition probility on the T_1 state spin quantum label, u. It is precisely this dependence wherein lies both the capability and the necessity for the use of phosphorescence microwave double resonance (PMDR) techniques[22] in the study of the properties of phosphorescent triplet states. As we shall show later (Chapter V), these techniques in fact require such a dependence if they are to succeed at all. Conversely, the existence of these dependences allow PMDR techniques to differentiate between the individual triplet spin sublevels and thereby to overcome the primary limitation of normal optical spectroscopic techniques in the study of molecular T_1 states.

The extension of equation (III-30) into an expression for the radiative lifetime τ_{1u}^{rad} of the state T_{1u} requires only that we explicitly include the vibrational wavefunctions χ, and realize that due to the extremely rapid rate of vibrational relaxation in the excited state T_{1u} radiates from the zeroth vibrational state, $\chi_o^{T_{1u}}$.[102] Thus,

$$1/\tau_u^{rad} \propto \sum_{\nu} \sum_{\ell}^{S} A_{\ell,u}^2 |\langle S_o|e\bar{r}|S_\ell\rangle|^2 |\langle\chi_\nu^{S_o}|\chi_o^{T_{1u}}\rangle|^2 \qquad \text{(III-31)}$$

Of course, T_{1u} may decay non-radiatively as well and the total lifetime, τ_{1u}, of T_{1u} has the form,

$$1/\tau_{1u} = 1/\tau_{1u}^{rad} + 1/\tau_{1u}^{nr} \propto \sum_{\nu} \sum_{\ell}^{S} A_{\ell,u}^2 |\langle S_o|e\bar{r}|S_\ell\rangle|^2 |\langle\chi_\nu^{S_o}|\chi_o^{T_{1u}}\rangle|^2$$

$$+ \sum_{\nu'} \sum_{\ell}^{S} A_{\ell,u}^2 |\langle S_o|\mathcal{H}_{nr}|S_\ell\rangle|^2 |\langle\chi_{\nu'}^{S_o}|\chi_o^{T_{1u}}\rangle|^2 \qquad \text{(III-32)}$$

where we have taken $\mathcal{H}_{nr}$ to represent a perturbation which causes electronic states to become non-stationary and thereby induced non-radiative transitions.[103,104]

An expression for the intersystem crossing rate, $k_{T_{1u}}^{I}$, into T_{1u} has a form similar to the non-radiative term in equation (III-32), i.e.,

$$k_{T_{1u}}^{I} \propto \sum_{\nu'\cong 0} \sum_{\nu} \sum_{\ell}^{S} A_{\ell,u}^2 |\langle S_\ell|\mathcal{H}'_{nr}|S_1\rangle|^2 |\langle\chi_\nu^{T_{1u}}|\chi_{\nu'\cong 0}^{S_1}\rangle|^2 \qquad \text{(III-34)}$$

Again, it is thought that the extremely rapid rate of vibrational relaxation within the excited singlet state manifold forces intersystem crossing to occur

primarily from low-lying vibrational states of the first excited singlet state, S_1.[102]

Finally, equation (III-28) indicates the obvious form of the expression for the energy of T'_{1u}:

$$E_{T'_{1u}} = E_{T^{\circ}_{1u}} - \sum_{\ell}^{S} A^2_{\ell,u} \cdot E_{S_\ell} - \sum_{i=-1}^{1} \sum_{m}^{T} B^2_{m,i,u} \cdot E_{T_{m,i}}$$

$$- \sum_{j=-2}^{2} \sum_{n}^{Q} C^2_{n,j,u} \cdot E_{Q_{n,j}} \qquad \text{(III-34)}$$

We wish to point out in conclusion that, while expressions (III-28, III-32, III-33) and (III-34) obviously illustrate the nature of spin-orbit effects on the properties of the T_1 state, they also demonstrate that measurements of the radiative strengths, lifetimes, intersystem crossing rates and energies of triplet state spin sublevels cannot by themselves yield a quantitative assessment of any specific spin-orbit interaction. Such an assessment requires significant additional information, e.g., various vibrational overlap factors, the oscillator strengths of a variety of singlet-singlet transitions, etc. A lack of necessary data thus requires that subsequent discussions of experimental results be restricted to the qualitative features of the spin-orbit interaction. These features are by no means uninformative, however, and are quite capable of leading to interesting conclusions.

IV. ADIABATIC INVERSION

In a recent publication, Harris discussed the application of several resonance techniques to the excited molecular triplet state spin system.[105] It has subsequently been established that under the influence of a microwave field a triplet state spin system in zero external field reacts in the interaction representation as does a spin one Zeeman system in the rotating frame.[39,106] Thus virtually any resonance technique which is applicable to a spin one Zeeman system may also be applied to a triplet state spin system in zero external field. One such resonance technique with which the present work is concerned is the technique of adiabatic rapid passage.[107] By this technique, the magnetization of a spin system may be adiabatically inverted by rapidly passing the system through resonance.

Harris[105] has shown that experimentally, conditions conducive to near complete inversion are easily attained for triplet state spin systems in solids at liquid helium temperatures. Essentially, there are three primary conditions necessary to achieve inversion of the magnetization of a spin system. First, the applied H_1 field must greatly exceed local dipolar fields within the sample. It has been shown that a triplet state spin system with non-degenerate spin sub-levels (i.e., a finite $|E|$ value) experiences in zero external magnetic field a quenching of dipolar coupling with non-resonant spins.[108] That is, an asymmetric zero-field splitting tensor reduces dipole-dipole

coupling of the triplet state spin system with non-identical spins in a manner analogous to the quenching of electron orbital angular momentum of paramagnetic ions by asymmetric crystal fields.[109] H_1 fields on the order of only 1 gauss are required to overcome these "quenched" local dipolar fields and thereby to achieve inversion of triplet state magnetizations.[105] A second obvious condition necessary for complete inversion is that $\frac{g\beta}{\hbar} H_1$ must be much larger than any spin-lattice relaxation rates of the triplet spin system. Since spin-lattice relaxation rates are commonly quite low at liquid helium temperatures this condition places no additional restraints upon the necessary H_1 field. Finally, the time derivative of the effective magnetic field must be much less than $\frac{g\beta}{\hbar} H_1{}^2$, and one must adjust the rate at which the system is swept through resonance to comply with this condition. For the spin systems with which we are concerned, and $H_1 \simeq 1$ gauss, this condition places a lower limit of about 10^{-7} sec on the time in which the system might be swept through resonance.[105] However, since the lifetimes of these spin systems are typically longer than 10^{-2} sec, this restriction leaves us with ample room in which to work.

As we have discussed, a suitable H_1 field may be used to invert triplet state magnetizations in the interaction representation. It is important to the subsequent discussion to note that these magnetizations correspond to the triplet state spin alignment in the laboratory frame. Thus, the adiabatic inversion of triplet magnetizations is equivalent to the inversion of the populations of triplet state spin subleveis in the laboratory frame.

V. EXPERIMENTS

A. Descriptions

1. Triplet State Dynamics

A full understanding of many of the experimental procedures employed during the course of this study requires a knowledge of the dynamics of spin polarization (i.e., spin sublevel populations) within the triplet spin ensemble. The following section deals with these dynamic considerations.

If the populations of the three spin sublevels of the phosphorescent triplet state ensemble are designated N_x, N_y and N_z, then the observed intensity, I_ν, into phosphorescence band ν may be represented by

$$I_\nu(t) \propto k_x^{r_\nu} N_x(t) + k_y^{r_\nu} N_y(t) + k_z^{r_\nu} N_z(t) \qquad \text{(V-1)}$$

where $k^{r_\nu}_{i=x,y,z}$ is the radiative rate constant from the triplet sublevel i into the phosphorescence band ν. For a solid phase trap T_1 state in the absence of an applied microwave field,

$$\frac{dN_x(t)}{dt} = N_x(t) \left\{ -[\sum^{\nu} (k_x^{r_\nu} + k_x^{nr_\nu})] - (k_{xy}^{SL} + k_{xz}^{SL}) - \sum_i^E k_{x_i}^{TE} \right\}$$

$$+ \sum_i^S N_{S_i}(t)\, k_{x_i}^I + \sum_i^E N_{E_i}(t)\, k_{x_i}^E + N_z(t)\, k_{zx}^{SL} + N_y(y)\, k_{yx}^{SL}$$

(V-2)

and similarly for $\frac{dN_y(t)}{dt}$ and $\frac{dN_z(t)}{dt}$; where the various symbols are defined:

$N_{S_i}(t) \equiv$ population of excited singlet state i at time (t);

$N_E(t) \equiv$ population of host exciton state i at time (t);

$k^I_{x_i} \equiv$ intersystem crossing probability from singlet state i into triplet sublevel x;

$k^E_{x_i} \equiv$ trapping probability from host exciton state i into sublevel x;

$k_x^{r_\nu} \equiv$ radiative relaxation rate from sublevel x into ground vibronic state ν;

$k_x^{nr_\nu} \equiv$ nonradiative relaxation rate from sublevel x into ground vibronic state ν;

$k^{SL}_{ij} \equiv$ spin-lattice relaxation rate from triplet spin sublevel i into sublevel j;

$k^{TE}_{x_i} \equiv$ detrapping rate from the trap spin sublevel x into host exciton state i.

This equation may be greatly simplified with the implementation of a few easily justified assumptions. First, since our experiments are performed at a temperature of $T \leq 1.5°K$, we may assume that k^{SL}_{ij} is small (i.e., $k^{SL}_{ij} << k^{r_\nu}, k^{nr_\nu}$), and secondly, since the trap depths of the trap T_1 states with which we are concerned are typically tens of wavenumbers, we will assume that $\sum_i^E k^{TE}_{k_{m_i}} << k_m^{r_\nu}, k_m^{nr_\nu}$. Then, if $\sum^\nu (k_x^{nr_\nu} + k_x^{r_\nu}) = K_x = \frac{1}{\tau_{1x}}$ (see equation III-32), the expression for $\frac{dN_x(t)}{dt}$ becomes

$$\frac{dN_x(t)}{dt} = -K_x N_x(t) + \sum_i^S N_{S_i}(t)\, k_{x_i}^I + \sum_i^E N_{E_i}(t)\, k_{x_i}^E \qquad \text{(V-3)}$$

Under the influence of continuous excitation the triplet spin system should be able to reach a steady-state condition in a time t' such that $\frac{dN(x,y,z)(t>t')}{dt} = 0$ and $N_{(x,y,z)}^{(t>t')} = N_{(x,y,z)}^{SS}$. If the populating rate, $k_{j=x,y,z}^P$ is defined such that

$$k_{j=x,y,z}^P = \sum_i^S N_{S_i}(t>t')\, K_{j,i}^I + \sum_i^S N_{E_i}(t>t')\, k_{j,i}^E \quad , \qquad \text{(V-4)}$$

then

$$N_{j=x,y,z}^{SS} = \frac{k_j^P}{K_j} \quad . \qquad \text{(V-5)}$$

Obviously, if the excitation is terminated at some time t" > t', then

$$N_j(t>t'') = N_j^{SS}\, e^{-K_j(t-t'')} \qquad \text{(V-6)}$$

and

$$I_\nu(t>t'') \propto \sum_{j=x,y,z} k_j^{r\nu}\, N_j^{SS}\, e^{-K_j(t-t'')} \qquad \text{(V-7)}$$

The steady state populations N_x^{SS}, N_y^{SS} and N_z^{SS} will usually assume different values since, in general, $k_x^P \neq k_y^P \neq k_z^P$ and $K_x \neq K_y \neq K_z$.

Alternatively, when the system is excited at t = 0 by a flash of short duration (i.e., flash duration << K_x, K_y, K_z), the populations of the spin sublevels immediately after excitation can be taken as

$$N_j(t=0) = N_j^o \approx k_j^P \tag{V-8}$$

and the phosphorescence decay which follows as

$$I_\nu(t) \propto \sum_{j=x,y,z} k_j^{r\nu} N_j e^{-K_j t} . \tag{V-9}$$

A slight digression, before continuing, seems appropriate here for clarification of the definition of $k^P_{j=x,y,z}$ in Eq.(V-4). Equation (V-4) shows that population finds its way into the triplet spin system via two distinct routes, intersystem crossing from the singlet manifold (i.e., $\sum_i^S N_{S_i}(t)\, k^I_{ji}$) and direct trapping from the host triplet exciton band (i.e., $\sum_i^E N_{E_i}(t)\, k^E_{j,i}$). These two routes can be investigated separately by appropriate filtering of the excitation light. That is, if excitation occurs only into the singlet manifold than $\sum_i^S N_{S_i}(t) >> \sum_i^E N_{E_i}(t)$ and the triplet spin system will populate primarily via the intersystem crossing route. Conversely, if excitation occurs only into the host triplet exciton band then $\sum_i^E N_{E_i}(t) >> \sum_i^S N_{S_i}(t)$ and the triplet spin system will populate primarily via trapping out of host exciton states.

2. Microwave Perturbations

Let us now examine the effects of various microwave perturbations upon the observed phosphorescence intensity. By including any proportionality constants implied by Eq.(V-1) into the definition of $k^{r_\nu}_{j=x,y,z}$, the steady state phosphorescence intensity into phosphorescence band may be represented by

$$I^{SS}_\nu = \sum_{j=x,y,z} k^{r_\nu}_j N^{SS}_j \quad . \qquad \text{(V-10)}$$

Upon application of a microwave field which suddenly saturates the spin sublevels x and y the immediately resultant phosphorescence intensity, I^{xy}_ν, becomes

$$I^{x,y}_\nu = k^{r_\nu}_x [\tfrac{1}{2}(N^{SS}_x+N^{SS}_y)] + k^{r_\nu}_y [\tfrac{1}{2}(N^{SS}_x+N^{SS}_y)] + k^{r_\nu}_z N^{SS}_z \qquad \text{(V-11)}$$

and the resultant change in phosphorescence intensity $\Delta I^{x,y}_\nu$ is given by

$$\Delta I^{x,y}_\nu = (I^{SS}_\nu - I^{x,y}_\nu) = \tfrac{1}{2} k^{r_\nu}_x [N^{SS}_x - N^{SS}_y] + \tfrac{1}{2} k^{r_\nu}_y [N^{SS}_y - N^{SS}_x]. \qquad \text{(V-12)}$$

Obviously, $\Delta I^{x,y}_\nu \neq 0$ as long as $N^{SS}_x \neq N^{SS}_y$ and $k^{r_\nu}_x \neq k^{r_\nu}_y$ and Eq.(V-12) thus displays the principle behind optical detection techniques in the electron spin resonance of the T_1 state. In other words, the zero-field ESR transitions of the T_1 state can be characterized using optical detection techniques by monitoring the phosphorescence intensity of a particular phosphorescence emission band while applying a microwave field

of frequency ω, and sweeping ω. The resultant ODMR spectra can then be recorded as $\Delta I_{\nu}^{i,j}$ vs. ω.

These spectra reveal the frequencies of the principal T_1 state zero-field transitions as well as, through associated fine structure, the strengths of nuclear quadrupole and electron-nuclear hyperfine interactions within the excited state.[24]

The PMDR[22] experiments represent an important variation on the ODMR technique. Once the zero-field microwave transitions of T_1 state are known, the microwave field can be tuned to saturate a particular transition, e.g., $T_{1x} \leftrightarrow T_{1y}$, while the phosphorescence detection system is set to monitor various phosphorescence emission bands. In this manner, the radiative characteristics of the T_{1x} and T_{1y} spin sublevels are investigated since

$$\begin{aligned} \Delta I_{\nu}^{x,y} &= \tfrac{1}{2}\,[N_x^{SS}-N_y^{SS}][k_x^{r_\nu}-k_y^{r_\nu}] \\ \Delta I_{\nu'}^{x,y} &= \tfrac{1}{2}\,[N_x^{SS}-N_y^{SS}][k_x^{r_{\nu'}}-k_y^{r_{\nu'}}] \end{aligned} \qquad \text{(V-13)}$$

and

$$\frac{\Delta I_{\nu}^{x,y}}{\Delta I_{\nu'}^{x,y}} = \frac{k_x^{r_\nu}-k_y^{r_\nu}}{k_x^{r_{\nu'}}-k_y^{r_{\nu'}}} \quad . \qquad \text{(V-14)}$$

The versatility of PMDR methods has been significantly increased through the implementation of microwave induced delayed phosphorescence[48] and adiabatic population inversion techniques.[39] The basic PMDR experiment (Eq. V-13 and V-14) acquired an enhanced sensitivity when coupled

with a capability for population inversion. Consider, for example, the steady state phosphorescence intensity to phosphorescence band ν (Eq. V-10). Upon the inversion of a certain fraction, f, of the steady state populations of spin sublevels T_{1x} and T_{1y} from each to the other the populations in T_{1x} and T_{1y} will immediately become

$$\begin{aligned} N_x &= (1-f)N_x^{SS} + f\,N_y^{SS} \\ N_y &= (1-f)N_y^{SS} + f\,N_x^{SS} \end{aligned} \qquad \text{(V-15)}$$

and the corresponding phosphorescence intensity into band ν becomes

$$I_\nu^1 = k_x^{r_\nu}[(1-f)N_x^{SS} + f\,N_y^{SS}] + k_y^{r_\nu}[(1-f)N_y^{SS} + f\,N_x^{SS}] + k_z^{r_\nu}\,N_z^{SS} \qquad \text{(V-16)}$$

(see Fig. V-1). If a second inversion is then performed after a time Δt which is short compared to all relaxation processes within the T_1 state, then a second fraction, f, of the T_{1x} and T_{1y} populations will be retransferred between them resulting in the final populations

$$\begin{aligned} N_x' &= [1-2f+2f^2]N_x^{SS} + [2f(1-f)]N_y^{SS} \\ N_y' &= [1-2f+2f^2]N_y^{SS} + [2f(1-f)]N_x^{SS} \end{aligned} \qquad \text{(V-17)}$$

and a final phosphorescence intensity of

Figure V-1 Graphic representation of the observed changes in steady state phosphorescence intensity upon application of successive population inversion operations. If phosphorescence originates from spin sublevel i, with $N_i^{SS} < N_j^{SS}$, then an inversion of the N_i^{SS} and N_j^{SS} populations at time t causes an increase in the phosphorescence intensity from I_ν^0 to I_ν^1. Upon re-inversion of these two populations at time $t+\Delta t$, the phosphorescence intensity changes to I_ν^2. I_ν^2 will be greater than I_ν^0 if the fraction of inversion is less than unity (see text). The dashed line indicates the phosphorescence decay which will be observed unless Δt is very much smaller than the lifetime of the two spin sublevels involved in the inversion.

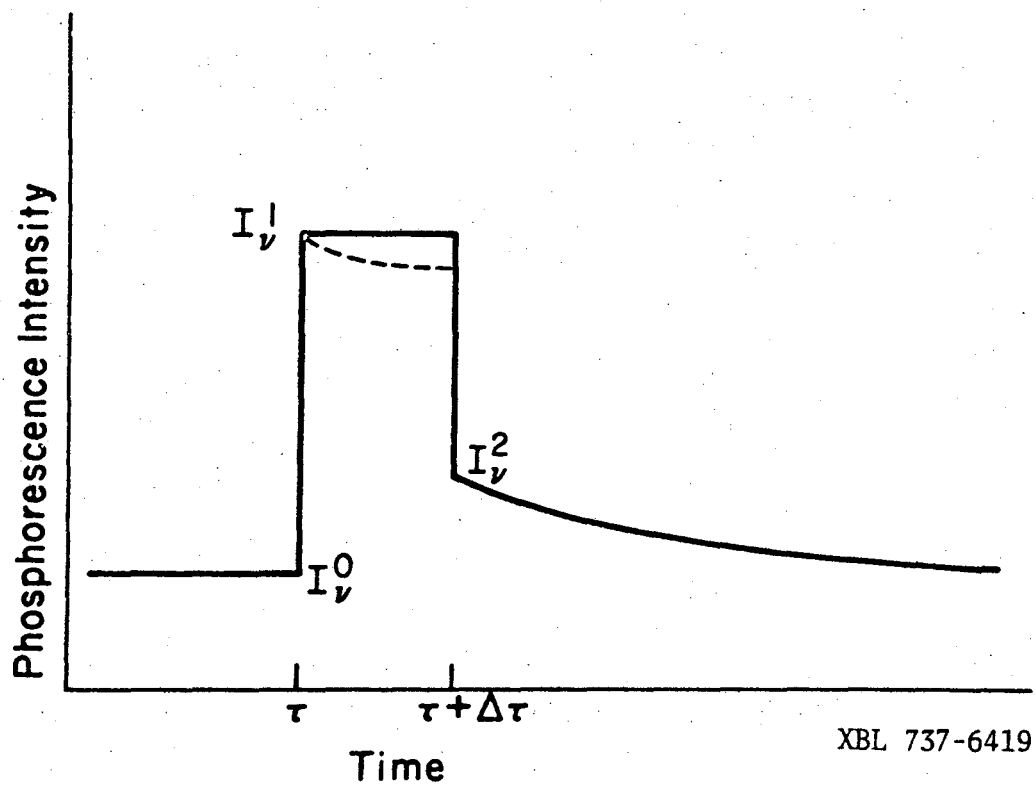
Phosphorescence Intensity
I_ν^1
I_ν^2
I_ν^0
τ
$\tau+\Delta\tau$
Time
XBL 737-6419

Figure V-1

$$I_\nu^2 = k_x^{r\nu}[1-2f+2f^2]N_x^{SS} + [2f(1-f)]N_y^{SS} + k_y^{r\nu}[1-2f+2f^2]N_y^{SS}$$

$$+ [2f(1-f)]N_x^{SS} + k_z^{r\nu} N_z^{SS} \quad . \qquad \text{(V-18)}$$

It is easily verified from equations V-14, V-17 and V-18 that the fraction of inversion, f, is accurately determined from experimentally measured phosphorescence intensities through the relationship[39]

$$f = 1 - \tfrac{1}{2}\left[\frac{I_\nu^2 - I_\nu^0}{I_\nu^1 - I_\nu^0}\right] \qquad \text{(V-19)}$$

Obviously, when $f = \frac{1}{2}$ the situation is identical to that of saturation and

$$I_\nu^2 = I_\nu^1; \quad I_\nu^1 - I_\nu^0 = I_\nu^{x,y} \quad . \qquad \text{(V-20)}$$

Another experimental technique which, when used in conjunction with the adiabatic inversion technique, enhances the capabilities of PMDR methods has been developed by Schmidt, Veeman and van der Waals.[48] The value of this technique, called microwave induced delayed phosphorescence (MIDP), lies in its ability to facilitate the examination of phosphorescence emission from a single spin sublevel in the absence of emission from the other two and also in its ability to facilitate the examination of non-radiative sublevels. For example, consider a triplet spin system with the following conditions: $K_x << K_y \approx K_z$, $N_x^{SS} \approx N_y^{SS} \approx N_z^{SS}$ and $k_x^{r\nu} \approx 0$, $k_y^{r\nu} \approx k_z^{r\nu}$, for all ν. An attempt to

completely characterize this system by previously mentioned experimental techniques would encounter obvious difficulties. These difficulties can be surmounted, however, by the following procedure (see Fig. V-2).

Assuming an initial condition at time t = 0 of

$$N_{j=x,y,z}(0) = N_j^0 \quad \text{(in the case of flash excitation)}$$

or

$$N_{j=x,y,z}(0) = N_j^{SS} \quad \text{(in the case of CW excitation)}$$

and

$$I_\nu(0) = \sum_{j=x,y,z} k_j^{r_\nu} N_j(0) \quad , \qquad \text{(V-21)}$$

we will allow the system to relax until at some time t_1,

$$N_y(t_1) = N_y(0)\, e^{-K_y t_1} \cong 0 \quad ,$$

$$N_z(t_1) = N_z(0)\, e^{-K_z t_1} \cong 0 \quad , \qquad \text{(V-22)}$$

$$N_x(t_1) = N_x(0)\, e^{-K_x t_1} \neq 0 \quad ,$$

and

$$I_\nu(t_1) = k_x^{r_\nu} N_x(0)\, e^{-K_x t_1} \cong 0 \qquad \text{(V-23)}$$

since $k_x^{r_\nu} \cong 0$.

Figure V-2 Graphic representation of the decay of phosphorescence intensity with a population inversion operation performed at time $t = t_1$. Events occur as follows. Phosphorescence intensity is allowed to decay from time $t = 0$ until at time $t = t_1$ population remains <u>only</u> in the non-radiative spin sublevel T_{1i}. At time $t = t_2$ a fraction, f, of the population $N_i(t_1)$ is placed into the radiative spin-sublevel T_{1j}, resulting in an increase in phosphorescence intensity at time $t = t_2 \approx t_1$ from $I_\nu(t_1)$ to $I_\nu(t_2)$. The subsequent phosphorescence intensity at time $t > t_2$ decays with the characteristic decay constant K_j of the spin subelvel T_{1j}.

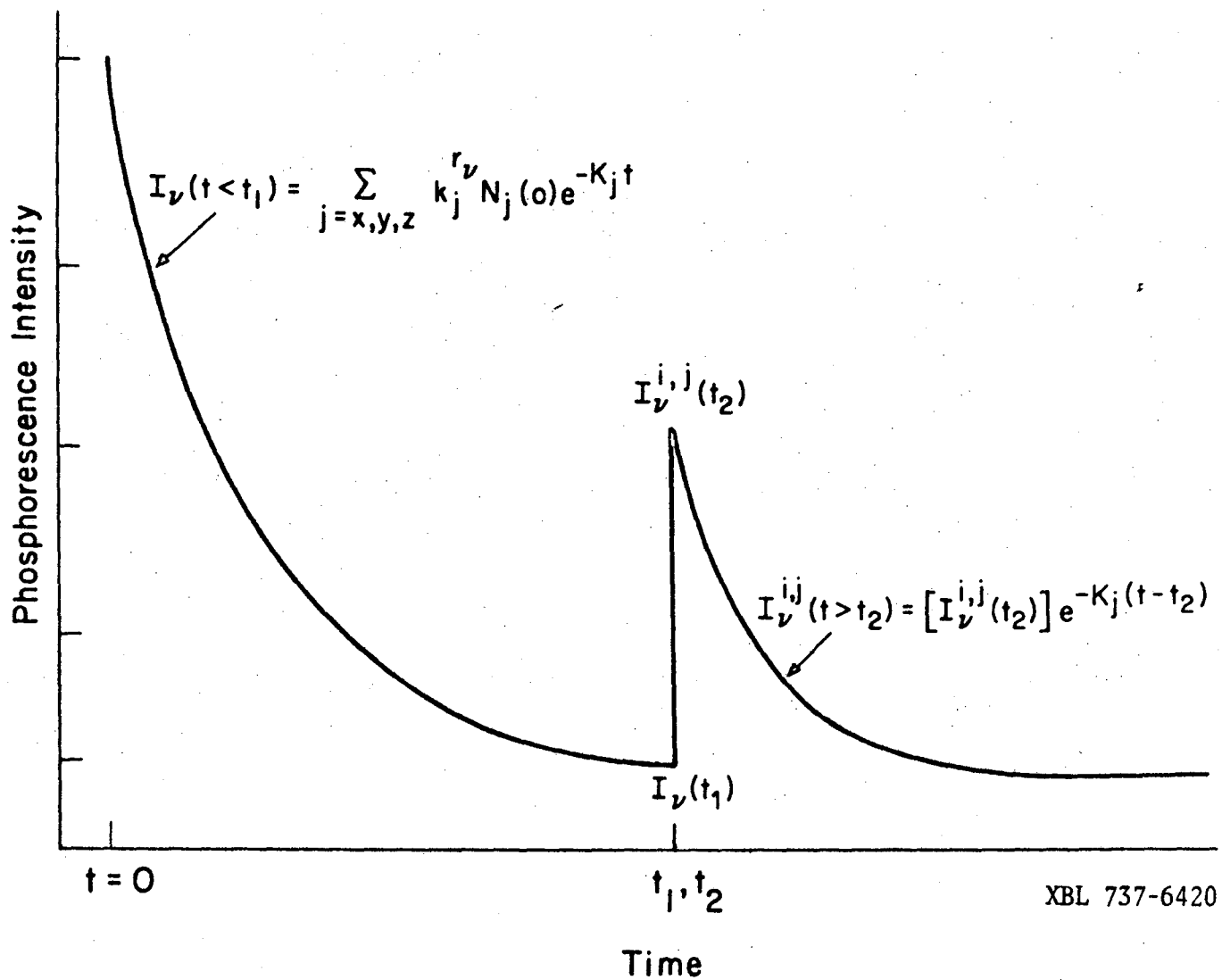

Figure V-2

0 0 0 0 3 9 0 0 4 6 2

At this point, the sample can be subjected to a brief microwave perturbation (i.e., adiabatic inversion) which affects the transfer of a fraction, f, of the population $N_x(t_1)$, into either of the now empty spin sublevels T_{1y} or T_{1z}. Immediately after such a transfer into T_{1z} at $t_2 \cong t_1$, we have

$$N_z(t_2) = f[N_x(t_1)]$$
$$N_x(t_2) = (1-f)[N_x(t_1)] \qquad \text{(V-24)}$$

and

$$I_\nu^{xz}(t_2) = k_z^{r_\nu} N_z(t_2) = k_z^{r_\nu} f[N_x(t_1)]$$
$$= k_z^{r_\nu} f[N(0)\, e^{-K_x t_1}] \neq 0 \quad , \qquad \text{(V-25)}$$

which will then decay as

$$I_\nu^{xz}(t>t_2) = [I_\nu^{xz}(t_2)]\, e^{-K_z(t-t_2)}$$
$$= k_z^{r_\nu} f[N_x(0)\, e^{-K_x t_1}]\, e^{-K_z(t-t_2)} \quad . \qquad \text{(V-26)}$$

If, on the other hand, the microwave perturbation at $t = t_1$ had affected a transfer into T_{1y}, then

$$I_\nu^{xy}(t_2) = k_y^{r_\nu} f'[N_x(0)\, e^{-K_x t_1}] \neq 0 \qquad \text{(V-27)}$$

and

$$I_{\nu}^{xy}(t>t_2) = [I_{\nu}^{xy}(t_2)]\, e^{-K_y(t-t_2)} \quad . \qquad \text{(V-28)}$$

Clearly, a plot of $\ell n[I_{\nu}^{xz}(t>t_2)]$ vs. t will return an accurate value for the decay constant, K_z, while a plot of $\ell n[I_{\nu}^{xy}(t>t_2)]$ vs. t will similarly return a value for the decay constant, K_y. Moreover, by varying the time t_1 at which the microwave perturbation is performed, one obtains either $I_{\nu}^{xy}(t_2)$ or $I_{\nu}^{xz}(t_2)$ as a function of t_1. A plot of $\ell n[I_{\nu}^{xy}(t_2)]$ or $\ell n[I_{\nu}^{xz}(t_2)]$ vs. t_1 then produces an accurate value for the T_{1x} decay constant, K_x, an otherwise unmeasurable quantity due to the non-radiative character of T_{1x}, i.e., $k_x^{r\nu} \approx 0$ for all ν. Additionally, since the inversion factors f and f' in equations V-26 and V-27 can be precisely determined (cf. above, equation V-19), the ratio of the radiative rates $k_y^{r\nu}/k_z^{r\nu}$ is determined by

$$\frac{I_{\nu}^{xy}(t_2)}{I_{\nu}^{xz}(t_2)} = \frac{k_y^{r\nu}\, f'[N_x(0)\, e^{-K_x t_1}]}{k_z^{r\nu}\, f[N_x(0)\, e^{-K_x t_1}]} = \left(\frac{k_y^{r\nu}}{k_z^{r\nu}}\right)\left(\frac{f'}{f}\right)$$

$$= \text{Constant} \times \left(\frac{k_y^{r\nu}}{k_z^{r\nu}}\right) \qquad \text{(V-29)}$$

Once the ratio $k_y^{r\nu}/k_z^{r\nu}$ is known, the ration $N_y(0)/N_z(0)$ is subsequently determined from phosphorescence decay curve decompositions (i.e., values for $k_i^{r\nu}N_i(0)/k_j^{r\nu}N_j(0)$ are obtained from decay curve decomposition (cf. Eq. V-21 and Fig. VI-4)) and the ratio k_y^P/k_z^P is thereby determined from the relationship

$$N_i(0) = \left\{ \begin{array}{l} N_j^0 \approx k_j^P \\ \\ N_j^{SS} = \dfrac{k_j^P}{K_j} \end{array} \right\} . \qquad \text{(V-30)}$$

The ODMR and PMDR methods described above are obviously valuable and versatile experimental methods. We conclude this section with the following summary of quantities which are easily obtainable for the T_1 state of a variety of molecules through the use of the ODMR and PMDR methods. ODMR experiments are capable of measuring:

(1) Frequencies of zero-field transitions;

(2) Strengths of nuclear quadrupole and electron-nuclear hyperfine interactions.

PMDR methods can yield values for:

(1) Absolute decay constant (or lifetimes) for the three spin sublevels;

(2) Relative radiative rates from the three spin sublevels to various phosphorescence bands;

(3) Relative populating rates into the three spin sublevels from either intersystem crossing or triplet exciton trapping.

B. Experimental Procedures

In this section the procedures and equipment used in performing the ODMR, PMDR, and delayed inversion experiments are described.

1. Basic Equipment

A block diagram of the basic apparatus is shown in Fig. V-3. Two primary systems comprise the apparatus: a microwave supply system and an optical detection system. The microwave system consists mainly of a microwave signal supplied by a Hewlett-Packard model 8690-B sweep oscillator and amplified by a Servo Corp. traveling wave tube amplifier (1 to 12 HGz at 1 watt, #3003; 1 to 2 GHz at 20 watts, #2210; 2 to 4 GHz at 20 watts, #2220; and 4 to 8 GHz at 20 watts, #2230). Microwave power is applied to the sample through a rigid 50 Ω coaxial rod which is terminated by a helical slow wave structure. Samples are mounted in the helical slow wave structure and the rod is suspended in a liquid helium dewar. Temperatures below 4.2°K are obtained by maintaining suitable low pressures over the liquid helium. A Hewlett-Packard PIN diode (models 33222A-020, 120 and 220) placed on the output of the sweep oscillator provides microwave switching capability. The optical detection system consists mainly of a Jarrell-Ash model 48-490, 3/4 meter Czerny-Turner spectrometer equipped at the exit slit with a thermo-electrically cooled (-20°C) EMI 6256S Photomultiplier which has its cathode maintained at -1600 to -1800 V by a Fluke 415B power supply. Sample phosphorescence is collected at a 90° angle to the exciting light

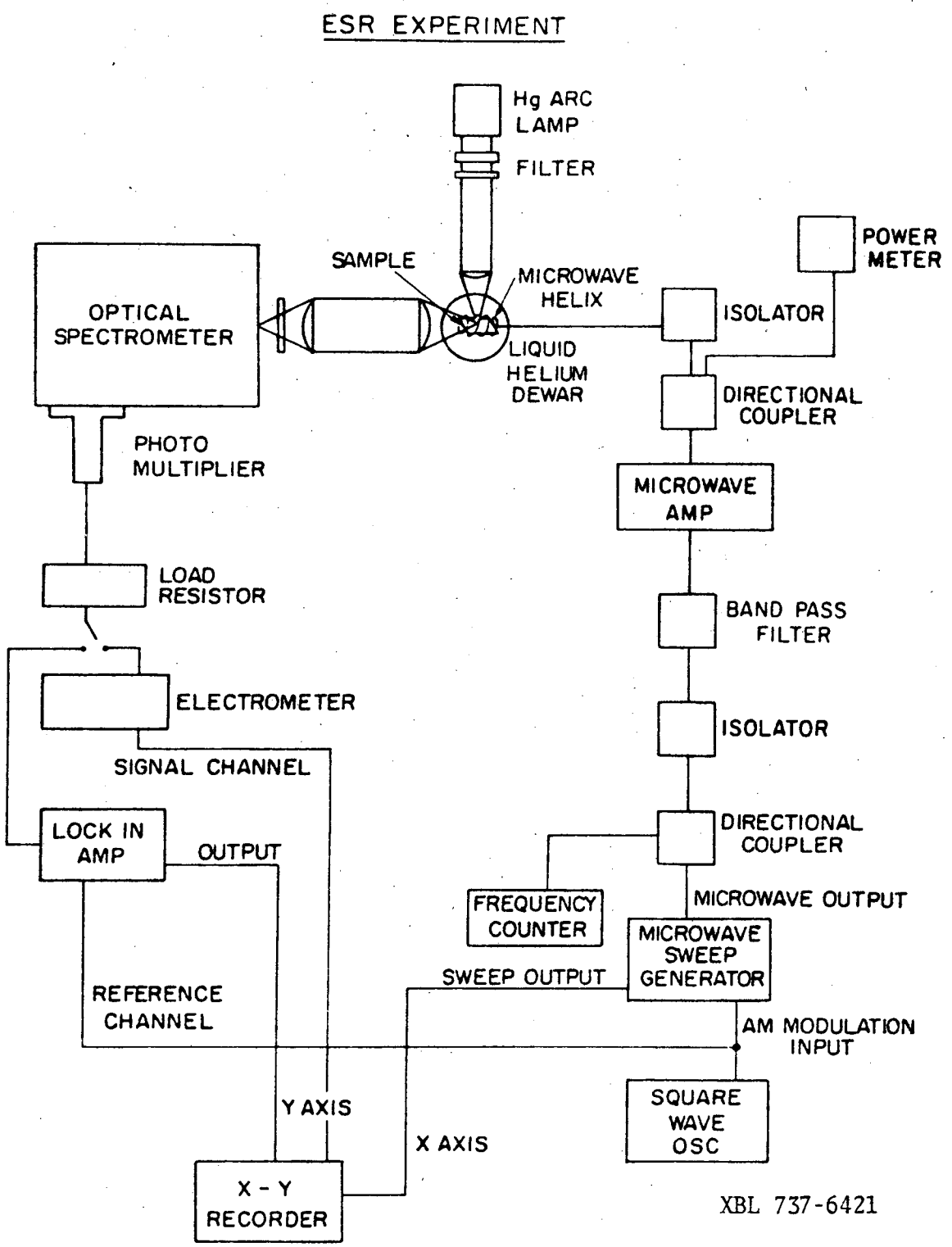

Figure V-3 Block diagram of the basic ODMR experimental arrangement.

and focussed through appropriated Corning filters (to remove scattered light) onto the spectrometer entrance slits. Exciting light is supplied by either a PEK 100-watt mercury short arc lamp (for continuous optical pumping) or by an EG&G 100 Joule flash lamp (~20 μsec duration). In either case, appropriate Corning glass and solution filters in conjunction with Schott interference filters (centered at 2500 Å, 2800 Å, or 3100 Å) provide the necessary control over the excitation wavelength.

Normal phosphorescence spectra were observed in the absence of any applied microwave power by connecting the anode of the photomultiplier tube through a load resistor to the input of a Keithly model 610 CR electrometer. A strip chart recorder then served to display the output of the electrometer as the sample phosphorescence was scanned via the optical spectrometer.

2. ODMR and PMDR Experiments

The zero-field OMDR experiments were performed by monitoring the change in the intensity of a given phosphorescence band of the sample while varying the frequency of an AM modulated microwave field. The majority of the ODMR spectra were obtained by square wave amplitude modulation with a frequency of 10 to 20 Hz and a modulation depth $\geq$ 30 db. Phosphorescence intensity was phase detected by connecting the anode of the photomultiplier tube through an adjustable lead resistor and into the signal channel of a PAR model HR-8 lock-in amplifier. A square wave oscillator provided a reference signal for the lock-in

amplifier and was connected to the PIN diode via an integrated circuit device (PIN driver) which supplied the appropriate voltages.

The output of the lock-in amplifier drove the Y-axis of an X-Y recorder while a ramp voltage from the microwave sweep oscillator drove the X-axis. In this manner a spectrum of phosphorescence intensity was observed as a function of microwave frequency.

The PMDR experiments required only a slight variation on this basic procedure. The optical spectrometer was set to scan the sample phosphorescence while the microwave field was AM modulated and set to saturate a single ESR transition; then, using phase sensitive detection, the emission from only two triplet spin sublevels was observed through the entire phosphorescence spectrum. PMDR spectra were obtained by connecting the output of the lock-in amplifier to a strip-chart recorder. Phase sensitive detection limits the observed intensity to only that due to the emission from the two spin sublevels which are connected by the microwave field. PMDR spectra therefore reveal the qualitative differences in the radiative rates of the two microwave connected spin sublevels to the various vibronic bands in the phosphorescence spectrum. A comparison of the normal phosphorescence spectrum with the three PMDR spectra (one for each of the three microwave transitions) can thereby yield information of significant value for the characterization of the various phosphorescence bands and of the phosphorescent triplet state itself.

3. Adiabatic Inversion

The achievement of an adiabatic inversion of the populations of two triplet spin sublevels requires a rapid sweeping of the microwave field through the zero-field ESR resonance. We obtained the required frequency sweep by applying a ramp voltage to the FM input of the microwave sweep oscillator. The ramp voltage was adjusted so that at V_0 the microwave frequency was ω_0, the center of the zero-field ESR transition being used for inversion. The FM voltage was swept linearly from $V_0 - \frac{1}{2}V$ to $V_0 + \frac{1}{2}V$ in a time τ so that the microwave frequency changed from $\omega_0 - \frac{1}{2}\omega$ to $\omega_0 + \frac{1}{2}\omega$ in the time τ (see Fig. V-4). Thus by varying τ and ω, one varies dH_1/dt. Maximum inversion was achieved by adjusting the power, the time τ (~100 μsec), and the ramp voltage V. Optimum inversion was obtained at a rate of ~10 MHz/100 μsec. Microwave power was applied to the sample only during passage through resonance. A General Radio type 1395-A pulse/delay generator supplied the necessary AM and FM modulation signals (see Fig. V-5).

Simple phosphorescence decay studies at 1.3°K show that the DCB phosphorescent triplet state possesses two short-lived spin sublevels and one relatively long-lived sublevel. Using the adiabatic inversion technique, experiments similar to those reported by Schmidt, Veeman and van der Waals were performed.[48]

The fraction of inversion, f, was measured under steady-state excitation conditions (see Section V-A). During each event sequence the microwave frequency was swept from $\omega_0 - \frac{1}{2}\omega$ to $\omega_0 + \frac{1}{2}\omega$ and then, after a time Δ, swept back from $\omega_0 + \frac{1}{2}\omega$ to $\omega_0 - \frac{1}{2}\omega$. A PAR waveform eductor

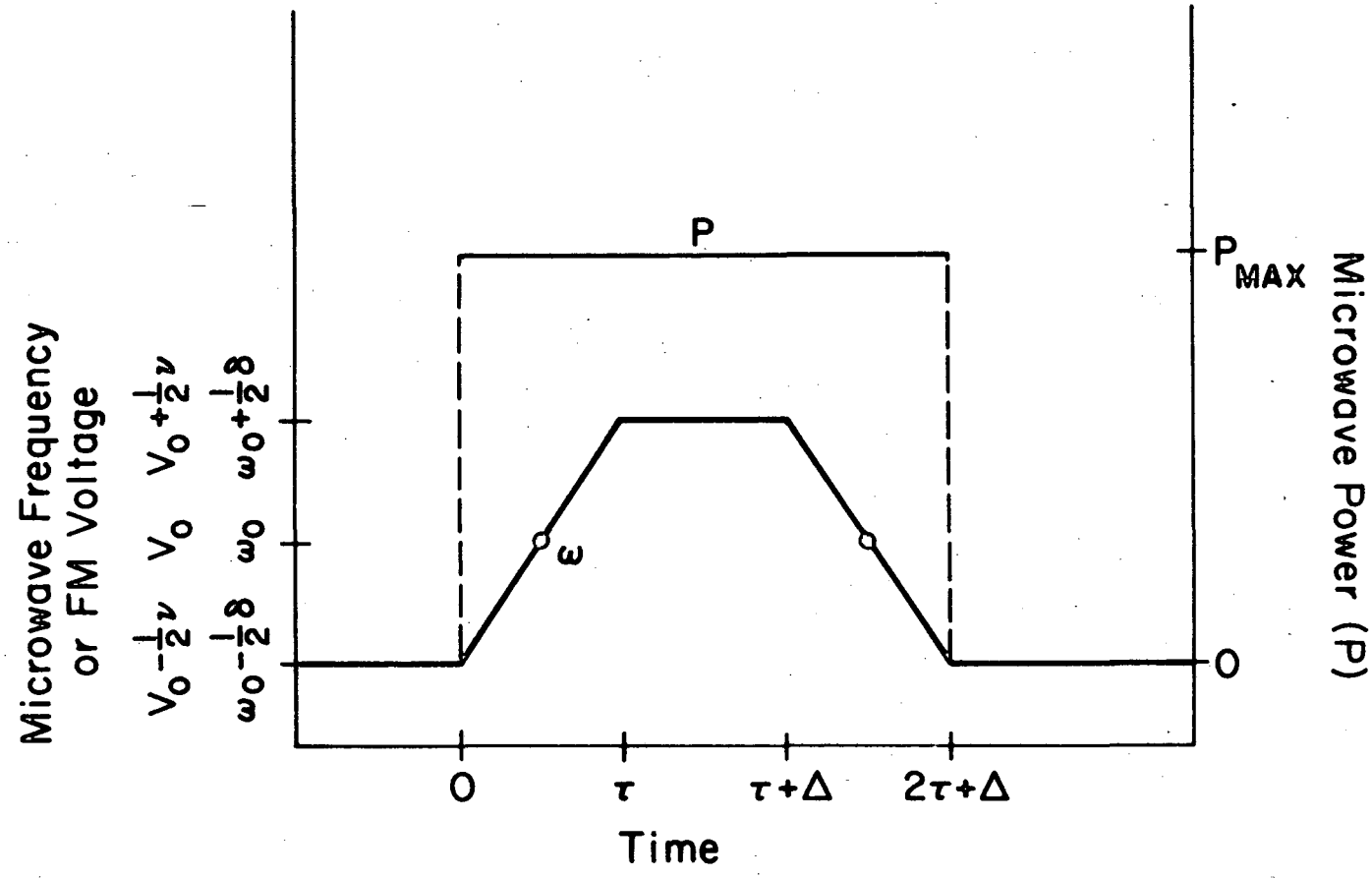

XBL 716-6895

Figure V-4 Graphic representation of the microwave signal used to adiabatically invert (and/or reinvert) triplet spin-sublevel populations (see text). The frequency (ω) and power (P) are shown as a function of time.

0 0 0 0 3 9 0 3 1 6 8

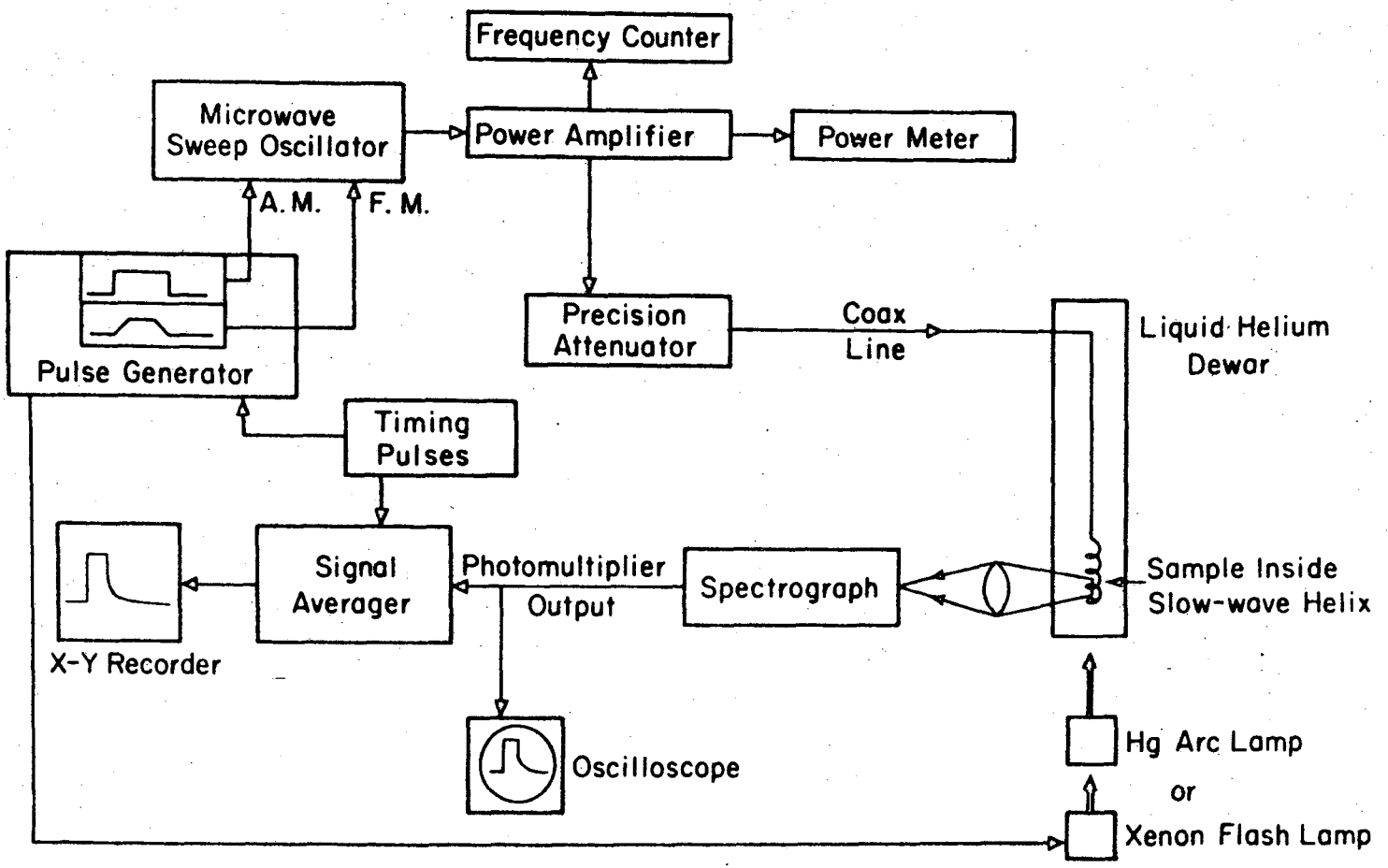

INSTRUMENTAL ARRANGEMENT FOR DELAYED INVERSION EXPERIMENTS

XBL 737-6422

Figure V-5 Block diagram of the instrumental arrangement employed in adiabatic inversion experiments.

again served to store the output from successive event sequences and thereby improve the signal-to-noise ratio.

0 0 0 0 3 9 0 0 4 6 9

VI. p-DICHLOROBENZENE -- PRELIMINARY STUDIES

Initially, the principal objective of this investigation of the properties of the lowest excited triplet state (T_1) of p-dichlorobenzene (DCB) was the unambiguous assignment of its orbital symmetry. The problem of establishing such assignments for the T_1 states of benzene derivatives has occupied a significant portion of the available literature concerning these molecules (see Section I-B). However, due to the spin forbidden nature of phosphorescence transitions, definitive orbital symmetry assignments for the T_1 state of most benzene derivatives have not generally been possible from ordinary spectroscopic studies.[18-20] The techniques of phosphorescence microwave double resonance, outlined in Chapter III, offered the prospect of uniquely determining the spin-orbit character of individual triplet magnetic sublevels, and thereby the unambiguous assignment of the orbital symmetry of the T_1 state. We therefore applied these techniques to the problem of establishing the orbital symmetry of the T_1 state of DCB, since this molecule is an important benzene derivative and its T_1 assignment remains unconcluded (see Section I-B).[79-81,93]

A. Experiment and Results

1. Sample

Samples of Eastman Organic paradichlorobenzene (DCB) were degassed and extensively zone-refined (200 passes at two inches/hour). Single

crystals of DCB were grown by Bridgman techniques and mounted inside a helical slow wave structure which was suspended in a liquid helium dewar. When polarized data were collected crystals were aligned coniscopically to detect phosphorescence from the crystallographic bc face. The exciting light was incident on the a'b face and was indicent from a direction perpendicular to the bc face. Temperatures lower than 4.2°K were obtained by pumping on the liquid helium.

2. Phosphorescence Microwave Double Resonance Spectroscopy (PMDR)

PMDR spectra were obtained as described in Section V-B. The three zero-field transitions of DCB were observed at 5.362 GHz, 3.605 GHz and 1.758 GHz, as reported by Buckley and Harris.[32]

In addition to the reported exciton phosphorescence[110] of DCB (origin = 27890 cm^{-1}), emission from a shallow trap which will be referred to as the x trap (origin = 27865 cm^{-1}) and a deep trap which will be referred to as the y trap (origin = 27807 cm^{-1}) was observed. The DCB sample was found to be extremely sensitive to its recent thermal history. The emission of both the exciton and the x trap was observed at 4.2°K with approximately equal intensity. Upon cooling the sample to 1.3°K only the x trap emission was observed. If the temperature of the DCB crystal was lowered to 4.2°K rapidly (approximately 20 minutes), exciton emission was not observed, but the emission from the y trap was observed in addition to that from the x trap. Upon cooling the sample below 4.2°K, the intensity of the x trap emission increased while the intensity of the y trap emission decreased until at 1.3°K

only the x trap emission was observed. The y trap emission is believed to be due to triclinic inclusions in the monoclinic DCB lattice. This was tested by preparing a triclinic sample of DCB which contained approximately 0.01 mole percent p-dimethoxybenzene as an impurity to stabilize the triclinic form at helium temperatures. Since the same phosphorescence origin as well as the same ODMR transition frequencies were observed for both the y trap and the triclinic form of DCB, the y trap is presumably due to triclinic inclusions.

We will concentrate in the remaining discussion on the monoclinic form, i.e., the x trap. Each of the PMDR spectra illustrated in Fig. VI-1 was obtained while saturating one of the three microwave zero-field transitions. The microwave field was amplitude modulated at 25 cps and the spectra were obtained by standard phase detection techniques as described in Section V-B. All of the vibronic transitions increase in intensity for each of the PMDR experiments. Since a lock-in amplifier was used, any decrease in intensity while monitoring the emission to a vibrational level of the ground state would have caused the PMDR transition to go negative rather than positive. The relative increase in intensity of the vibronic band at 0,0-1579 cm^{-1} (denoted by * in Fig. VI-1) compared to the origin is striking. The relative increase in intensity of the vibronic band is greatest while saturating the 3.604 GHz transition, while the relative increase in intensity of the origin is greatest for the 5.362 GHz transition. Other vibrations which have been assigned as a_g behave in a manner similar to the origin and therefore it is clear that the vibration at 0,0-1583 cm^{-1} is not exclusively

Figure VI-1 (a) Unpolarized phosphorescence spectrum in p-dichlorobenzene.

(b) The 5.362 GHz (D+|E|) zero-field PMDR spectrum.

(c) The 3.604 GHz (D-|E|) zero-field PMDR spectrum.

(d) The 1.758 GHz (2|E|) zero-field PMDR spectrum.

All spectra were obtained at 1.3°K.

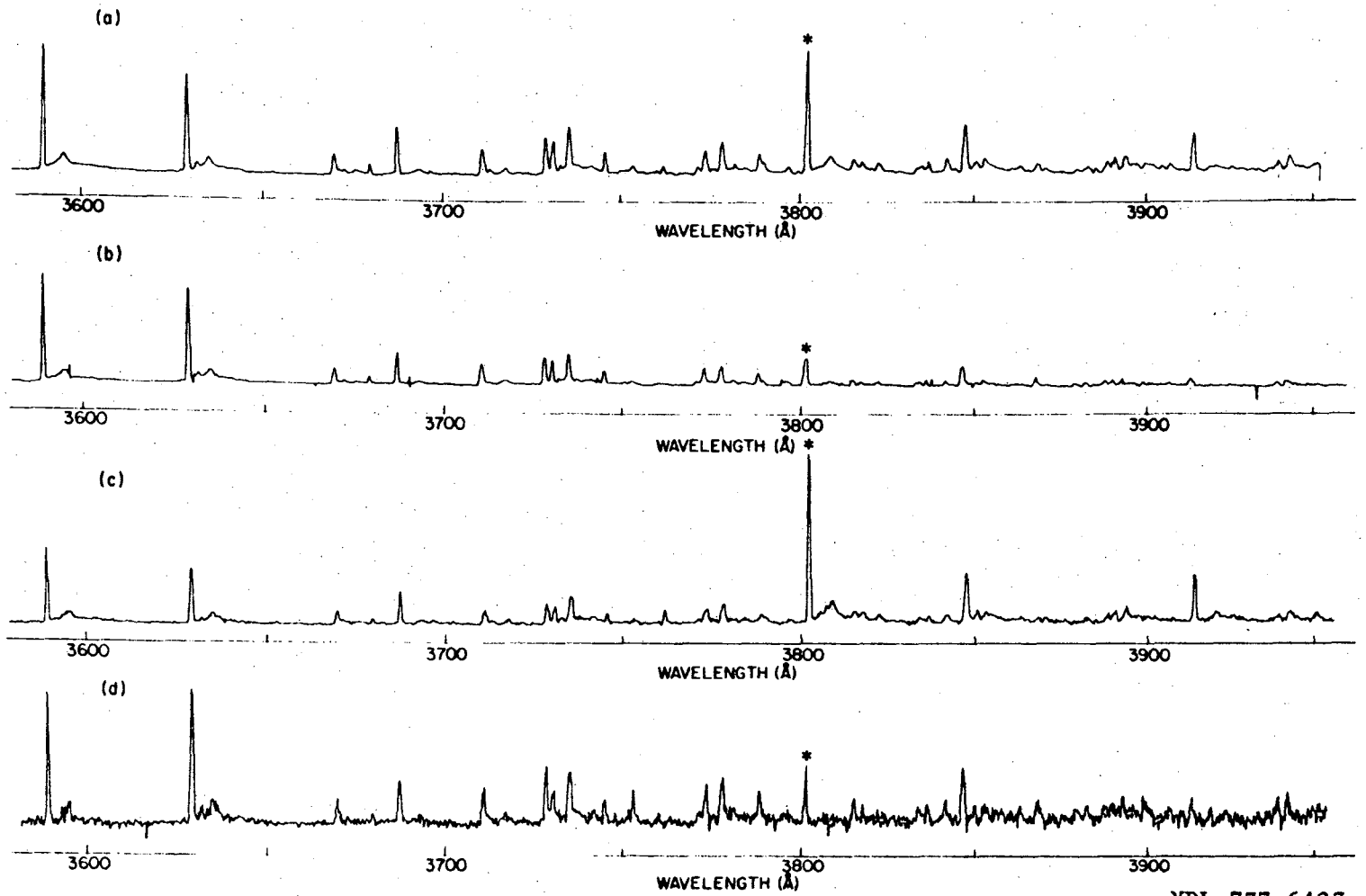

XBL 737-6423

Figure VI-1

an a_g vibration as previously assigned, since all vibrations with the same symmetry should maintain a constant intensity ratio within all three PMDR spectra.

3. Adiabatic Inversion

The inversion experiments were conducted at 1.3±0.05°K employing the procedures outlined in Section V-B. Simple phosphorescence decay studies at 1.3°K show that the DCB triplet state possesses two short-lived sublevels and one relatively long-lived sublevel (Fig. VI-2). Using the inversion technique the lifetimes of all three sublevels were measured in the same manner as reported by Schmidt, Veeman and van der Waals.[48] The experiment depends upon an examination of the time evolution of the emission intensity to a chosen vibrational band in the phosphorescence spectrum. The event sequence occurred as follows. The excitation source, a 100 joule flash lamp (~20 μsec duration) was triggered first, with the excitation light focussed on the sample through a water filter and a Schott 3100 Å interference filter. A PAR waveform eductor was triggered a short time after the excitation flash (~100 μsec) and the population inversion operation[39] was performed after a variable delay which was adjusted to allow the two short-lived spin sublevels to decay. The waveform eductor served to store output from successive event sequences and thereby improve the signal-to-noise ratio. Successive event sequences were separated by a four second delay to insure complete decay of the triplet sublevels. However, only the first one second of each sequence was sampled and stored in the waveform eductor.

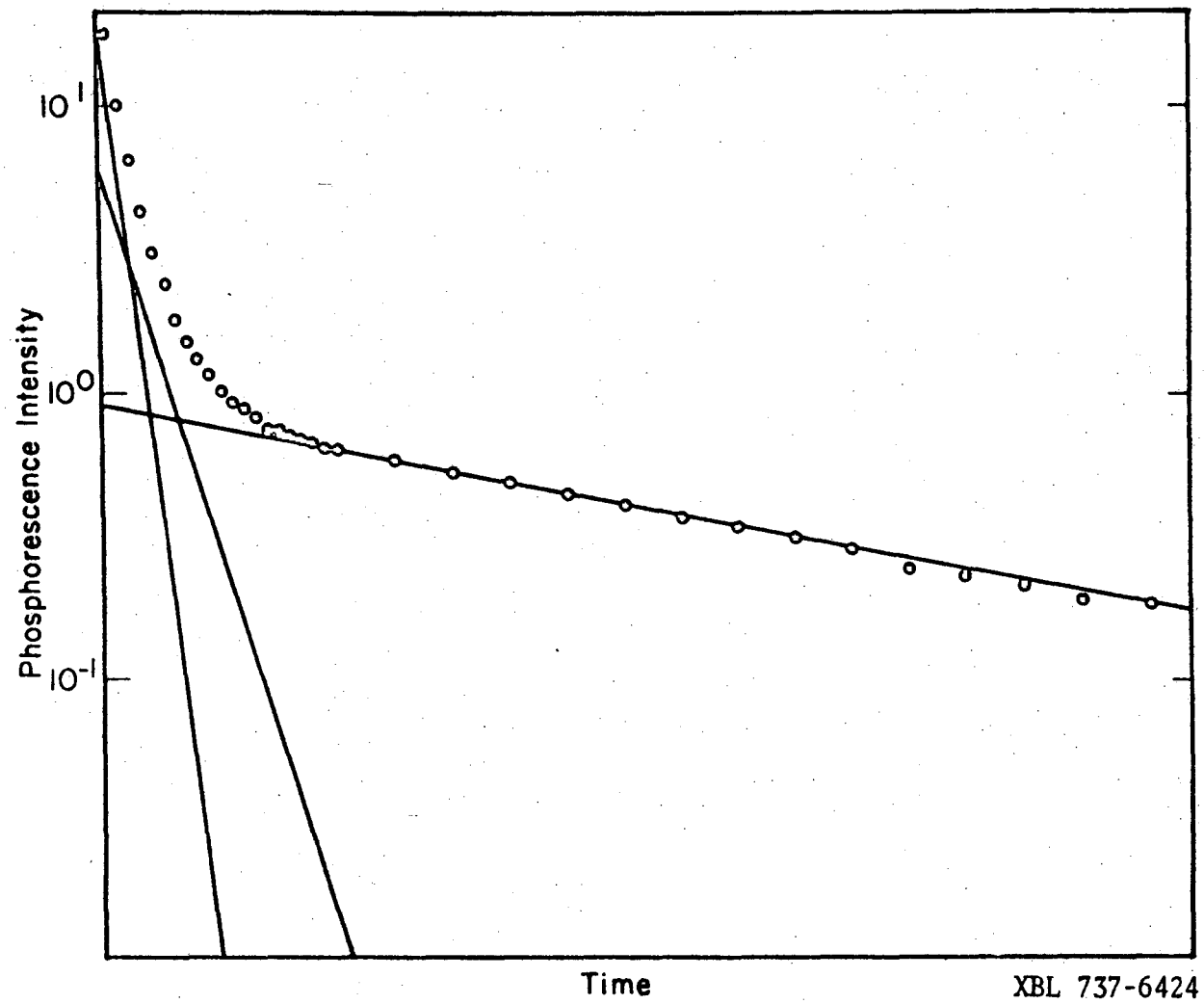

Figure VI-2 A semi-logarithmic plot of a typical DCB x-trap phosphorescence decay. Filled circles indicate experimental points while the solid lines approximate the three exponential functions whose sum will reproduce the experimental curve. Note that two of these experimental functions decay rapidly relative to the third.

0 0 0 0 3 9 0 4 7 0

These observations confirmed the simple decay data, showing the sublevels with 1/3 lifetimes of 13±1.5 msec, 46±3 msec, and about 600 msec, and, further, established the long-lived sublevel to be common to both the 5.362 and the 3.604 GHz transitions. Inversion was observed at times as long as several seconds after excitation, thereby establishing that at very low temperatures (~1.3°K) spin-lattice relaxation may be neglected.

Figure VI-3 illustrates the phosphorescence to the origin in the inversion experiment described above from the accumulation of time average experiments. Following the excitation flash, the two short-lived spin sublevels decay, thus depleting their populations. The inversion operation is triggered after a time long compared to the short lifetimes (~90 msec) thereby placing population from the long-lived sublevel selectively into one of the now almost empty short-lived sublevels. In this manner one can obtain ratios of radiative rate constants from the ratio of intensity of the inversion signal at τ = 90 msec (5.362/3.604 GHz).

From PMDR spectra, vibronic bands of varying symmetries were identified and a systematic series of the 5.362 and 3.604 GHz inversions was also applied to several of the prominent vibrational bands in the phosphorescence spectrum which yielded the data listed in Table VI-1. Monitoring emission from the crystallographic[111] bc face, polarization ratios obtained for this same series of inversions are reported in Table VI-2.

0 0 0 0 3 9 0 0 0 7 1

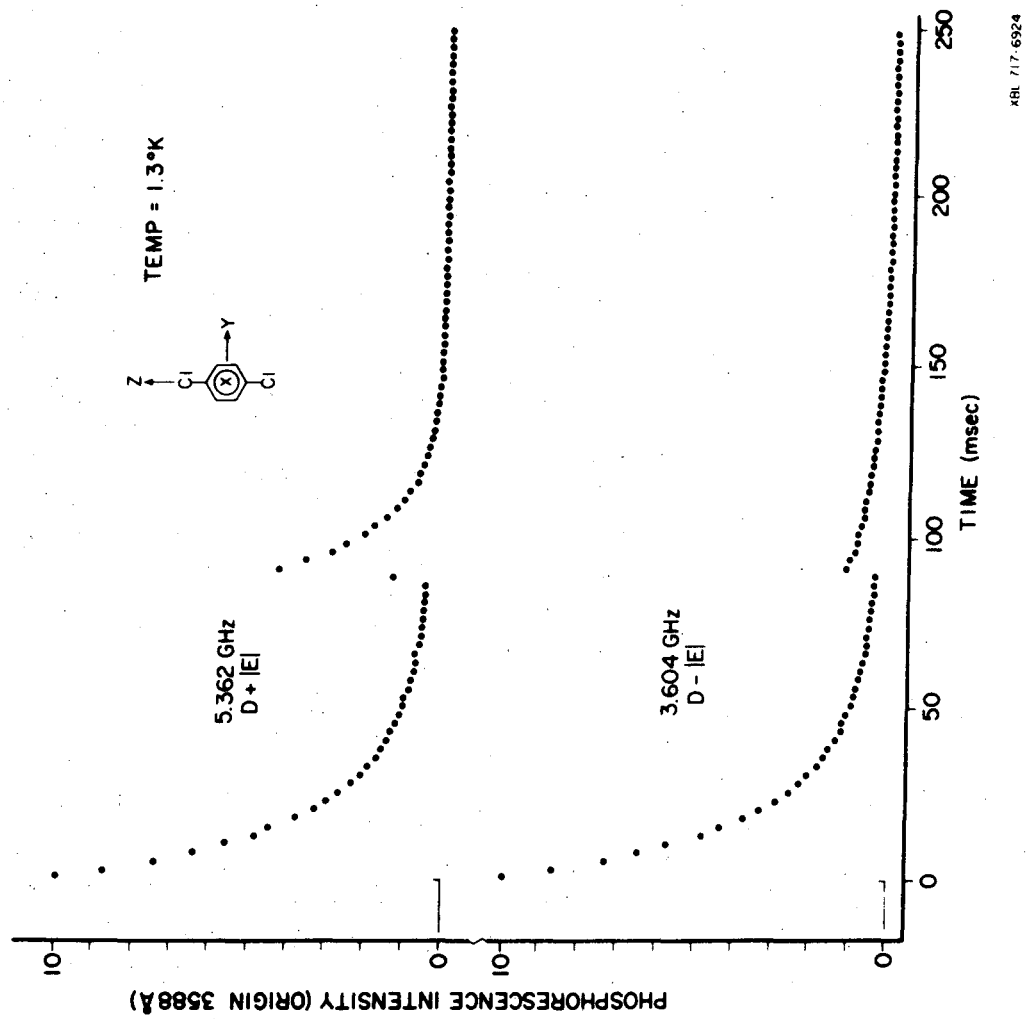

Figure VI-3 The phosphorescence decay and microwave induced inversion monitoring the x-trap origin at 1.3°K in p-dichlroboenzene from 168 accumulations in a 100 channel averager. The fraction of inversion in both transitions was 0.85.

Table VI-1

Relative Inversion Heights

(Normalized to phosphorescence intensity)

	$D+\|E\|$	$D-\|E\|$	Ratio $\frac{D+\|E\|}{D-\|E\|}$ [b]
Origin (0,0)	0.50	0.12	4.1:1
b_{1g}(0,0-(1579+309) cm^{-1})[a]	0.47	0.18	2.6:1
b_{2g}(0,0-309 cm^{-1})	0.53	0.12	4.6:1
b_{3g}(0,0-1579 cm^{-1})[a]	0.40	0.28	1.4:1

[a] See text for discussion of assignments of these bands.

[b] These ratios are approximately equal to the radiative rate constant ratios (τ_y/τ_z) in the bands listed.

Table VI-2

Polarized Inversion Heights (b/c ratio)

	D+|E|	D-|E|
Origin (0,0)	0.49	1.45
b_{1g} (0,0-(1579+309) cm^{-1})[a]	0.95	1.38
b_{2g} (0,0-309 cm^{-1})	0.83	1.67
b_{3g} (0,0-1579 cm^{-1})[a]	0.65	1.00

[a] See text for a discussion of assignment of these bands.

In addition, polarization of emission from the long-lived spin sublevel was measured by eliminating the inversion operation and monitoring the polarized emission in the tail of the phosphorescence decay to vibronic bands at 3629 Å and 3849 Å. Table VI-3 illustrates these data.

B. Discussion

The $T_1 \rightarrow S_0$ phosphorescence, because of its spin-forbidden nature, derives its transition probability from singlet states admixed into the triplet state via spin-orbit coupling (see Sections III-B and III-C). It has been shown that within molecules of relatively high point symmetries the triplet state spin sublevels generally exhibit selective spin-orbit coupling with excited singlet states; consequently, one and sometimes two spin sublevels contribute the majority of phosphorescence intensity (see Sections III-B and III-C).

A completely unambiguous assignment of the orbital symmetry of the triplet states requires, in addition to the polarization of the phosphorescence from the active spin sublevels, a knowledge of the magnetic orientation of these spin sublevels relative to the molecular axes. An explicit consideration of the spin-orbit symmetries for paradichlorobenzene (DCB) in both a $^3B_{1u}$ and a $^3B_{2u}$ state will easily demonstrate this requirement.

Zeroth order wavefunctions for each triplet sublevel, taken as a product of spatial (orbit) and spin functions, transform as the direct product of the irreducible representations of each part. Eigenfunctions

Table VI-3

b/c Polarization Ratios in the Phosphorescence Decay*

	Origin	b_{1g}	b_{2g}	b_{3g}
τ_y, τ_z (0-25 msec)	0.7	1.4	1.4	0.7
τ_x (200 msec - 1 sec)	0.5	0.8	1.1	0.6

* The a'c face shows similar a'/c ratios.

of the spin angular momentum operator transform, in zero magnetic field, as rotations which in the point group D_{2h} are B_{1g} (R_z), B_{2g} (R_y), and B_{3g} (R_x). Table VI-4 outlines the total spin-orbit symmetry of the sublevels for the above orbital symmetries for the lowest triplet state of paradichlorobenzene in D_{2h}.

An examination of Table VI-4 reveals that the only difference between the $^3B_{1u}$ and the $^3B_{2u}$ assignments are: (1) the spin-orbit symmetry of the τ_x spin sublevel, and (2) the magnetic orientation of the B_{3u} and A_u (τ_z or τ_y) spin-orbit states.

We have neglected to consider the two other possible symmetry assignments for the lowest triplet state in DCB (^3A_u and $^3B_{3u}$), since they correspond to $n\pi^*$ or $\sigma\pi^*$ configurations. Experimental evidence indicates a $\pi\pi^*$ configuration is correct. Early support for this contention came from the observation that the DCB $T_1 \rightarrow S_0$ absorption spectrum exhibits a significant amount of out-of-plane polarization.[93,110] Furthermore, the experimental values for the zero-field parameters D and D* ($D^* = (D^2 + 3E^2)^{1/2}$) of DCB differ by only a few percent from those of benzene.[32,112] Finally, measurement of the chlorine hyperfine interaction[32] indicates that the para-chlorines of DCB possess a much smaller spin density than might be expected for a $^3n\pi^*$ state.[113]

By analogy to benzene[112,114] and from previous studies of aromatic molecules in $\pi\pi^*$ triplet states,[115] it is reasonable to assume that in DCB the zero-field parameter D is positive and that the largest component of the electron spin-spin tensor in its principal axis system is along the molecular axis normal to the plane. In the coordinate system

0 0 0 0 3 9 0 6 4 7 3

Table VI-4

The Spin-Orbit Symmetries of the Individual Magnetic Sublevels in Paradichlorobenzene in the states $^3B_{1u}$ and $^3B_{2u}$

Orbital Symmetry	Magnetic Sublevel	Spin-orbit Symmetry	Vibrational Band Polarization* a_g	b_{1g}	b_{2g}	b_{3g}
	τ_y	B_{3u} $(n\pi^*)$	X	Y	Z	-
$^3B_{1u}$ $(\pi\pi^*)$	τ_z	A_u $(n\pi^*)$	-	Z	Y	X
	τ_x	B_{2u} $(\pi\pi^*)$	Y	X	-	Z
	τ_z	B_{3u} $(n\pi^*)$	X	Y	Z	-
$^3B_{2u}$ $(\pi\pi^*)$	τ_y	A_u $(n\pi^*)$	-	Z	Y	X
	τ_x	B_{1u} $(\pi\pi^*)$	Z	-	X	Y

* Z and Y are in-plane long and short axes, respectively, according to the coordinate system in Fig. VI-4, while X is out-of-plane.

illustrated in Figure IV-4, the lowest energy triplet sublevel would then be τ_x.

The observation that the long-lived (~600 msec) spin sublevel is common to both the 3.604 GHz (D-|E|) and 5.362 GHz (D+|E|) zero-field transitions, together with the above considerations, allows us to assign the lowest energy subelvel as the long-lived sublevel. The remaining spin sublevels, τ_y and τ_z, are then associated with spin eigenfunctions of the zero-field Hamiltonian asymmetry parameter E, and have either B_{3u} or A_u spin-orbit symmetry.

It is apparent from the delayed adiabatic inversion data listed in Table VI-1 that the B_{3u} and A_u spin-orbit states contribute most to the dipole activity in DCB phosphorescence. This activity and our observation that the lowest triplet state of DCB possesses two short-lived (lifetimes: 13±1.5 msec and 46±3 msec) and one relatively long-lived spin sublevel (~600 msec) can be understood when further aspects of the chlorine perturbations are considered more explicitly.

Intrinsic emission lifetimes of the triplet sublevels are inversely proportional to the radiative and/or radiationless transition probability, and thereby proportional to the amount of singlet character mixed into the triplet state primarily by spin-orbit coupling. The measured magnitudes of the DCB triplet sublevel lifetimes (τ_y and τ_z) are about a factor of 10^3 shorter than those of benzene.[123] This observation points to a significant amount of spin-orbit coupling presumably due to the addition of two chlorine nuclei to the benzene ring. A natural assumption then is that the most effectively spin-orbit coupled singlet states

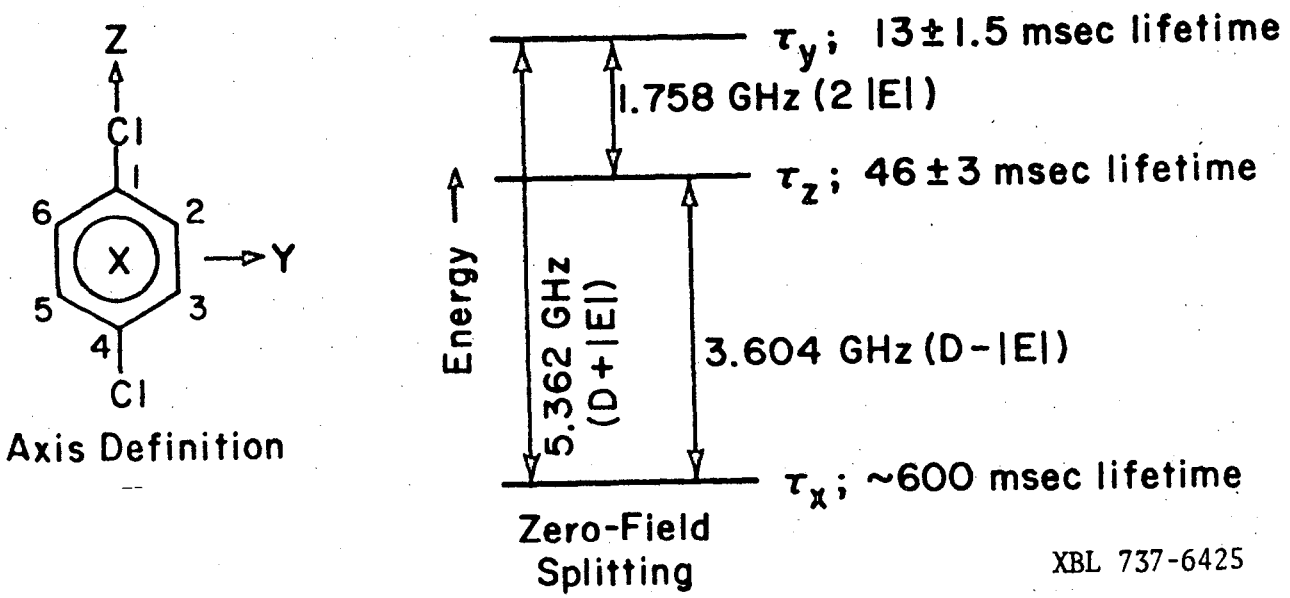

Figure VI-4 Para-dichlorobenzene zero-field splittings for the phosphorescent triplet triplet state in the coordinate system illustrated.

would be those states formed from molecular orbitals which include to a large degree the atomic orbitals of the two para-chlorines. The symmetries of these possible chlorine perturbing orbitals using all chlorine valence electrons except the out-of-plane p_π are b_{1u}, a_g, b_{2u}, b_{3g}.

The lowest unoccupied molecular orbital in benzene has e_{2u} symmetry.[124] In the point group D_{2h} the e_{2u} MO reduces to a b_{3u} and an a_u MO. Singlet states fashioned from the combinations of these molecular orbitals and the molecular orbitals admixed with para-chlorine atomic orbitals will transform as the direct products of their respective irreducible representations. Singlet states which might admix any electric dipole character into the triplet sublevels must be antisymmetric with respect to inversion. This restriction limits the consideration of possible perturbing singlet states to $^1B_{3u}$ ($b_{3g} \times a_u(B)$; $a_g \times b_{3u}(B)$) and ^1A_u ($a_g \times a_u(B)$; $b_{3g} \times b_{3u}(B)$) (where B denotes MO derived from benzene e_{2u} in D_{2h} symmetry). Also, the presence of carbon-chlorine bonds (as opposed to carbon-hydrogen bonds) would lower the energy of some $\sigma\pi^*$ states of A_u and B_{3u} symmetry relative to those in benzene. Finally, the A_u and B_{3u} states have one-center spin-orbit coupling matrix elements with the τ_z and τ_y sublevels while the $^1\pi\pi^*$ character associated with τ_x arises only from two-center spin-orbit terms.[125] Consequently one might expect most of the phosphorescence to originate from τ_y and τ_z as the experimental data demonstrate.

The ordering of the spin-orbit states in DCB has been established by determining which spin sublevel has the largest radiative dipole activity to the phosphorescence origin. Since in D_{2h} the spin sublevel

that transforms as A_u is formally dipole forbidden, the principal activity should be from the spin sublevel that transforms as B_{3u}. In the $^3B_{1u}$ or $^3B_{2u}$ states this would correspond to τ_y or τ_z, respectively. Delayed adiabatic inversion data illustrated in Fig. VI-2 and Table VI-1 demonstrate that the principal activity is from the upper spin sublevel. The important point of Fig. VI-2 is that the ratio of the radiative rates (τ_y/τ_z) is much greater than unity.

The order of the spin-orbit states is then ((τ_x)B_{1u} or B_{2u}) < A_u < B_{3u} (cf. Fig. VI-4). The orbital symmetry of the triplet state could now be concluded if the magnetic orientation of either the B_{3u} or A_u spin-orbit state could be established (cf. Table VI-4).

The application of an external magnetic field could, in principle, establish the magnetic orientation of these spin-orbit states. Such a field application has been attempted on DCB in this laboratory; however, the unfavorable orientation of the two molecules in the DCB unit cell prevented us from obtaining conclusive data by a low magnetic field ODMR study.

Further considerations of the possible chlorine perturbations on the benzene π molecular orbitals along with estimates of the in-plane electron spin-spin dipole interactions will show that the established order of the triplet spin-orbit states also leads to a definite orbital symmetry assignment.

In the absence of appreciable spin-orbit coupling contributions to the zero-field splittings, the effect on the carbon spin densities with the addition of chlorine substituents to a benzene ring can be understood

qualitatively in terms of the one-electron molecular orbitals that form the basis for the excited state. Figure VI-5 illustrates two possible perturbations that can occur with chlorine para-substitution. Since the chlorine out-of-plane p-orbitals (π) form linear combinations that transform as b_{2g} and b_{3u} in D_{2h} and since the energies of these orbitals would be approximately at the chlorine valence state ionization potential[122] and thus somewhere between the benzene[124] a_{2u} and e_{1g} orbitals, the $b_{2g}(2)$ MO derived from the benzene e_{1g} MO would be raised in energy while the predominantly chlorine $b_{2g}(1)$ MO would be lowered. The b_{3u} interactions unfortunately cannot be easily predicted from first order perturbation theory. Two possible orderings are apparent depending upon the magnitude of the chlorine-benzene interactions. First, the $b_{3u}(3)$ orbital derived from the benzene e_{2u} MO could be lowered via chlorine interactions. This would depend upon many factors, few of which can be even qualitatively estimated. The participation of <u>empty</u> chlorine d-orbitals would, for instance, lower this state relative to its $a_u(1)$ degenerate partner since the a_u state has a node through the para-positions and cannot interact with out-of-plane orbitals. The other possibility is for the $b_{3u}(3)$ MO to increase in energy via carbon-chlorine bonding. The more electronegative the substituent (as would be the case in fluorine substitution) the most likely this situation. In either of the above cases the symmetry of the lowest occupied MO in the ground state of DCB is expected to be $b_{2g}(2)$; therefore two excited state orbital symmetries can arise. B_{1u} is derived from a $b_{2g} \rightarrow b_{3u}$ transition while the state B_{2u} is derived from the transition $b_{2g} \rightarrow a_u$ (cf. Figs. VI-5 and VI-6).

These excited states may now be represented by properly anti-symmetrized wavefunctions formed from the appropriate molecular orbitals (see Section II-B). Thus,

$$B_{1u} = \frac{1}{\sqrt{2}} (b_{2g} b_{3u} - b_{3u} b_{2g})$$

and

$$B_{2u} = \frac{1}{\sqrt{2}} (b_{2g} a_u - a_u b_{2g})$$

Approximating the spin distribution in the molecular planes as delta function spins localized at the atomic centers, calculations of the electron spin-spin dipole interactions along the two in-plane molecular axes have been performed (see Appendix I). For generality, two other orbital state functions have also been considered. There are the two states which would be formed from excitation out of the high lying occupied b_{1g} MO into either the a_u or b_{3u} MO's and have state functions

$$B'_{1u} = \frac{1}{\sqrt{2}} (b_{1g} a_u - a_u b_{1g})$$

$$B'_{2u} = \frac{1}{\sqrt{2}} (b_{1g} b_{3u} - b_{3u} b_{1g})$$

Figure VI-7 illustrates on an arbitrary scale the relative energies for the B_{3u} and A_u spin-orbit states within each of the four possible lowest excited orbital states B_{1u}, B'_{1u}, B_{2u} and B'_{2u}. The possibility of

Figure VI-5 The one-electron π molecular orbitals of benzene and paradichlorobenzene with a qualitative assessment of two possible effects of the para-chlorine substitution.

0 0 0 0 5 9 0 4 7 7

Qualitative Effects of Parachlorine Substitution in the Benzene π-Orbitals.

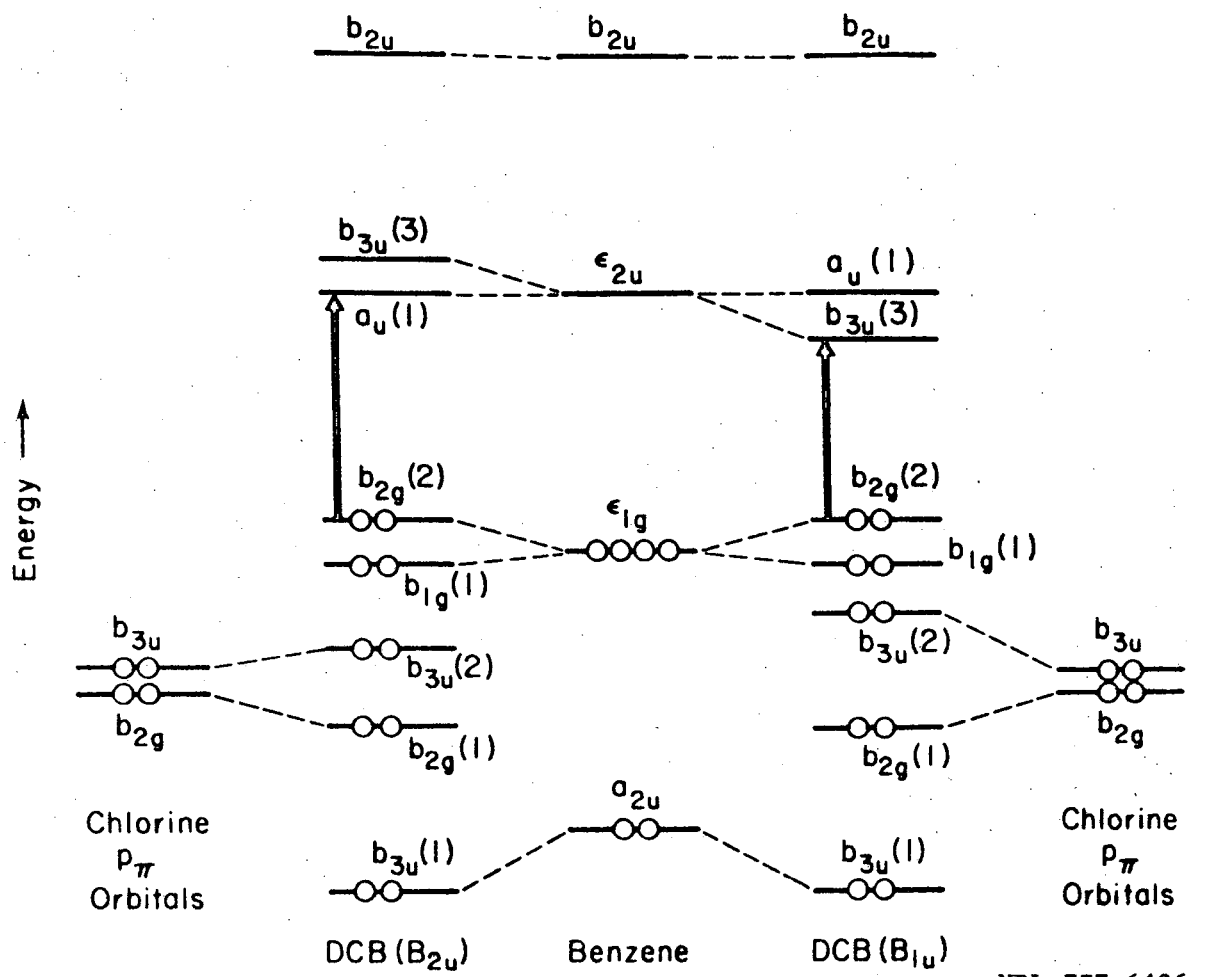

XBL 737-6426

Figure VI-5

Figure VI-6 The symmetries of various benzene one-electron molecular orbitals in D_{2h} along with approximate spin density distributions on the individual carbon atoms in the appropriate molecular orbitals.

0 0 0 0 3 9 0 0 4 7 8

Symmetry and Spin Density Distribution in Substituted Benzene One-Electron Molecular Orbitals.

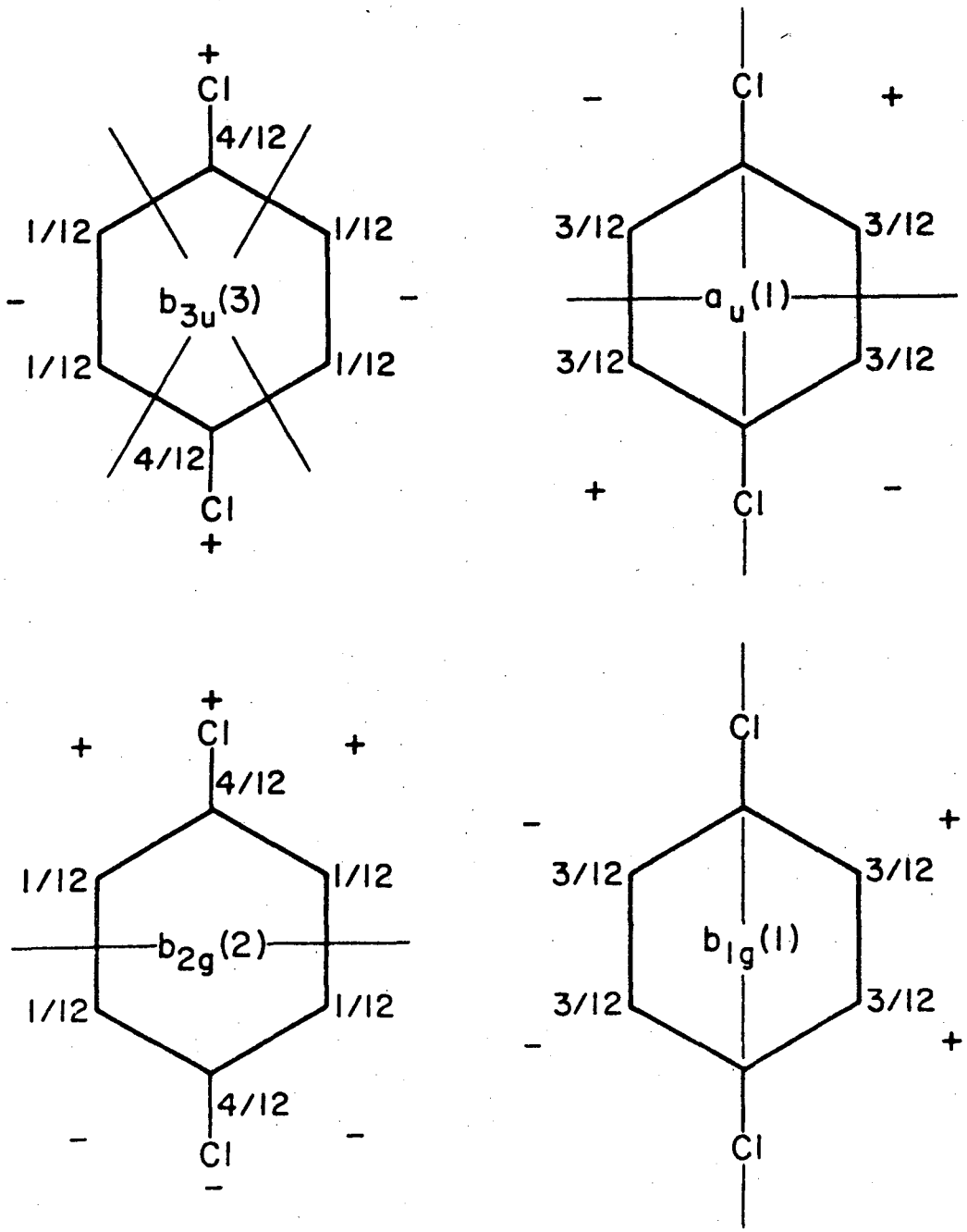

XBL 737-6427

Figure VI-6

Figure VI-7 Graphic representation of the relative energies of the DCB B_{3u} (broken line) and A_u (solid line) spin sublevels within the four triplet states of orbital symmetries B_{1u}, B'_{1u}, B_{2u} and B'_{2u} (see text). The influence of configurational mixing (between triplet orbital states of like symmetry) is included in terms of an angular mixing parameter, θ, such that $\theta = 45°$ denotes an equal admixture of the appropriate two orbital states. The vertical axis indicates energy on an arbitrary scale (see Appendix I).

(a) depicts the case where the B_{1u} orbital state lies lowest (i.e., the B_{1u} state is the T_1 state) and shows the relative B_{3u} and A_u spin sublevel energies within both the B_{1u} (T_1) orbital state and the necessarily higher lying B'_{1u} orbital state. The relative energies of the two spin sublevels are shown within both orbital states as a function of the amoung of configurational mixing (θ) occurring between the two orbital states. (b), (c) and (d) similarly depict the relative spin sublevel energies for cases in which the B'_{1u}, B_{2u} and B'_{2u} orbital states lie lowest in energy, respectively. Note that the B_{3u} spin sublevel of the lowest orbital state lies higher than the A_u spin sublevel only in (a).

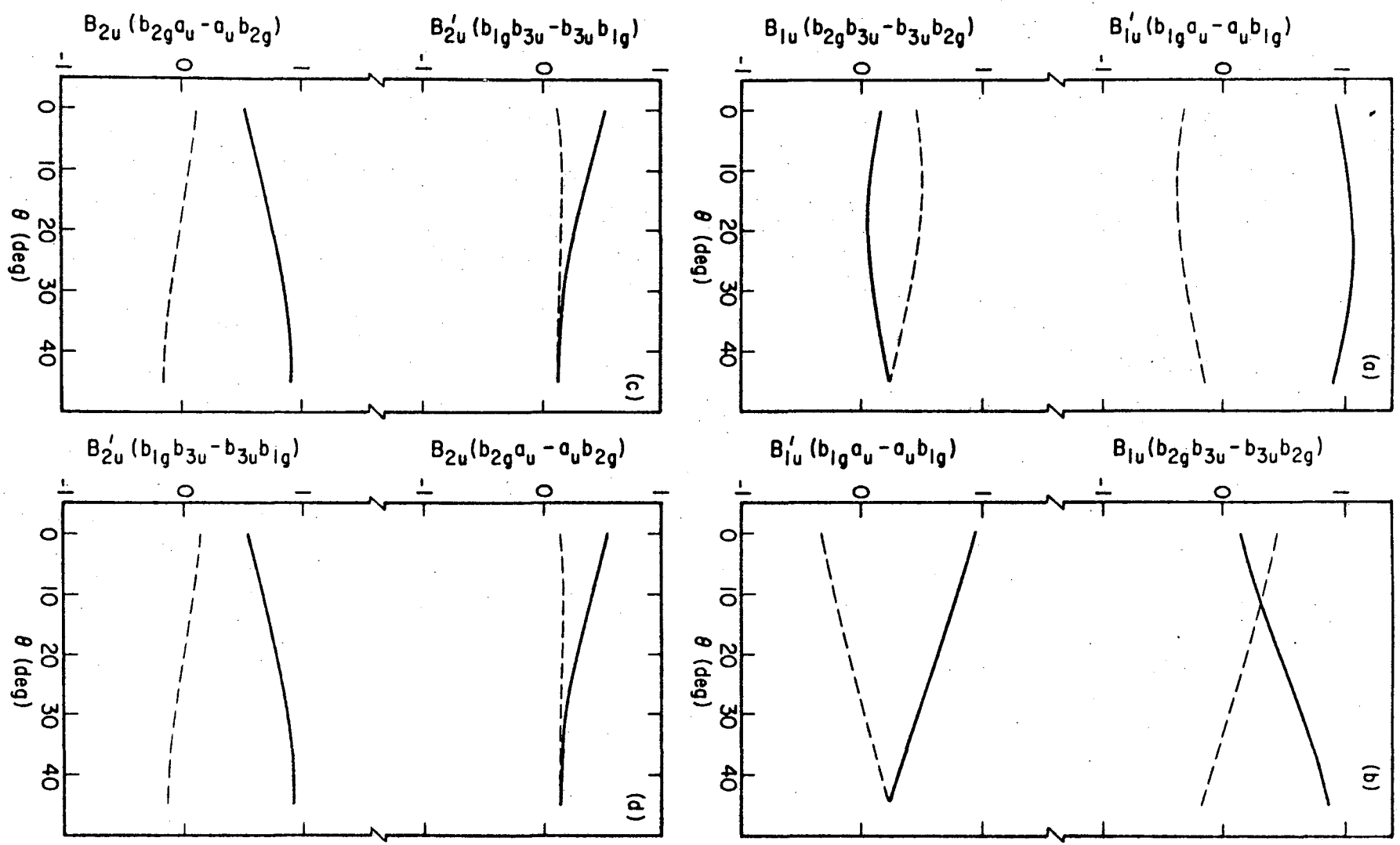

XBL 737-6428

Figure VI-7

configurational mixing has been included in the calculations and Fig. VI-7 shows the relative A_u(SO) and B_{3u}(SO) energies for varying degrees of mixing.

The delayed inversion data (Table VI-1) has conclusively established that the spin-orbit states lie $B_{3u} > A_u > X(B_{1u}$ or $B_{2u})$, and Fig. VI-7 shows that this ordering of SO states may be associated with <u>only</u> the B_{1u} ($b_{2g} \rightarrow b_{3u}$) lowest triplet state. Thus, by the experimentally established order of the tripl spin-orbit states, the orbital symmetry of the DCB phosphorescent triplet state is conclusively assigned as $^3B_{1u}$ with $Y(B_{3u}) > Z(A_u) > X(B_{2u})$ in energy.

The $^3B_{1u}$ assignment is further substantiated by polarization measurements (cf. Table VI-3) taken while monitoring emission from the DCB crystallographic bc face[111] in the tail of the phosphorescence decay to vibrational bands at 3529 Å (0,0-309 cm^{-1}) and 3849 Å (0,0-(1579+309) cm^{-1}) which have been assigned as a b_{2g} fundamental[93,126] and a $b_{1g}(b_{3g} \times b_{2g})$ combination band,[127a,b] respectively. These measurements indicate that emission from the long-lived sublevel (τ_x) is out-of-plane polarized to the b_{1g} band, while polarization is mixed to the b_{2g} band. In addition, phosphorescence from τ_x to the b_{1g} band is about two and one-half times as intense as that to the b_{2g} when the emission is normalized to their respective total phosphorescence intensity. These data point to a B_{2u} spin-orbit symmetry for the τ_x sublevel consistent with the $^3B_{1u}$ orbital assignment (cf. Table VI-4).

We have excluded from discussion vibronic coupling in the singlet and triplet manifolds. This topic deserves special attention and is the subject of another investigation.[128]

While the ODMR techniques employed in this study have helped remove the primary ambiguities (i.e., spin sublevel origins of phosphorescence), the present observations of DCB phosphorescence are subject to other ambiguities which also plagued previous investigators, i.e., crystal field effects and possible changes in the excited state geometry. In fact, both the polarized and nonpolarized inversion data (Tables VI-1 and VI-2) point to a significant relaxation of D_{2h} symmetry restrictions in the phosphorescence emission.

The D_{2h} symmetry restrictions require that emission to any totally symmetric vibration should originate from the τ_y (B_{3u}) sublevel, while the τ_z (A_u) sublevel should be completely inactive to such vibrations. The measured value of the radiative rate constant ratio for $\tau_y(B_{3u}):\tau_z(A_u)$ to the origin (Table VI-1) is only about 4:1. Moreover, while emission from τ_y shows predominantly out-of-plane polarization as expected, emission from τ_z displays a slight in-plane polarization. Further, it is found that the primary emission route to <u>every</u> vibrational band in the phosphorescence spectrum is from the τ_y (B_{3u}) sublevel, and that every band also derives a significant amount of intensity from the τ_z (A_u) sublevel. This can be seen from the ratios reported in Table VI-1 which are approximately equal to the spin sublevel radiative rate constant ratios for the vibrational bands listed. The PMDR spectra shown in Fig. VI-1 clearly reveal that all optical transitions are coupled by all three microwave transitions.[24]

The vibrational band found at 3804 Å (0,0-1579 cm^{-1}) is most perplexing in this respect. This band has been assigned as an a_g fundamental by some investigators.[93,129,130] PMDR spectra (Fig. VI-1) clearly show that it behaves differently than other a_g vibrations. A tentative b_{3g} assignment was therefore made on the basis of reported laser Raman studies;[126] however, the microwave inversion data subsequently failed to display the expected b_{3g} behavior for this band. Any b_{3g} band in the phosphorescence spectrum would be expected to exhibit a reversal of activity from spin sublevels τ_y and τ_z compared to the origin (or any totally symmetric vibration). Even taking into account a slight relaxation of symmetry restrictions we would expect most of its intensity to be derived from the τ_z ($A_u \times b_{3g} = B_{3u}$) sublevel. Our observations, in fact, show a marked increase in emission from the τ_z sublevel in the PMDR's. However, most of the emission remains from τ_y, as evident from the radiative rate constant ratios from τ_y and τ_z, i.e., $k_{r_{\tau_y}}^{(0,0-1579)}:k_{r_{\tau_z}}^{(0,0-1579)} = 1.4:1$. These anomalous characteristics allow us to <u>suggest</u> that the (0,0+1579 cm^{-1}) band is, in actuality, associated with both an a_g and a b_{3g} vibration which our instruments were unable to resolve.[127b]

A definitive explanation for the mixed phosphorescence observed in DCB is beyond the scope of data currently available. We have, however, considered various possibilities. Explicit considerations of the crystal field effects focussed on the surrounding chlorine atoms, since the reduction of molecular symmetry D_{2h} to C_i site symmetry would occur in all likelihood via the chlorine crystal field contributions (e.g., the heavy

atom effect). An analysis of the DCB crystal structure[111] shows that the sum of weighted $(1/|r|^2)$ vectors from each of the 24 nearest chlorine atoms surrounding any DCB molecule yields a resultant vector $0.87\ \hat{x} + 0.31\ \hat{y} + 0.38\ \hat{z}$, relative to the DCB molecular axes. Such a field vector could mix both the in-plane zero-field spin sublevels and the out-of-plane spin sublevel with each in-plane spin state. Obviously, this chlorine-field vector possesses suitable geometry to account for the mixed DCB phosphorescence, but a quantitative assessment of the strength of the external chlorine influence will be necessary before we can venture any definite conclusions.

Aside from crystal-field effects, the relaxation of symmetry restrictions observed in DCB trap phosphorescence might also be due to a distortion of the molecule itself. However, the question of the exact nature of this distortion remains as yet unanswered. The distortion may be caused by a rearrangement of the nuclear skeleton either under the influence of the excited state electronic potential or as an inherent characteristic of the trap. It is noteworthy, however, that the chlorine field gradient in the excited state is substantially lower than in the ground state. As has been discussed[32] this can be due in part to a distortion and in part to increased carbon-chlorine π bonding in the excited state. The average decrease in chlorine field gradients in $\pi\pi^*$ states in those molecules thus far investigated where no distortion is suspected is about 3% (8-chloroquinoline,[31] 1,2,4,5-tetrachlorobenzene,[128] and 1,4-dichloroquinoxaline[131]). An average decrease of 3%

may well represent the increased π character of the C-Cl bond. DCB, on the other hand, shows an 8% decrease in the chlorine field gradient. Perhaps the additional 5% decrease is due to an out-of-plane chlorine distortion. The PMDR and inversion data do not exclude this possibility. Further experiments are needed to resolve this question adequately.

VII. p-DICHLOROBENZENE -- ENVIRONMENTAL EFFECTS

Although our preliminary investigation of the DCB T_1 state achieved its primary objective with the conclusion of a $^3B_{1u}$ orbital symmetry assignment for the state, it also left many questions concerning the seemingly "anomalous" mixed phosphorescence of the DCB x-trap largely unanswered. Our succeeding efforts were therefore directed toward the establishment of suitable explanations for this "anomalous" phosphorescence.

At the conclusion of the preliminary DCB investigation two possible explanations were proposed. DCB x-trap phosphorescence might be understood in terms of a distortion of the x-trap molecule from the D_{2h} configuration, either under the influence of the T_1 state electronic potential or as an inherent characteristic of the trap itself. Alternatively, the observed mixed DCB x-trap phosphorescence might be explained in terms of an external crystal field effect, e.g., external heavy atom effect.

Kothandaraman and Tinti recently completed a study of the properties of the T_1 states of several di-substituted benzenes in xylene host crystals.[44] Their results for the p-dichlorobenzene T_1 state within a p-xylene host crystal (DCB/PXY) are listed in Tables VII-1,2. These data strongly suggest that external spin-orbit coupling contributions to the DCB x-trap T_1 state are significant and must be considered to explain the anomalous phosphorescence of the DCB x-trap. They found that the DCB/PXY T_1 state exhibits essentially the same chlorine quadrupole frequencies as does the DCB x-trap. Therefore, the excited state geometry

Table VII-1

Zero-Field Splitting Parameters in DCB/Host Systems

	$\nu_{0,0}$ (cm^{-1})	D (MHz)[a]	E (Mhz)[a]
DCB/PXY[b]	27410	4323.5	-684.5
DCB-h_4/DCB-d_4	27886	4517.0	-928.5
DCB x-trap	27865[c]	4483[d]	-878[d]
DCB/DBB	27863	4446	-860

[a] D = 3/2 X and E = 1/2(Z-Y) where the X axis is normal to the molecular plane and the Z and Y axes are the long and short in-plane axes, respectively, as shown in Fig. VI-4.

[b] Reference 44.

[c] Reference 43.

[d] Reference 32.

Table VII-2

DCB T_1 State Properties in Various DCB/Host Systems

	Lifetimes (msec) (±10%)	Relative Radiative Rates (Emission Band) (±10%)		Relative Populating Rates (Host Excitation Band) (±20%)	
		(0,0)	b_{2g}	S_1	T_1
DCB/PXY 1.2°K [a]					
Y	14	50	100	25	-----
Z	142	1.2	6.2	25	-----
X	1470	1.0	1.0	1	-----
DCB-h /DCB-d 1.4°K					
Y	20	43	5	3	1.8
Z	78	1.0	1.0	5	1.0
X	~400	< 1.0	< 1.0	1	<< 1.0
DCB x-trap 1.3°K [b]					
Y	13	4.1	4.6	-----	-----
Z	46	1.0	4.6	-----	-----
X	~600	-----	-----	-----	-----

Table VII-2 (continued)

	Lifetimes (msec) (±10%)	Relative Radiative Rates (Emission Band) (±10%)		Relative Populating Rates (Host Excitation Band) (±20%)	
		(0,0)	b_{2g}	S_1	T_1
DCB x-trap 1.4°K					
Y	13.5	30	-----	2.5	1.7
Z	38	5.0	-----	3.0	1.0
X	~400	1.0	-----	1.0	1.4
DCB/DBB 1.2°K[c]					
Y	11	5.2	15	-----	-----
Z	20	3.6	5.0	-----	-----
X	93	1.0	1.0	-----	-----
DCB/DBB 1.4°K					
Y	12	7.0	-----	1	1
Z	17	5.0	-----	3	1
X	79	1.0	-----	2	1

[a] Reference 44.

[b] Reference 43.

[c] G. Kothandaraman, unpublished results.

must be quite similar within both systems. Yet, unlike the DCB x-trap, the DCB/PXY phosphorescence displays strict D_{2h} symmetry selection rules, as evidenced by the absence of dipole activity from the A_u spin-orbit state (see coordinate system, Fig. VI-4) to the phosphorescence (0,0) band (and other totally symmetric vibronic bands).

PMDR spectra (Fig. VII-1)[43] also illustrate the strict observance of D_{2h} selection rules within the DCB/PXY phosphorescence and further show that the phosphorescence band near (0,0-1579 cm^{-1}) actually consists of two bands, a b_{3g} (0,0-1574 cm^{-1}) and an a_g (0,0-1577 cm^{-1}) fundamental. Thus, the earlier suggestion of the preliminary DCB investigation (Section VI-B) regarding the nature of the corresponding x-trap emission band appears to be correct.

In the following investigation, we intend to more completely characterize the nature of crystal influences on the DCB T_1 state in various crystalline environments and, at the same time, explore the nature of the DCB neat crystal x-trap.

A. Experiment and Results

1. Systems Chosen for Study and Comparison

To complement previous studies of the DCB T_1 state we have chosen to conduct experiments on the DCB x-trap T_1 state as well as on DCB/DBB and DCB-h_4/DCB-d_4 phosphorescent triplet states. The DCB-h_4/DCB-d_4 system was chosen for the obvious reason that the difference in nuclear potentials of DCB-h_4 vs. DCB-d_4 causes the DCB-h_4 T_1 state to form an

Figure VII-1 †

(a) phosphorescence spectrum of DCB/PXY.

* denotes the DCB trap origin (27410 cm^{-1}).

** denotes an unidentified trap origin, most probably due to either a DCB dimer or a DCB trap modified by an anomalous local PXY host structure.

\+ denotes the vibronic band near (0,0-1575 cm^{-1}) which the PMDR spectra reveal is actually two nearly coincident fundamentals; an a_g at (0,0-1577 cm^{-1}) and a b_{3g} at (0,0-1574 cm^{-1}) (see text).

++ denotes the coincident $b_{1g}(b_{2g} \times b_{3g})$ and $b_{2g}(b_{2g} \times a_g)$ combination bands built off of these fundamentals.

(b) $2|E|$ zero-field PMDR spectrum of the DCB/PXY system.

(c) $D+|E|$ zero-field PMDR spectrum of the DCB/PXY system.

† These spectra taken in this laboratory by W. G. Breiland.

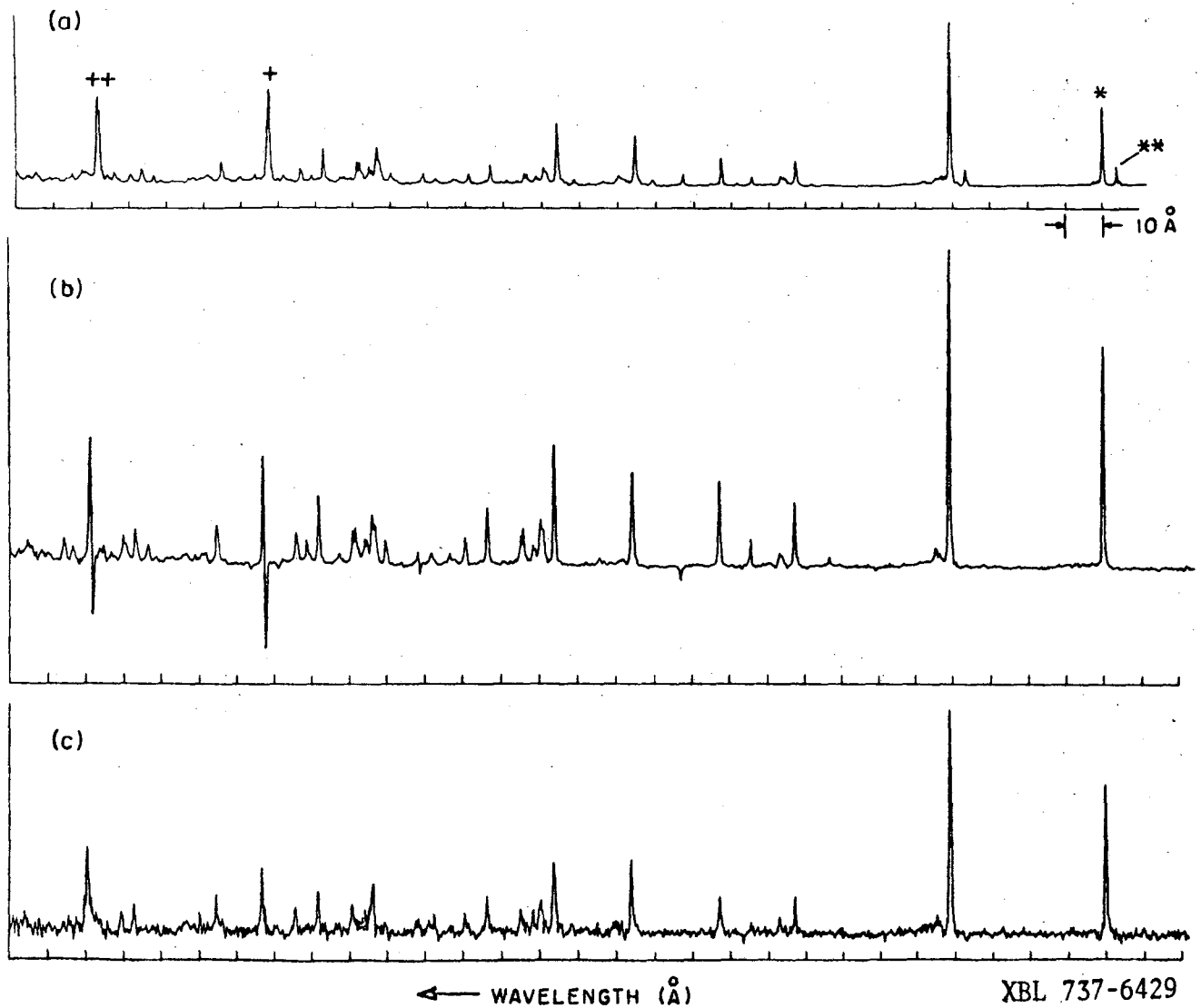

Figure VII-1

intrinsic trap relative to the DCB-d_4 T_1 exciton band. Thus the phosphorescent triplet state is expected to rest on an isomorphously equivalent molecular site. The x-trap T_1 state of the DCB neat crystal, on the other hand, is not necessarily required to rest on any such isomorphously equivalent molecular site. A comparison of experimental results for these two systems should thereby elucidate many aspects of the nature of DCB crystal field influences on the DCB T_1 state and of the DCB x-trap itself.

A similar reasoning applies to the choice of the DCB/DBB system. The structure of the para-dibromobenzene (DBB) host crystal is very much the same as that of DCB. Therefore, the crystal field influence on the DCB trap T_1 state from the DBB host crystal should be nearly the same as that of the DCB crystal except for the replacement of chlorine atoms with bromine atoms on the molecules which surround the phosphorescent T_1 state. Data collected on this system should then allow a semi-quantitative scaling factor to be designated for the magnitude of any external heavy atom effects of the crystal field.

2. Sample Preparation

Samples of p-dichlorobenzene (DCB) were purified by extensive zone refining (200 passes at approximately 2 in/hr).

Samples of p-dibromobenzene (DBB) were purified by first passing a solution of DBB in spectrograde cyclohexane through a column of alumina. The DBB collected from recrystallization out of this solution was then vacuum sublimed several times.

Samples of p-dichlorobenzene-d_4 were prepared by performing five successive exchanges of DCB-h_4 with concentrated deuterium sulfate according to the procedures of Renaud, Kovachic and Letich.[132] The recovered DCB-d_4 was then vacuum sublimed and extensively zone refined (200 passes at approximately 2 in/hr).

Single cyrstals of near DCB as well as 1% m/m DCB/DBB and 1% m/m DCB-h_4/DCB-d_4 mixed crystals were grown by standard Bridgeman techniques in vacuo.

All experiments were performed on single crystals which were mounted inside a slow wave helix affixed to a section of 50 Ω rigid coaxial rod and suspended in a liquid helium dewar which could be pumped to temperatures below 4.2°K. Details of the experimental arrangement are described in Section V-B.

3. ODMR and PMDR Spectra

The zero-field optically detected magnetic resonance (ODMR) spectra of DCB-h_4/DCB-d_4 and DCB/DBB mixed crystals were obtained monitoring appropriate trap phosphorescence bands at 1.4°K, using phase detection as described in Section V-B. PMDR spectra of the DCB/PXY, DCB/DBB and DCB-h_4/DCB-d_4 systems were also obtained at 1.4°K using phase detection as described in Section V-B.

The measured zero-field splittings of the DCB/DBB and DCB-h_4/DCB-d_4 T_1 states are listed in Table VII-1 in terms of the zero-field parameters D and E. The $D+|E|$ ODMR spectrum of DCB/DBB is illustrated in Fig. VII-2. An important feature of the DCB/host ODMR spectra is the observation that

the frequencies of chlorine quadrupole transitions observed in the fine structure of DCB T state ODMR spectra were virtually identical for all DCB/host systems studied. Phosphorescence and various PMDR spectra for the DCB/DBB and DCB-h_4/DCB-d_4 systems were obtained at 1.4°K with a 20 μ slit width on the optical spectrometer. These spectra are illustrated in Figs. VII-3 and VII-4.

4. Delayed Inversion Experiments

Delayed adiabatic inversion experiments were conducted at 1.4°K for DCB x-trap, DCB-h_4/DCB-d_4 and DCB/DBB systems and again at 1.2°K for the DCB/DBB and DCB-h_4/DCB-d_4 systems. These experiments were conducted employing essentially the same procedures used in the preliminary study and yielded accurate measurements of the total decay lifetimes of all three triplet spin sublevels as well as values for the relative radiative rate constants from individual spin sublevels to various vibronic bands in the phosphorescence spectrum. Lifetime values were obtained from the intensity decay following the delayed adiabatic inversion of spin-sublevel populations, and relative radiative rate constant values were obtained from the ratios of the intensities of appropriate delayed inversion signals. These data are listed in Table VII-2.

Additional information was obtained from these experiments in the form of relative populating rates into the individual triplet spin sublevels. A least-squares computer fit program[134] aided in the decomposition of intensity decays which followed a flash (~50 μsec) excitation. Flash decay curves were decomposed into their three exponential decay components and values of the fractional intensity from all three triplets

0 0 0 0 3 9 0 0 4 8 7

Figure VII-2

D+|E| ODMR spectrum of the DCB/DBB T_1 state.

A - denotes the pure electronic transition

B - denotes chlorine quadrupole wings (see Reference 32).

C - denotes ^{81}Br quadrupole wings.

D - denotes ^{79}Br quadrupole wings.

Frequencies differences between the Br quadrupole wings correspond to p-DBB ground state quadrupole frequencies at ~1.4°K.[a]

[a] G. K. Simin and E. I. Defin, Zh. Struk. Khim. 1, No. 2, 252 (1960); 1, No. 4, 464 (1960).

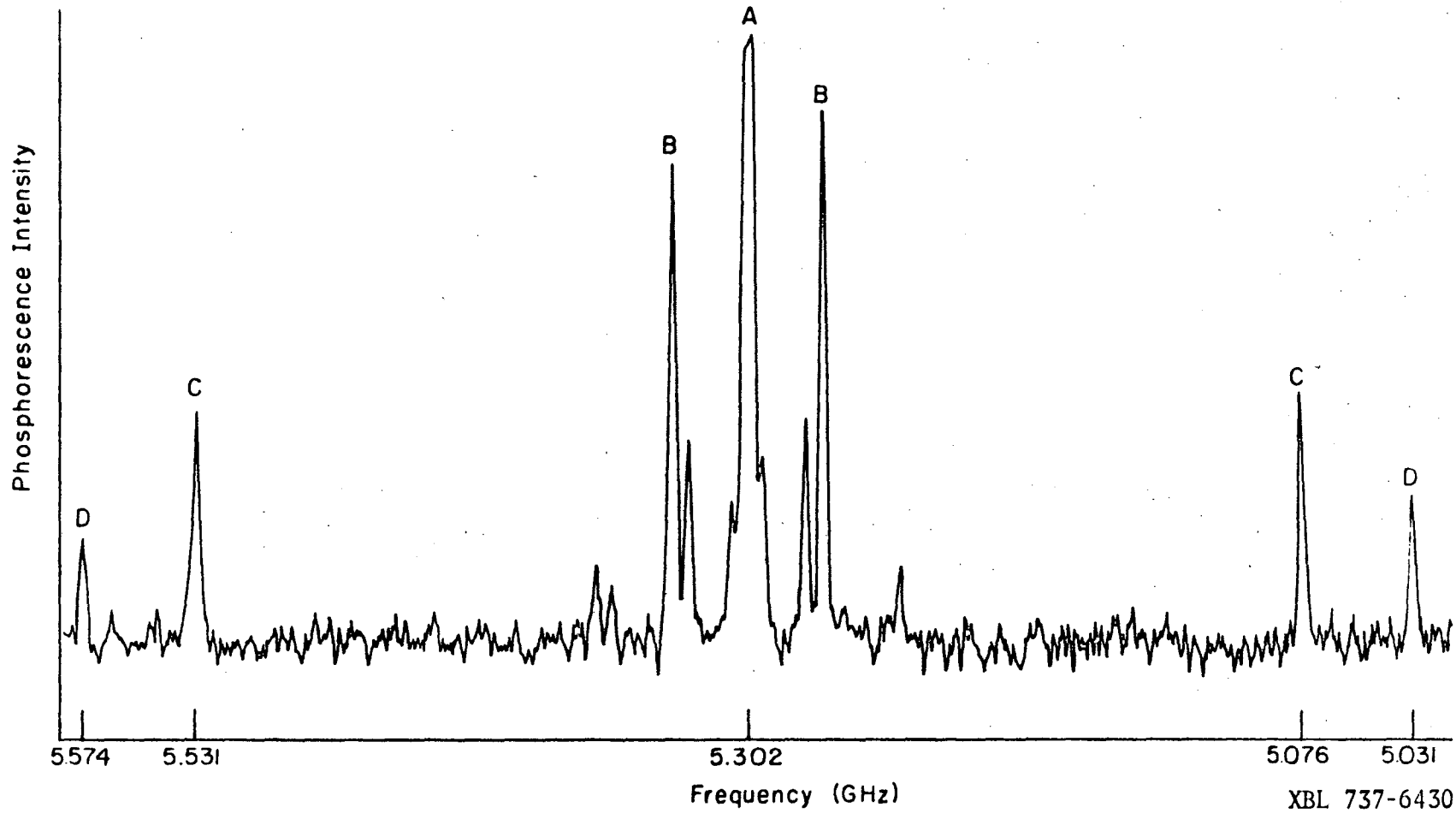
Phosphorescence Intensity
D
C
B
A
B
C
D
5.574
5.531
5.302
5.076
5.031
Frequency (GHz)
XBL 737-6430

Figure VII-2

0 0 0 0 3 9 0 0 4 8 8

Figure VII-3

(a) Phosphorescence spectrum of the DCB/DBB phosphorescent triplet state.

* denotes the DCB electronic origin (27863 cm^{-1}).

\+ denotes the coincident b_{3g} and a_g fundamentals near (0,0-1575 cm^{-1}) (see text).

(b) D+|E| zero-field PMDR spectrum of DCB/DBB system.

(c) D-|E| zero-field PMDR spectrum.

(d) 2|E| zero-field PMDR spectrum.

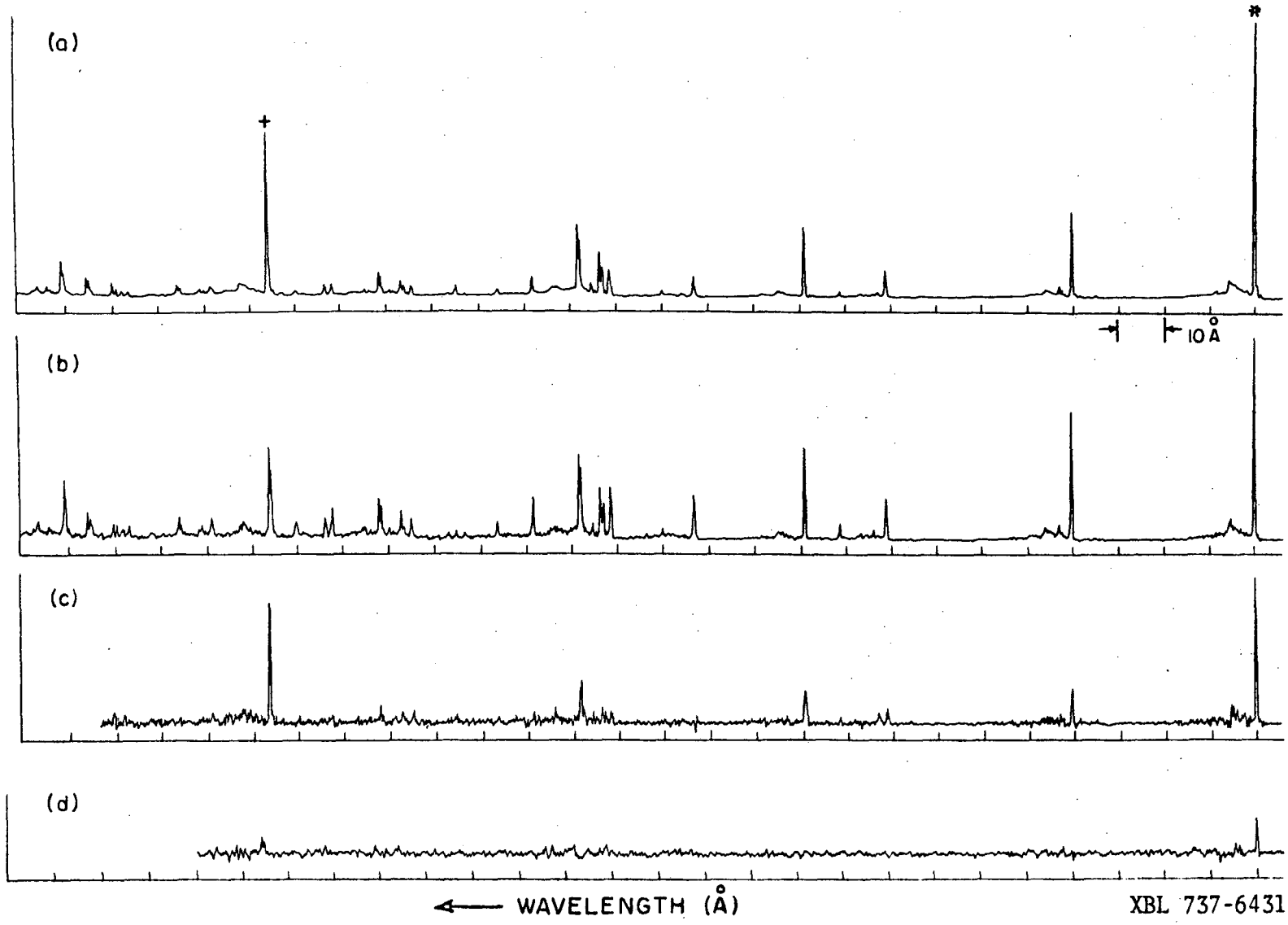

Figure VII-3

0 0 0 0 3 9 0 0 4 8 9

Figure VII-4

(a) Phosphorescence spectrum of the DCB-h_4/DCB-d_4 system.

* denotes the DCB-h_4 phosphorescence origin (27886 cm^{-1}).

** denotes most probably the DCB-d_4 x-trap phosphorescence origin.

\+ denotes the position of partially resolved b_{3g} and a_g fundamentals.

++ denotes the $b_{1g}(b_{2g} \times b_{3g})$ and $b_{2g}(b_{2g} \times a_g)$ combination bands built off of these fundamentals.

(b) $2|E|$ zero-field PMDR spectrum of the DCB-h_4/DCB-d_4 T_1 state.

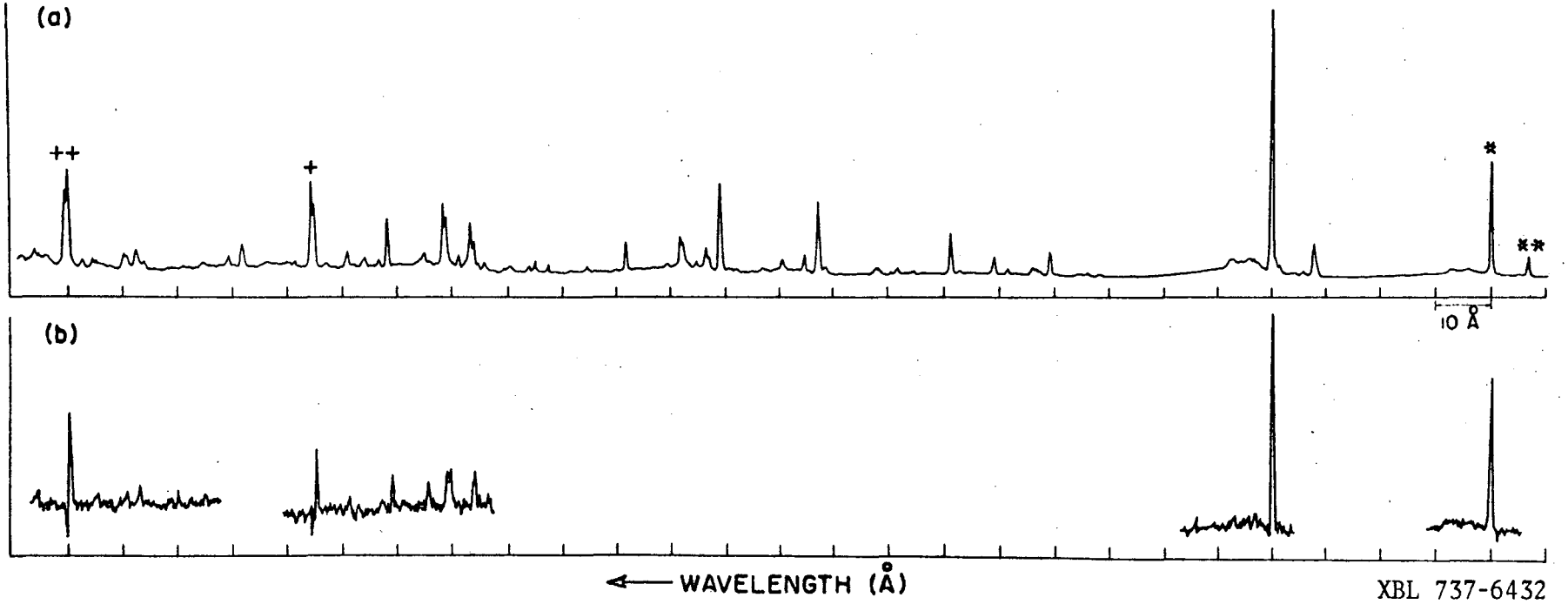

Figure VII-4

spin sublevels were obtained and extrapolated to time t = 0. In this manner, the relative populations of individual spin sublevels were obtained at t = 0 once the relative radiative rates were known, or conversely (as in the case of DCB-h_4/DCB-d_4) relative radiative rates were obtained once the relative populations of the spin-sublevels at t = 0 were known. Since excitation was effectively from an "instantaneous" source, then relative populations at t = 0 reflect the correct values for the relative populating rates into the individual triplet spin-sublevels.

Values for the time t = 0 relative populations of the triplet state spin sublevels were obtained for each system under the influence of excitation into two distinct energy regions. The first excitation band was obtained by filtering the emission from the flash lamp (100 J Xenon) through a Schott 2500 Å interference filter and gave excitation into the 2500-2800 Å region. A second excitation into the 3100-3550 Å region was produced by filtering the flash lamp emission through a Schott 3100 Å interference filter in conjunction with a Corning 0-54 pyrex glass filter and a one centimeter pyrex cell containing a 0.5 M DCB in benzene solution. For the solid systems with which we are concerned, the 2500-2800 Å and 3100-3550 Å excitation bands served to excite the samples into their lowest excited singlet band and lowest excited triplet band respectively. The measured values of the relative populating rates into the individual triplet spin-sublevels of each sample are included in Table VII- 2 for excitation into both regions.

B. Discussion

Initially, the most important comparisons are to be made between the properties of the DCB T_1 state in the DCB/PXY system and in the DCB-h_4/DCB-d_4 system. The DCB/PXY system may be approximated as demonstrating a DCB T_1 state under "free molecule" conditions, i.e., in the absence of any external heavy atoms. Results from this system therefore exhibit the characteristics of a DCB T_1 state with only internal spin-orbit coupling contributions. An examination of Table VII-1 shows that all of the data concerning the dynamic characteristics of this system are consistent with the "free molecule" interpretation. As we have already mentioned, Table VII-1 shows that the DCB/PXY phosphorescence clearly follows the expected D_{2h} symmetry selection rules. Moreover, Table VII-1 shows that spin-orbit coupling occurs primarily into the A_u and B_{3u} spin-orbit states of the DCB/PXY system as would be predicted from group theoretical considerations only (see Section VI-B).[43] This conclusion is supported by the DCB/PXY relative populating rate data for S_1 state excitation and by the measured values for the lifetimes of the three DCB/PXY triplet spin sublevels. For excitation into the S_1 state (first excited singlet state) the relative populating rates correspond to relative intersystem crossing rates from the DCB S_1 state into each of the three triplet spin sublevels. Since intersystem crossing rates are roughly proportional to the amount of singlet character which has been admixed into the individual triplet spin sublevels, principally through spin-orbit coupling (see Section III-C, equation III-33), the relative intersystem crossing values of $25(B_{3u}):25(A_u):1(B_{1u})$

for the DCB/PXY system indicate a large preference of spin-orbit coupling into the A_u and B_{3u} spin-orbit states. Additional indications in this respect are seen when the lifetimes of the three DCB/PXY spin sublevels are compared to the corresponding benzene phosphorescence lifetime.[133] Since total decay lifetimes are, to a crude approximation, inversely proportional to the singlet character within the spin sublevel (see Section III-C, equation III-32), the measured values of 14 msec (B_{3u}), 142 msec (A_u) and 1.47 sec (B_{2u}) for the three DCB/PXY T_1 lifetimes again point to preferential spin-orbit coupling into the A_u and B_{3u} spin-orbit states, and B_{3u} spin-orbit states, representing approximate reduction factors of 10^3 (B_{3u}), 10^2 (A_u), and 10^1 (B_{2u}) over the benzene phosphorescence lifetime (~12 sec at 20°K).[133]

The relative radiative rate data offer an explanation for the apparent discrepancy between the relative intersystem crossing data ($A_u \approx B_{3u}$) and the measured lifetimes ($B_{3u} \approx A_u/10^1$). That is, the relative radiative rates of the B_{3u} and A_u spin-orbit states to the b_{2g} (0,0-303 cm^{-1}) phosphorescence band (to which they are <u>both</u> dipole allowed) shows that the singlet state(s) admixed into the A_u spin-orbit state must possess a much lower oscillator strength than that which is admixed into the B_{3u} spin-orbit state. The A_u lifetime would thus be expected to be longer than the B_{3u} lifetime. Also, the relative intersystem crossing rate data fail to consider the actual details of the populating mechanism (i.e., vibronic overlap factors, etc.) and therefore cannot be relied upon as a strict quantitative measure of the magnitude of spin-orbit coupling contributions.

With the preceeding considerations in mind, we will therefore take the DCB/PXY system to illustrate the dynamic characteristics of the DCB T_1 state when only magnetic contributions from the electron spin-spin dipolar interaction and the internal spin-orbit interactions are included.

If we now consider the DCB-h_4/DCB-d_4 system, we may ascertain the contributions to the phosphorescent triplet state wave functions due to the external spin-orbit coupling influences of the DCB neat crystal. The data list in Table VII-1 demonstrate several significant characteristics of the DCB-h_4/DCB-d_4 T_1 state. First, measured ^{35}Cl and ^{37}Cl quadrupole frequencies for the DCB-h_4/DCB-d_4 T_1 state (~32-33 MHz and ~25-26 MHz, respectively) are unchanged from those of the DCB-PXY T_1 state, indicating that no significant change in the T_1 state nuclear geometry has occurred which could change the σ-π mixing of the chlorine electron distribution. Secondly, the D_{2h} symmetry selection rules appear to be maintained within the DCB-h_4/DCB-d_4 system. The overall appearances of phosphorescence and PMDR spectra of this system are quite similar to those of the DCB/PXY system. The relative radiative rate data show that, as in the DCB/PXY system, the transition from the A_u spin-orbit state to the phosphorescence origin is still dipole forbidden. Finally, the data indicate that the change from the DCB/PXY system to the DCB-h_4/DCB-d_4 has markedly increased the singlet character of both the A_u and B_{2u} spin-orbit states while leaving the B_{3u} spin-orbit state relatively unaffected. These increases in the A_u and B_{2u} singlet characters are demonstrated by the observed decreases in the total decay lifetimes of these states as well as their increased intersystem

crossing rates relative to the B_{3u} spin-orbit state. Consistent with these observations, the DCB-h_4/DCB-d_4 A_u spin-orbit state additionally exhibits increased radiative activity to the dipole allowed b_{2g} phosphorescence band.

It should be noted that the lifetime data and intersystem crossing rate data are both subject to influence from spin-lattice relaxation. The presence of this additional relaxation mechanism within the DCB/host systems, as indicated in Table VII-2 by lifetime data taken at various temperatures, therefore necessitates the use of a certain degree of caution when analyzing dynamic rate data for these systems.

Our confidence in the conclusion that external spin-orbit coupling in the DCB-h_4/DCB-d_4 system affects only the A_u and B_{2u} T_1 spin-orbit states is, however, reinforced by one further consideration. That is, the conclusion is consistent with our previous observation that the DCB-h_4/DCB-d_4 phosphorescence appears to adhere to the D_{2h} symmetry selection rules. As long as external influences can only affect a mixing between the inactive B_{2u} (which has only three center, $\pi\pi^*$ singlet character) and the A_u (which has an $n\pi^*$ or $\sigma\pi^*$ singlet character of low oscillator strength to the ground state) spin-orbit states, then the dipolar selection rules cannot become significantly relaxed from those of the DCB/PXY system.

Following arguments similar to those which we have just presented for the DCB/PXY and DCB-h_4/DCB-d_4 systems, our analysis of the DCB x-trap and DCB/DBB data (Table VII-2) provided some additional information. Consider first the DCB x-trap data. Since we have eliminated (due to

lack of any measurable difference between the DCB/PXY, DCB-h_4/DCB-d_4 DCB xptrap and DCB/DBB T_1 state chlorine quadrupole frequencies) a nuclear skeleton deformation as a possible explanation for the seemingly "anomalous" mixed phosphorescence of this system, then the behavior of the DCB x-trap must obviously be significantly influenced by crystal field (i.e., external spin-orbit coupling) effects. In other words, external spin-orbit coupling influences have affected a mixing of the spin-orbit characters of all three of the DCB x-trap T_1 state spin sub-levels. It is obvious from the PMDR spectra[43] (Fig. VI-1) and radiative rate data that the x-trap A_u and B_{3u} spin-orbit states have each acquired some characteristics of the other. That is, the unusually high radiative activity of the A_u spin-orbit state to the (0,0) band and behavior of the b_{3g}(0,0-1579 cm^{-1}) transition in the DCB x-trap PMDR spectra[43] (Fig. VI-1) may be explained in terms of an external spin-orbit mixing of the x-trap A_u and B_{3u} spin-orbit states.

A comparison of the results for the DCB x-trap T_1 state with those of the DCB-h_4/DCB-d_4 T_1 shows also that the x-trap molecule must rest in a non-isomorphously equivalent position within the DCB crystal. That is, since the DCB x-trap T_1 state seems to experience a significantly different external spin-orbit coupling influence from that which is experienced by the isomorphously substituted DCB-h_4/DCB-d_4 T_1 state, then the x-trap molecule cannot exist in an isomorphously equivalent position within the DCB neat crystal. This altogether unsurprising conclusion merely affirms the fact that the x-trap molecule has the properties of a "trap" and thus the x-trap T_1 state must experience a

different environment than the T_1 state of a molecule within the DCB triplet exciton band.

We can, however, cite further observations which allow a limited speculation as to the nature of the DCB x-trap. The first of these observations concerns the relative populating rate data for both the DCB-h_4/DCB-d_4 and DCB x-trap systems when excitation occurs only into the host T_1 exciton band (see Table VII-1). Since we may assume that the DCB-h_4 molecule substitutes isomorphously into the DCB-d_4 crystal, then we may also assume that the zero-field splitting axes of the phosphorescent triplet state of the DCB-h_4/DCB-d_4 system are translationally equivalent to the zero-field splitting axes of molecules within the DCB-d_4 T_1 exciton band. Thus, in the absence of significant relaxation processes (e.g., spin-lattice relaxation, cross-chain hopping, etc.), the relative populating rates into the DCB-h_4/DCB-d_4 T_1 state spin-sublevels when excitation is limited to the host (DCB-d_4) T_1 exciton band directly reflect the spin polarization within the host T_1 exciton band.[135] Table VII-1 shows that for DCB-h_4/DCB-d_4 the measured relative populating rates from the host exciton band into the phosphorescent triplet state spin-sublevels are: 1.8 (y), 1 (z), and << 1 (x).

If we now assume that these figures reflect not only the spin polarization which host $S_0 \rightarrow T_1$ excitation produces in the DCB-d_4 T_1 exciton band but also the spin polarization which such excitation will produce within the DCB-h_4 neat crystal T_1 exciton band, then the relative populating rates out of the neat crystal T_1 exciton band into the DCB x-trap T_1 state spin sublevels will alternatively yield information on the orientation of the x-trap T_1 state zero-field splitting axes relative

to those of molecules within the exciton band. The measured relative populating rates from the DCB neat crystal T_1 exciton band into the x-trap spin-sublevels are given in Table VII-2 as: 1.7 (y), 1 (z), and L.4 (x). Based on the above assumptions, these figures indicate that the DCB x-trap molecule must be rotated principally about the molecular z-axis relative to the zero-field axes of molecules within the exciton band.

Additional information is also obtained through further considerations of the quadrupole resonances which are observed in ODMR spectra of the phosphorescent triplet state of DCB/host systems. Throughout the course of this work, and in previous studies of the DCB x-trap T_1 state,[32] the only chlorine quadrupole resonances which were observed in the structure of ODMR spectra for the DCB x-trap as well as the DCB-h_4/DCB-d_4 T_1 state were those associated with the T_1 excited state. Chlorine quadrupole resonances which could be assigned as DCB ground state quadrupole resonances have not been observed in the ODMR spectra of these T_1 states.[32] Since ground state chlorine quadrupole resonances can only be observed in the T_1 state ODMR spectra through the action of a transferred nuclear quadrupole coupling and are therefore dependent on the presence of an intermolecular nuclear-electron hyperfine interaction,[33] the failure to observe any such ground state chlorine resonances suggests that any significant intermolecular interactions among molecular electronic wavefunctions are absent within both the DCB-h_4/DCB-h_4 and DCB x-trap phosphorescent triplet states.

This suggestion then also concerns the nature of the external spin-orbit coupling interaction in these phosphorescent states. That is, we

consider the influence of external heavy atoms to be manifested through two principal mechanisms: (1) External heavy atoms can mix intramolecular singlet character into the phosphorescent state by their influence on the electrostatic field of the phosphorescent molecule;[27,136] (2) External heavy atoms can mix singlet character from external molecules into the phosphorescent state through intermolecular interactions with associated spin-orbit coupling occurring in the external molecule.[136] We can then postulate that the suggested absence of significant intermolecular interaction of electronic wavefunctions demonstrates that the first mechanism must bear responsibility for the external spin-orbit coupling effects observed in the DCB-h_4/DCB-d_4 and DCB x-trap systems.

The DCB/DBB system, on the other hand, presents an even less discernible picture. The data in Table VII-1 illustrate that in the presence of the surrounding DBB crystal the DCB T_1 state spin sublevels have become almost completely mixed. The external spin-orbit are thus much stronger in this system than in the DCB-h_4/DCB-d_4 or DCB x-trap systems as expected for bromine-chlorine substitution in the DCB T_1 state environment (Z dependence of spin-orbit interaction).[27] In fact, the spin sublevel lifetime data and the relative radiative rate data show that the external spin-orbit copuling interaction competes favorably with the internal spin-orbit coupling interaction in this system.

This very qualitative description of the magnitude of external spin-orbit coupling interaction within the DCB/DBB system unfortunately represents all that may be accurately assessed. Although DCB and DBB have very similar crystal structures,[111] a comparison of external

spin-orbit effects on the DCB T_1 state in these two crystals cannot yield any accurate assessment of the external spin-orbit interaction (e.g., Z proportionality) since the interaction appears to occur by different mechanisms in the two crystalline environments. That is, while we have already postulated that intermolecular interactions between molecular electronic states are insignificant in both the DCB-h_4/DCB-d_4 and DCB x-trap systems, the same postulate cannot be made for the DCB/DBB system. The presence of prominent ground state bromine nuclear quadrupole resonance in the ODMR spectra of the DCB/DBB T_1 state (See Fig. VII-2) demonstrate that intermolecular interactions are significant between the DCB and the DBB molecular electronic wavefunctions within the DCB/DBB system. Moreover, unlike the DCB-h_4/DCB-d_4 and DCB x-trap systems the first excited singlet state of the phosphorescent DCB molecule lies higher in energy than the corresponding singlet state of the surrounding DBB host in the DCB/DBB system.[93,110] Intersystem crossing into the DCB T_1 state of DCB/DBB must thereby occur either directly from the DBB S_1 state or via an intermediate DBB T_1 state. Beyond these few comments, the exact nature of the DCB/DBB system remains unexplained.

Throughout the discussion to this point we have omitted any explicit consideration of the possible effects which the host environment might produce on the DCB T_1 state zero-field splitting parameters D and E. The preceding discussion represents an assessment of the possible spin-orbit interactions present in the various DCB/host systems studied and as such it has concerned itself with parameters whose value can be primarily

attributed to the spin-orbit interaction, i.e., dynamic quantities. The values of D and E, on the other hand, do not derive directly from the spin-orbit interaction and we have thus reserved consideration of these parameters until now.

A cursory examination of Table VII-1 immediately reveals that the D and E values of the DCB T_1 state are dramatically affected by the host environment. A more detailed examination of Table VII-1 will additionally show that the variations which occur in D and E upon transition from one environment to another do not strictly correlate with the accompanying variations in the dynamic characteristics of the individual DCB T_1 state spin sublevels. For example, consider the two environmental transitions DCB/PXY → DCB-h_4/DCB-d_4 and DCB-h_4/DCB-d_4 → DCB/DBB.

In the case of the former transition, we have previously noted that the lifetime data indicate that the environmental change has resulted in a significant increase in the singlet characters of both the A_u and B_{2u} spin sublevels of the DCB T_1 state while at the same time leaving the B_{3u} spin-sublevel relatively unaffected. In terms of the zero-field splittings of the DCB T_1 state, this result would tend to lower the energies of both the A_u and B_{2u} spin sublevels relative to the B_{3u}. Thus both $|D|$ and $|E|$ should increase and indeed they have. However, before any conclusions are drawn from these data we should also examine the latter example, the DCB-h_4/DCB-d_4 → DCB/DBB transition.

In this case the lifetime data again indicate that the environmental transition has caused a significant increase in the singlet characters of both the A_u and B_{2u} T_1 state spin-sublevels while leaving the B_{3u}

spin sublevel relatively unaffected. Thus, similar to the former example, the environmental transition would be expected to cause an increase in both $|D|$ and $|E|$. What is in fact observed is that the transition from DCB-h_4/DCB-d_4 to DCB/DBB results in a decrease in both the $|D|$ and $|E|$ values of the phosphorescent triplet state.

Of course, the obvious conclusion to be drawn from these considerations is that the environmental factors which most strongly influence the dynamic characteristics (i.e., external spin orbit coupling) of the three DCB T_1 state spin-sublevels are not primarily responsible for the observed environmental effects in the zero-field splittings of the DCB T_1 state.

Most probably the primary responsibility for the observed changes in zero-field splittings of the DCB T_1 state within various hosts can be attributed to the host environment's influence on the configuration interaction within the DCB triplet manifold. A recent publication by Harrigan, Wong and Hirota has offered an assessment of the electronic structures of the lowest excited triplet states of some substituted benzenes and pyridines.[137] In this publication, these authors correlated the experimentally determined zero-field splittings of the T_1 state of many such molecules with calculated values obtained using electronic structures which were based on the excited configurations of benzene.[112,114] Their results showed that the zero-field splittings of $\pi\pi^*$ triplet states of substituted benzenes were extremely sensitive to small interactions among the excited electronic configurations of the triplet manifold and further that this configuration interaction was in turn sensitive to substitution onto the benzene ring.

In view of these observations it seems reasonable to propose that, while external spin-orbit coupling factors must also contribute, the host dependent variations in the zero-field splittings of the DCB T_1 state which the present study has revealed may be understood principally in terms of an environmental influence on the interaction between excited benzene electronic configurations which form the basis for our description of the DCB T_1 state electronic structure.

By now the reader must undoubtedly realize the high complexity of the crystal field perturbations which exert an influence on the behavior of the DCB T_1 state in crystalline solids. While this complexity has to a large degree rendered our assessment of such crystal field perturbations highly speculative, we have managed to arrive at several significant observations. These observations are summarized as follows:

(1) Crystal field perturbations on the DCB T_1 state within crystalline solids are indeed strong and cannot be neglected in any complete treatment of the state.

(2) The behavior of the DCB x-trap T_1 state may be explained entirely in terms of crystal field effects. A distortion of the DCB nuclear skeleton from D_{2h} symmetry is not a necessary consequence of the observed behavior of this state.

(3) The behavior of the DCB x-trap T_1 state does, however, provide evidence for the proposal that the x-trap molecule is rotated (principally about the molecular z-axis) with respect to the orientation of translationally related molecules.

(4) At 1.4°K, the intermolecular overlap of molecular electronic wavefunctions is significantly larger in DBB crystals than in DCB crystals.

Appendix I. DCB In-Plane Spin-Spin Calculations

In section VI-B we presented the results of calculations which were designed to demonstrate the relative magnitudes of the in-plane electron magnetic dipole-dipole interactions for various T_1 states of p-dichlorobenzene (DCB). The following presentation explains the nature of these calculations.

It can be shown that in a plane the interaction between two magnetic point dipoles with spin S_i and S_j (represented by equations III-1 and III-2 in Chapter III) along a direction μ may be represented as

$$D_\mu \propto (S_i \cdot S_j) \frac{1 - 3\cos^2\theta_\mu}{|\hat{r}_{ij}|^3} , \qquad \text{(AI-1)}$$

where the vector $\hat{r}_{ij}$ joins the two spins, the plane of the interaction is defined by $\hat{\mu}$ and $\hat{r}_{ij}$, and θ_μ is defined as in Fig. AI-1. Our implementation of this planar representation of the electron dipole-dipole interaction in the specific problem of evaluating the in-plane spin-spin interaction of the Π state of DCB took the following form.

Within a given electronic triplet state the quantities S_i and S_j in equation AI-1 may be directly related at any given time to the probability of finding electrons at the positions labeled i and j. These quantities were therefore derived from properly antisymmetrized two-electron wavefunctions which were formed from one-electron M.O.'s (see section VI-B). For example, the $^3B_{1u}$ ($\pi\pi^*$) state function discussed in Section VI-B is given by

0 0 0 0 3 9 0 0 4 9 7

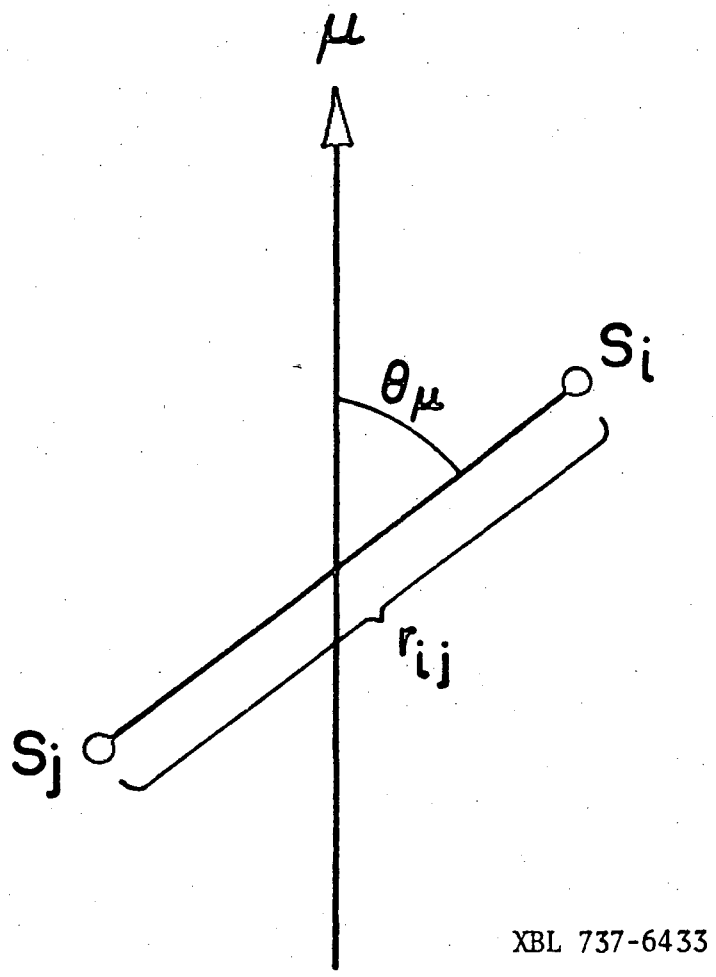

Figure AI-1 Pictorial display of parameters employed in equation AI-1 for description of magnetic dipole-dipole interaction between spins S_i and S_j.

$$^3B_{1u} = \frac{1}{\sqrt{2}} [b_{2g}\, b_{3u} - b_{3u}\, b_{2g}] \quad , \tag{AI-2}$$

or, in terms of the out-of-plane carbon atomic p-orbitals, χ_i, by

$$^3B_{1u} = \frac{1}{6\sqrt{2}} \begin{Bmatrix} -2\,\chi_1\chi_2 + 4\,\chi_1\chi_4 + 2\,\chi_2\chi_1 - \chi_2\chi_3 - \chi_2\chi_5 + \chi_3\chi_2 \\ -2\,\chi_3\chi_4 + \chi_3\chi_6 - 4\,\chi_4\chi_1 + 2\,\chi_4\chi_3 + 2\,\chi_4\chi_5 + \chi_5\chi_2 \\ -2\,\chi_5\chi_4 + \chi_5\chi_6 + 2\,\chi_6\chi_1 - \chi_6\chi_3 - \chi_6\chi_5 - 2\,\chi_1\chi_6 \end{Bmatrix} \tag{AI-3}$$

since

$$b_{2g} = - [2\,\chi_1 + \chi_2 - \chi_3 - 2\,\chi_4 - \chi_5 + \chi_6]$$

and (AI-4)

$$b_{3u} = \frac{1}{\sqrt{12}} [2\,\chi_1 - \chi_2 - \chi_3 + 2\,\chi_4 - \chi_5 - \chi_6] \ ,$$

where χ subscripts label the DCB carbon positions as shown in Fig. AI-2.

For our construction of the DCB problem we approximated the atomic orbitals χ_i as delta functions localized on the appropriate carbon atomic sites. Our $^3B_{1u}$ state function may then be represented solely by the numerical coefficients contained in Eq. AI-4 and given in matrix form by

$$^3B_{1u} = \{\Psi(I,J)\} = \frac{1}{6\sqrt{2}} \begin{Bmatrix} 0 & -2 & 0 & 4 & 0 & -2 \\ 2 & 0 & -1 & 0 & -1 & 0 \\ 0 & 1 & 0 & -2 & 0 & 1 \\ -4 & 0 & 2 & 0 & 2 & 0 \\ 0 & 1 & 0 & -2 & 0 & 1 \\ 2 & 0 & -1 & 0 & -1 & 0 \end{Bmatrix} \tag{AI-5}$$

0 0 0 0 3 9 0 5 4 9 8

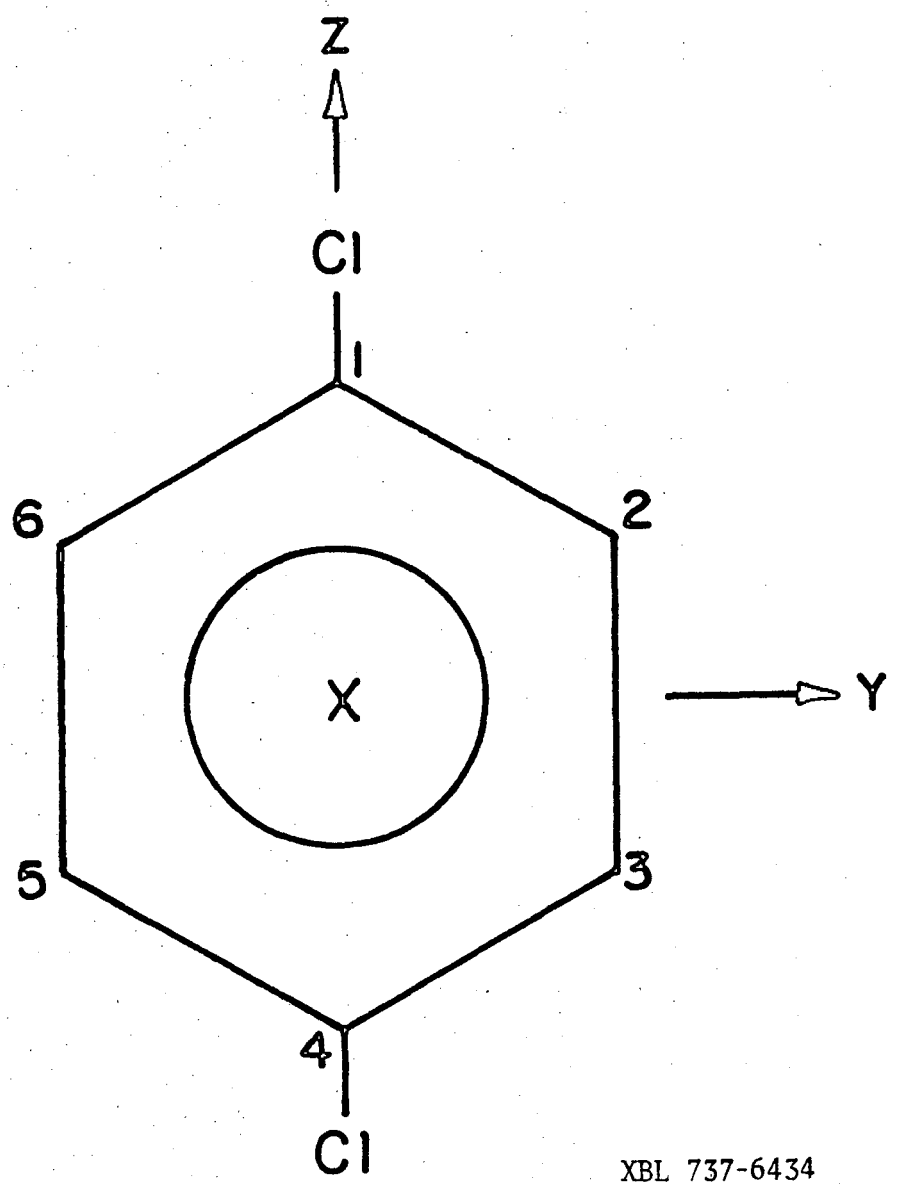

XBL 737-6434

Figure AI-2 Illustrates the coordinate system and carbon numbering system which is employed throughout this thesis.

From this state function matrix, we may form two other matrices, a probability matrix and a correlation matrix. The probability matrix has the elements

$$P(I) = \sum_{J=1}^{6} [\Psi(I,J)]^2 \qquad \text{(AI-6)}$$

and each element P(I) then represents the total probability of finding a given electron on the carbon site labeled by I. The correlation matrix, on the other hand, has elements

$$S(I,I) = 1.0$$

and (AI-7)

$$\underset{I \neq J}{S(I,J)} = \frac{[\Psi(I,J)]^2}{\sum_{J=1}^{6} [\Psi(I,J)]^2}$$

and represents the probability of finding the second electron on carbon site J provided the first electron has been placed on carbon site I. For our $^3B_{1u}$ example, these two matrices are

$$\{P(I)\} = \begin{Bmatrix} 1/3 \\ 1/12 \\ 1/12 \\ 1/3 \\ 1/12 \\ 1/12 \end{Bmatrix} \quad \text{and} \quad \{S(I,J)\} = \begin{Bmatrix} 1 & 1/6 & 0 & 2/3 & 0 & 1/6 \\ 2/3 & 1 & 1/6 & 0 & 1/6 & 0 \\ 0 & 1/6 & 1 & 2/3 & 0 & 1/6 \\ 2/3 & 0 & 1/6 & 1 & 1/6 & 0 \\ 0 & 1/6 & 0 & 2/3 & 1 & 1/6 \\ 2/3 & 0 & 1/6 & 0 & 1/6 & 1 \end{Bmatrix} \qquad \text{(AI-8)}$$

In order to employ the "spin" factor embodied in the matrices $\{P(I)\}$ and $\{S(I,J)\}$ in the evaluation of D_μ (equation AI-1) over the appropriate triplet state function, it is convenient to additionally express the factors θ_μ and r_{ij} in matrix form. Taking the distance between neighboring carbon atoms as equal to unity, the r_{ij} factors for any DCB state composed of delta function atomic orbitals can be expressed by

$$r_{ij} = \{R(I,J)\} = \begin{Bmatrix} 0 & 1 & 2\cos\frac{\pi}{6} & 2 & 2\cos\frac{\pi}{6} & 1 \\ 1 & 0 & 1 & 2\cos\frac{\pi}{6} & 2 & 2\cos\frac{\pi}{6} \\ 2\cos\frac{\pi}{6} & 1 & 0 & 1 & 2\cos\frac{\pi}{6} & 2 \\ 2 & 2\cos\frac{\pi}{6} & 1 & 0 & 1 & 2\cos\frac{\pi}{6} \\ 2\cos\frac{\pi}{6} & 2 & 2\cos\frac{\pi}{6} & 1 & 0 & 1 \\ 1 & 2\cos\frac{\pi}{6} & 2 & 2\cos\frac{\pi}{6} & 1 & 0 \end{Bmatrix} \qquad \text{(AI-9)}$$

Of course, the θ_μ factors cannot be specified until the direction μ is defined. For the DCB problem, the two axes of interest are the z-axis and the y-axis defined in Fig. AI-2. A separate θ matrix may then be defined for each of these two axes. Obviously, since we are interested in the function $\cos^2\theta_\mu$ the elements of the θ_μ matrix may be limited to the range $0 \rightarrow \pi/2$. Then

$$\theta_y = \{\theta_y(I,J)\} = \begin{Bmatrix} \emptyset & \frac{\pi}{6} & \frac{\pi}{3} & \frac{\pi}{2} & \frac{\pi}{3} & \frac{\pi}{6} \\ \frac{\pi}{6} & \emptyset & \frac{\pi}{2} & \frac{\pi}{3} & \frac{\pi}{6} & 0 \\ \frac{\pi}{3} & \frac{\pi}{2} & \emptyset & \frac{\pi}{6} & 0 & \frac{\pi}{6} \\ \frac{\pi}{2} & \frac{\pi}{3} & \frac{\pi}{6} & \emptyset & \frac{\pi}{6} & \frac{\pi}{3} \\ \frac{\pi}{3} & \frac{\pi}{6} & 0 & \frac{\pi}{6} & \emptyset & \frac{\pi}{2} \\ \frac{\pi}{6} & 0 & \frac{\pi}{6} & \frac{\pi}{3} & \frac{\pi}{2} & \emptyset \end{Bmatrix} \qquad \text{(AI-10)}$$

$$\theta_z = \{\theta_z(I,J)\} = \begin{Bmatrix} \emptyset & \frac{\pi}{3} & \frac{\pi}{6} & 0 & \frac{\pi}{6} & \frac{\pi}{3} \\ \frac{\pi}{3} & \emptyset & 0 & \frac{\pi}{6} & \frac{\pi}{3} & \frac{\pi}{2} \\ \frac{\pi}{6} & 0 & \emptyset & \frac{\pi}{3} & \frac{\pi}{2} & \frac{\pi}{3} \\ 0 & \frac{\pi}{6} & \frac{\pi}{3} & \emptyset & \frac{\pi}{3} & \frac{\pi}{6} \\ \frac{\pi}{6} & \frac{\pi}{3} & \frac{\pi}{2} & \frac{\pi}{3} & \emptyset & 0 \\ \frac{\pi}{3} & \frac{\pi}{2} & \frac{\pi}{3} & \frac{\pi}{6} & 0 & \emptyset \end{Bmatrix} \qquad \text{(AI-11)}$$

where the symbol $\emptyset$ denotes an undefinable element.

At this point we have defined all of the parameters necessary to evaluate equation AI-1 for our construction of the DCB problem. For the subsequent evaluation, we were interested in the relative magnitudes of the quantities D_y and D_z defined by the relationships:

$$D_y = \frac{M}{2} \sum_{I=1}^{6} \sum_{\substack{J=1 \\ J\neq K}}^{6} \sum_{K=L}^{6} [P(I)][S(I,J)][S(I,K)] \left\{ \frac{1 - 3\cos^2[\theta_y(J,K)]}{[R(J,K)]^3} \right\} \quad \text{(AI-12)}$$

and

$$D_z = \frac{M}{2} \sum_{I=1}^{6} \sum_{\substack{J=1 \\ J\neq K}}^{6} \sum_{K=1}^{6} [P(I)][S(I,J)][S(I,K)] \left\{ \frac{1 - 3\cos^2[\theta_z(J,K)]}{[R(J,K)]^3} \right\} \quad \text{(AI-13)}$$

where the factor M is an arbitrary proportionality constant and the factor 1/2 merely accounts for the redundancy of terms encountered in the summations.

As a further clarification to the meaning of the above equations, the terms in the summations may alternatively be defined in the following manner. The indices J and K label the "spin" (electron density) on carbon sites J and K, while the index I labels the specific electron configuration in which one electron is localized on carbon site I. Thus, since the factors R(J,K) and $\theta_{\mu=y,z}(J,K)$ contain respectively the length and the direction (with respect to the axis $\mu = y,z$) of the vector $\hat{f}_{JK}$ (joining carbon J and carbon K), the sum over J and K (with the restriction that $J \neq K$) sums all two-center dipole-dipole terms within the Ith electron configuration while the sum over I sums the contributions due to each configuration, weighting each configuration by its probability which is contained in P(I).

The resultant values for D_y and D_z indicate the relative energies of the two DCB triplet state in-plane spin sublevels, providing a

knowledge of the third, the out-of-plane, spin sublevel is available from other considerations. The summations given by equations AI-12 and AI-13 were evaluated for various DCB T_1 state functions with the aid of a computer program and the results are presented in Section VI-B.

0 0 0 0 3 9 0 0 3 0 0

References

1. E. Widemann, Ann. Phys. 34, 446 (1888).
2. J. Dewar, Proc. Roy. Soc. (London) 36, 164 (1880).
3. J. Dewar, Proc. Roy. Soc. (London) 43, 1078 (1888).
4. J. Dewar, Proc. Roy. Inst. G. B. 12, 557 (1888).
5. G. N. Lewis, D. Lipkin and T. T. Magel, J. Am. Chem. Soc. 63, 3005 (1941).
6. A. Terenin, Acta Physicochim. URSS 18, 210 (1943).
7. A. Terenin, Zhur. Fiz. Khim. 18, 1 (1944).
8. G. N. Lewis and M. Kasha, J. Am. Chem. Soc. 66, 2100 (1944).
9. G. N. Lewis and M. Kasha, J. Am. Chem. Soc. 67, 994 (1945).
10. G. N. Lewis and M. Calvin, J. Am. Chem. Soc. 67, 1232 (1945).
11. G. N. Lewis, M. Calvin and M. Kasha, J. Chem. Phys. 17, 804 (1949).
12. D. F. Evans, Nature 176, 777 (1955).
13. C. A. Hutchison, Jr. and B. W. Mangum, J. Chem. Phys. 29, 952 (1958).
14. C. A. Hutchison, Jr. and B. W. Mangum, J. Chem. Phys. 34, 908 (1961).
15. W. Heisenberg, Z. Physik 39, 499 (1926).
16. A. Carrington and A. D. McLachlan, Introduction to Magnetic Resonance (Harper & Row, 1967), Chapter 8.
17. S. Geschwind, G. E. DeVlin, R. L. Cohen and S. R. Chinn, Phys. Rev. 137, A 1087 (1965).
18. J. Brossel and A. Kastler, Compt. Rend. 229, 1213 (1949).
19. M. J. Sharnoff, J. Chem. Phys. 46, 3263 (1967).
20. A. L. Kwiram, Chem. Phys. Letters 1, 272 (1967).

21. J. Schmidt and J. H. van der Waals, Chem. Phys. Letters 2, 640 (1968).

22. D. S. Tinti, M. A. El-Sayed, A. H. Maki and C. B. Harris, Chem. Phys. Letters 3, 343 (1969).

23. C. B. Harris, D. S. Tinti, M. A. El-Sayed and A. H. Maki, Chem. Phys. Letters 4, 409 (1969).

24. M. J. Buckley, Ph.D. Thesis, University of California, Berkeley (1971), and references therein.

25. G. Kothandaraman, Ph.D. Thesis, University of California, Davis (1973), and references therein.

26. A. Nishimura, Ph.D. Thesis, University of California, Davis (1972), and references therein.

27. S. P. McGlynn, T. Azumi and M. Kinoshita, Molecular Spectroscopy of the Triplet State (Prentice-Hall, 1969), and references therein.

28. See References 12-14, 19-21, 24-27, 29-36, 39-44, 48-61, 112, 113, 121, 128, 133.

29. I. Y. Chan, J. Schmidt and J. H. van der Waals, Chem. Phys. Letters 4, 269 (1969).

30. M. J. Buckley, C. B. Harris and A. H. Maki, Chem. Phys. Letters 4, 591 (1970).

31. M. J. Buckley and C. B. Harris, Chem. Phys. Letters 5, 205 (1970).

32. M. J. Buckley and C. B. Harris, J. Chem. Phys. 56, 137 (1972).

33. M. D. Fayer, C. B. Harris and D. A. Yuen, J. Chem. Phys. 53, 4719 (1970).

34. A. H. Francis, C. B. Harris and A. M. Nishimura, Chem. Phys. Letters 14, 425 (1972).

0 0 0 0 3 9 0 5 5 0 1

35. A. H. Francis and C. B. Harris, J. Chem. Phys. 57, 1050 (1972).

36. C. A. Hutchison, Jr., J. V. Nicholas and G. W. Scott, J. Chem. Phys. 53, 1906 (1970).

37. See References 23, 24, 30-36.

38. See References 23, 24, 30-35.

39. C. B. Harris and R. J. Hoover, J. Chem. Phys. 56, 2199 (1972).

40. A. M. Nishimura, D. S. Tinti and J. S. Vincent, Chem. Phys. Letters 12, 360 (1971).

41. S. W. Mao, T. C. Wong and N. Hirota, Chem. Phys. Letters 13, 199 (1972).

42. D. Schweitzer, J. Zuclich and A. H. Maki, Chem. Phys. Letters 18, 24 (1973).

43. M. J. Buckley, C. B. Harris and R. M. Panos, J. Am. Chem. Soc. 94, 3692 (1972).

44. G. Kothandaraman and D. S. Tinti, Chem. Phys. Letters 19, 225 (1973).

45. See References 39, 43, 44, 52.

46. See References 35, 39, 43, 44, 48, 50-52.

47. See References 50, 51.

48. J. Schmidt, W. S. Veeman and J. H. van der Waals, Chem. Phys. Letters 4, 341 (1969).

49. W. G. Breiland, C. B. Harris and A. Pines, Phys. Rev. Letters 30, 158 (1973).

50. C. B. Harris, R. L. Schlupp and H. Schuch, submitted for publication to Phys. Rev. Letters (1973).

51. J. P. Wolfe, Chem. Phys. Letters 10, 212 (1971).

52. H. C. Brenner and C. A. Hutchison, Jr., J. Chem. Phys. 58, 1328 (1973).

53. J. Schmidt, I. A. M. Hesselmann, M. S. de Groot, and J. H. van der Waals, Chem. Phys. Letters 1, 434 (1967).

54. J. Schmidt and J. H. van der Waals, Chem. Phys. Letters 3, 546 (1969).

55. M. A. El-Sayed, D. S. Tinti and D. Owens, Chem. Phys. Letters 3, 339 (1969).

56. M. A. El-Sayed, J. Chem. Phys. 52, 6432 (1970).

57. D. S. Tinti and M. A. El-Sayed, J. Chem. Phys. 54, 2529 (1971).

58. A. H. Francis and C. B. Harris, Chem. Phys. Letters 9, 181 (1971).

59. J. Schmidt, V. C. van Dorp and J. H. van der Waals, Chem. Phys. Letters 8, 345 (1971).

60. M. Sharnoff, Chem. Phys. Letters 2, 498 (1968).

61. R. F. Clements and M. Sharnoff, Chem. Phys. Letters 7, 4 (1970).

62. G. Herzberg, Electronic Spectra of Polyatomic Molecules, V. 3 (D. van Nostrand Co., Inc., 1967), pp. 555-561.

63. H. Spooner and E. Teller, J. Chem. Phys. 7, 382 (1939).

64. J. H. Callomon, T. M. Dunn and I. M. Mills, Phil. Trans. Roy. Soc. 259A, 499 (1966).

65. H. Sponer, G. Nordheim, A. L. Sklar and E. Teller, J. Chem. Phys. 7, 207 (1939).

66. M. Goepert-Mayer and A. L. Sklar, J. Chem. Phys. 6, 645 (1938).

67. R. G. Parr, D. P. Craig and I. G. Ross, J. Chem. Phys. 18, 1561 (1950).

68. F. M. Garforth and C. K. Ingold, J. Chem. Soc., 417,427 (1948).

69. F. M. Garforth and C. K. Ingold, J. Chem. Soc., 433,440 (1948).

70. A. L. Sklar, J. Chem. Phys. 5, 669 (1937).

71. G. N. Lewis and M. Kasha, J. Am. Chem. Soc. 67, 994 (1945).

72. H. Shull, J. Chem. Phys. 17, 295 (1949).

73. G. W. Robinson, J. Mol. Spec. 6, 58 (1961).

74. S. Leach and R. Lopez-Delgado, J. chim. phys. 61, 1636 (1964).

75. D. S. McClure, J. Chem. Phys. 17, 665 (1959).

76. D. P. Craig, J. Chem. Phys. 18, 236 (1950).

77. D. R. Kearns, J. Chem. Phys. 36, 1608 (1962).

78. D. W. Olds, J. Chem. Phys. 35, 2248 (1961).

79. A. C. Albrecht, J. Chem. Phys. 33, 156 (1960).

80. A. C. Albrecht, J. Chem. Phys. 33, 169 (1960).

81. A. C. Albrecht, J. Chem. Phys. 38, 354 (1963).

82. C. C. J. Roothan and R. S. Mulliken, J. Chem. Phys. 16, 118 (1948).

83. C. C. J. Roothan and R. G. Parr, J. Chem. Phys. 17, 1001 (1949).

84. K. J. Niira, J. Chem. Phys. 20, 1498 (1952).

85. K. J. Niira, J. Phys. Soc. Japan 8, 630 (1953).

86. J. A. Pople, Proc. Phys. Soc., London, Sect. A 68, 81 (1955).

87. R. Pariser, J. Chem. Phys. 24, 250 (1956).

88. N. S. Ham and K. Ruedenberg, J. Chem. Phys. 25, 1 (1956).

89. J. R. Platt, J. Mol. Spectrosc. 9, 288 (1962).

90. J. W. Moskowitz and M. P. Barnett, J. Chem. Phys. 39, 1557 (1963).

91. J. M. Schulman and J. W. Moskowitz, J. Chem. Phys. 43, 3287 (1965).

92. See References 5, 6, 16, 21-30.

93a. G. Castro and R. M. Hochstrasser, J. Chem. Phys. 46, 3617 (1967).

93b. R. M. Hochstrasser, private communication.

94. The discussion presented in this section is essentially the same as that which can be found in any standard quantum mechanics text. In particular our discussion parallels that of F. L. Pilar, Elementary Quantum Chemistry (McGraw-Hill, 1968) Chapter 11.

95. H. M. McConnell, Proc. Nat. Acad. Sci. (U.S.) 45, 172 (1959).

96. J. H. van Vleck, Rev. Mod. Phys. 23, 213 (1951).

97. M. Tinkham and M. W. P. Strandberg, Phys. Rev. 97, 937 (1955).

98. H. F. Hameka and L. J. Oosterhoff, Mol. Phys. 1, 358 (1958).

99. D. S. McClure, J. Chem. Phys. 20, 682 (1952).

100. J. H. van der Waals and M. S. de Groot, The Triplet State, Proceedings of the Beirut Symposium, 1967 (Cambridge University Press, 1967), pp. 101-133.

101. See Reference 27, Chapter 5.

102. M. Kasha, Disc. Faraday Soc. 9, 14 (1950).

103. G. W. Robinson and R. P. Frosh, J. Chem. Phys. 38, 1187 (1963).

104. G. W. Robinson and R. P. Frosh, J. Chem. Phys. 37, 1962 (1962).

105. C. B. Harris, J. Chem. Phys. 54, 972 (1971).

106. M. Schwab and E. L. Hahn, J. Chem. Phys. 52, 3152 (1970).

107. C. P. Slichter, Principles of Magnetic Resonance (Harper and Row, 1963), pp. 18-22.

108. G. W. Leppelmeier and E. L. Hahn, Phys. Rev. 141, 724 (1966).

109. J. H. van Vleck, Phys. Rev. 74, 1168 (1948).

110. G. A. George and G. C. Morris, Mol. Cryst. Liquid Cryst. 11, 61 (1970).

111. U. Croatto, S. Bezzi and E. Bua, Acta Cryst. 5, 825 (1952).

112. M. S. deGroot, I. A. M. Hesselmann and J. H. van der Waals, Mol. Phys. 16, 45 (1969).

113. L. T. Cheng and A. L. Kwiram, Chem. Phys. letters 4, 457 (1969).

114. M. Godfrey, C. W. Kern and M. Karplus, J. Chem. Phys. 44, 4459 (1966).

115. See References 13, 14, 36, 116-122.

116. M. Gouterman and W. Moffitt, J. Chem. Phys. 30, 1107 (1959).

117. M. Gouterman, J. Chem. Phys. 30, 1369 (1959).

118. B. Smaller, J. Chem. Phys. 37, 1579 (1962).

119. H. Hameka, J. Chem. Phys. 31, 315 (1959).

120. Y. N. Chin, J. Chem. Phys. 39, 2736 (1963).

121. N. Hirota, C. A. Hutchison, Jr., and P. Palmer, J. Chem. Phys. 40, 3717 (1964).

122. C. E. Moore, Nat. Bur. Stand. (U.S.), Circ. 457 (1949 and 1952).

123. D. S. McClure, J. Chem. Phys. 17, 905 (1949).

124. L. Salem, The Molecular Orbital Theory of Conjugated Systems (W. A. Benjamin, New York, 1966).

125. See Reference 27, Chapter 6.

126. M. Suzuki and M. Ito, Spectrochim. Acta, Part A 25, 1017 (1969).

127a. See later text for discussion of this band. We suggest that this band is actually a $b_{1g}(b_{3g} \times b_{2g})$ combination band coincident with a $b_{2g}(a_g \times b_{2g})$ combination band. This suggestion is based on the tentative assignment of the (0,0-1579 cm^{-1}) band as coincident a_g and b_{3g} fundamentals.

127b. We realize that a b_{3g} symmetry assignment represents an unusual assignment for a $^3\pi\pi^*$ phosphorescence band of such intensity. That is, since a b_{3g} vibration is an in-plane mode and as such cannot mix $\sigma\pi^*$ or $n\pi^*$ character into the $\pi\pi^*$ T_1 state, the intensity of the (0,0-1579 cm^{-1}) band is unusually high for a b_{3g} vibration. However, on the basis of the reported Raman active 1577 cm^{-1} ground state b_{3g} mode (see Ref. 126) and in light of possible crystal-field perturbations (Cf. Sec. VII), the b_{3g} assignment seems most probable.

128. A. H. Francis and C. B. Harris, Chem. Phys. Letters 9, 188 (1971).

129. A. Stojiljkovic and D. H. Wiffen, Spectrochim. Acta 12, 471 (1958).

130. J. R. Scherer and J. C. Evans, Spectrochim. Acta 19, 1739 (1963).

131. M. J. Buckley and C. B. Harris, unpublished work.

132. R. N. Renaud, D. Kovachic and L. C. Leitch, Can. J. Chem. 39, 21 (1961).

133. M. S. de Groot and J. H. van der Waals, Mol. Phys. 6, 545 (1963).

134. Least-squares fit program; LBL designated LSQVMT written by E. Beals of the LBL computer staff.

135. J. Gromer, H. Sixl and H. C. Wolf, Chem. Phys. Letters 12, 574 (1972).

136. G. W. Robinson, J. Chem. Phys. 46, 572 (1967).

137. E. T. Harrigan, T. C. Wong and N. Hirota, Chem. Phys. Letters 14, 549 (1972).

0 0 0 0 3 9 0 0 5 0 4

ACKNOWLEDGEMENTS

First, I would sincerely like to thank my research director, Professor Charles Harris, for his personal guidance throughout my graduate career. I would also like to thank Professor Harris' coworkers, especially Mr. Michael Fayer and Dr. Alan Nishimura for their constant aid and counsel. Additionally, I extend my gratitude to Professor D. S. Tinti of the University of California at Davis for freely offering his thoughts, and to Ms. Eileen Deusler for her aid in helping me to understand the computer mind.

Finally, heartfelt love and appreciation are extended to my parents, Mr. and Mrs. Charles Panos, for their continuing encouragement and unwavering confidence throughout many years of study, and to my wife, Jeanne, for all her extraordinary abilities, especially for being able to live with me.

This work was done under the auspices of the U. S. Atomic Energy Commission.

LEGAL NOTICE

This report was prepared as an account of work sponsored by the United States Government. Neither the United States nor the United States Atomic Energy Commission, nor any of their employees, nor any of their contractors, subcontractors, or their employees, makes any warranty, express or implied, or assumes any legal liability or responsibility for the accuracy, completeness or usefulness of any information, apparatus, product or process disclosed, or represents that its use would not infringe privately owned rights.

TECHNICAL INFORMATION DIVISION
LAWRENCE BERKELEY LABORATORY
UNIVERSITY OF CALIFORNIA
BERKELEY, CALIFORNIA 94720